ADDIS ABABA UNIVERSITY

ADDIS ABABA INSTITUTE OF TECHNOLOGY

AFRICAN RAILWAY CENTER OF EXCELLENCE

RAILWAY ENGINEERING (CIVIL INFRASTRUCTURE)

Effects of Flow Variability on Scouring of Bridges and Culverts between Sebeta and Adama Section of Ethio - Djibouti Railway Line

A Thesis in Civil Infrastructure Railway Engineering

This research thesis is submitted to the African Railway Centre of Excellence (ARCE) as a requirement for a Master's Degree in Civil Infrastructure (Railway Engineering) of Addis Ababa Institute of Technology, Addis Ababa University, Ethiopia

By:
Habeeb SOLIHU
GSR/6129/12

Advisor:

Dr. Belete Berhanu. Kidanewold

Addis Ababa, Ethiopia
August 2021

APPROVAL PAGE

The undersigned have examined the thesis entitled "Effects of Flow Variability on Scouring of Railway Bridges and Culverts within Sebeta – Adama Section of the Ethio – Djibouti Railway Line" presented by SOLIHU Habeeb (GSR/6129/12), submitted to African Railway Center of Excellence, Addis Ababa Institute of Technology, School of Graduate Studies in partial fulfillment of the requirement of the award of Degree of Masters of Science in Railway Engineering (Civil Infrastructure):

Submitted by:

SOLIHU Habeeb		
Student	Signature	Date

Approved by:

Belete Birhanu Kidanewold (PhD)		
Advisor	Signature	Date
Prof. Yilma Seleshi		
Examiner 1	Signature	Date
Fiseha Behulu (PhD)		
Examiner 2	Signature	Date
Abrham Gebre (PhD)		
Director ARCE		
Chairperson	Signature	Date

DECLARATION

This is to declare that the work which is being presented in this thesis work entitled “Effects of flow variability on Scouring of Bridges and Culverts (Railway Bridges & Culverts) between Sebeta and Adama Section of Ethio - Djibouti Rail Line” is the original work of my own, has not been presented for a degree of any other university and all the resource of materials used for this thesis have been duly acknowledged.

_____ _____

Habeeb SOLIHU
GSR/6129/12
soilhu.habeeb@aait.edu.et
+2347038949144

Date

ACKNOWLEDGMENT

Firstly, my profound gratitudes go to the Almighty Allah for giving me the opportunities to accomplish this milestone. None but Him alone is the Most Powerful.

Secondly, I will like to express my appreciation to my family (in general) for their prayers, moral, and financial supports to achieve this feat. For indeed, family is over everything.

Thirdly, my appreciation to the Department of Railway Center for allowing me to pursue my MSc Program in Civil Infrastructure Engineering under the African Railway Center of Excellence Postgraduate Scholarship. In addition, my appreciations specifically go to Mrs. Nigist and Mr. Tewodoros of the Ethiopian Railway Cooperation and the Ministry of Water, Irrigation, and Energy of Ethiopia respectively for their supports during the data acquisition for this study.

Moreso, my deepest appreciation to my MSc Advisor, Dr. Belete Berhanu Kidanewold of the Department of Hydrology and Hydraulics Engineering, Addis Ababa Institute of Technology for his moral advice and support throughout this study. Those pieces of advice were indeed invaluable. Again, my appreciations go to my undergraduate supervisors and mentors specifically in persons of Dr. S. O. Bilewu, Dr. Mrs. Mokuolu, Dr. Niyi Adeogun, and Engr. Abdulhameed Ayomaya for their moral support and for not getting tired of me whenever their inputs are needed. Again, my special appreciations go to Dr. Salim Ayomaya for being a mentor, a brother, and an advisor of all time.

However, this acknowledgment would not be completed without appreciating my friends and colleagues in no particular order: Abdulwaheed, Idrees, CVE class of 2017, Sakina Mrina (Tanzania), and Mr. Fallah (Liberia) just to mention but a few amongst the endless most intelligent people I have met so far as a family here in Aratkilo Hostel. You guys are wonderful and I appreciate you all.

Finally, to those who I failed to list here due to the limited space provided for this section, you are all wonderful people, and I appreciate you all.

Table of Contents

LIST OF FIGURES

LIST OF TABLES

ABSTRACT

This case study area is found within Uplands, Upper Valley, and Western Highlands of Awash river subbasins which is one of the major river flood-prone areas in part of Oromia region where the most significant part of the railway section is found. This study simulated the rainfall-runoff of the hydrological processes in the selected catchment using HEC-HMS hydrological model. The simulation was achieved using the ground-based rainfall datasets for the meteorological gauge stations within the catchment (Uplands, Upper valley, and Western Highlands of Awash river subbasins) for a period of twenty years (2000 – 2019); sourced from the National Meteorological Agency of Ethiopia. The model was calibrated with the observed time-series datasets between 2005 and 2014 at Awash Melka Kuntire, Awash @Hombole, and Mojo @MojoVI hydrological gauging Stations. These stations were selected not only because they are directly linked with the selected railway section but also the availability of full records. These datasets were sourced from the Ministry of Water, Irrigation, and Energy of Ethiopia. The model performance shows that NSE, PBIAS, and R^2 were respectively 0.932, 14.94%, and 0.9994 at Awash @Melka Kuntire; 0.923, 16.25%, and 0.9994 at Awash @Hombole; 0.859, 12.42%, and 0.992 at Mojo @MojoVI. It has also been established that there is flow variability in all the selected drainage structures with the coefficient of variance ranged from 0.645 to 1.034. The study has also developed Rainfall (mm) Duration Frequency and Rainfall Intensity (mm/hr) – Duration Frequency Curves for the selected catchment which was used as design rainfall as input for flood frequency modeling in HEC-HMS. The comparison results between the estimated peak flows and the designed peak flow extracted from the design documents, Q_{100} (m^3/s), showed that about 40% of the drainage structures are likely to experience flooding once every 100 years. However, this could only be true if and only if the probability distribution used for peak flow estimation is the same as that used for the design of peak flows in the document. The results of scour depth comparison for all the structure types indicated that the flow variability (in peak flows) has an effect on scouring depths and it varies at different return periods. Also, this study has estimated the median stone size for riprap materials and found it to be about 1.58 m as a mitigating measure to ameliorate the high risk of scouring (about 60%) estimated around a pier at bridge location K97+817.22 (Mojo-Adama No.3 Bridge). This study thereafter generated some relationship equations for the slab culverts and the NSE and R^2 were found to be (0.77, 0.90) and (0.82, 0.83) for scenario 1 (Estimated Q_{100}) and scenario 2 (Design Q_{100}) respectively. The study, thereafter, recommended the use of the generated scour depth equations for slab culverts in the other section of this railway line.

KEYWORDS:

Flood risk; scour depths; riprap size; flow variability; hydrological model; slab culvert; railway; Awash river sub-basins

ABBREVIATIONS & ACRONYMS

GIS	Geographical Information System
HEC	Hydrologic Engineering Center
HMS	Hydrologic Modeling System
DEM	Digital Elevation Model
GPS	Global Positioning System
MWIEE	Ministry of Water, Irrigation, and Energy of Ethiopia
CoV	Coefficient of Variance
R^2	Coefficient of Determination
NSE	Nash- Sutcliff Efficiency
LULC	LandUse LandCover
SS	Sums of Squares
SE	Standard Error
MS	Mean Square
df	Degree of Freedom
ANOVA	Analysis of Variance
NMAoE	National Meteorological Agency of Ethiopia

Chapter 1: INTRODUCTION

1.1 Background of the Study

Railway transport is a very important type of public transport that has a longstanding irreplaceable role especially in suburban transport and transport for distances up to 400 km **[1]**. Railway infrastructure is a system formed by railway tracks, rail switches, other engineering structures such as bridges, tunnels, and associated infrastructure of stations which includes platforms, security, and safety devices **[2]**. Railway infrastructure elements can be further classified as critical and routine. Railway bridges and tunnels are classified under the major critical elements which are characterized by their increased importance in the railway infrastructure network in which disruption or failure of these elements could lead to a significant negative impact on the lives and health of passengers and or economic losses of the operator **[3]**. Railway bridges must support the continuity of the track to ensure the same traffic safety and ride comfort throughout the entire length of the rail track **[4]**.

Ethiopia – Djibouti railway line otherwise known as Addis Ababa – Djibouti railway line is known as a major export and import connection linking landlocked Ethiopia with Djibouti Port in the Red Sea's international shipping routes **[6]**. This railway line connecting Ethiopia with Djibouti through Dire Dawa was about 780km with meter-gauge opened to traffic in 1917 but deteriorated due to a lack of maintenance and management **[7]**, and also because of lack of commercial motivation **[6]**. After the feasibility study conducted in 2007, taking into account the importance of this line concerning both economic and financial points of view, the line was set to modernization which involved the replacement of the meter-gauge with standard gauge, electrification at 25kV, and designed with 120 km/h traveling speed which was constructed in compliance with Chinese electrified railway standards by China Civil Engineering Construction Corporation (CCECC) inaugurated in November 2015 and October 2016 for freight services and passenger services respectively **[7]**.

However, after the modernization, the new line has a total length of 752.7km which involves laying double-track for the first 115km from Addis Ababa to Adama, and a single track for the remaining 600km to Djibouti **[7]**. There are 21 stations along this line with a prayer room in addition to the ticketing and refreshment facilities at each station and has a total number of sixty-one (61) bridges, thirty-seven (37) frame bridges, and four hundred and fifty-three (453) culverts along the route.

Bridge piers placed inside the river is one of the most common civil engineering practices whereby the bridge pier is in direct contact with the flowing water **[8]**, and **[9]** noted that in the Western part of China, bridges are most of the time inevitably constructed over canyons, and their piers are thought to be the most vulnerable to the hazards associated with debris flow. The scouring process

is known to be the main issue associated with the interaction of flowing water and the bridge pier and this is known as local scour **[8]**. Also, Lagasse et. al. **[10]** stated that the foremost cause of bridge failure globally is scouring, which is the removal of riverbed material at bridge foundations due to the flow of water. It is also the bridge management risk most likely to be affected by climate change **[11]**. Global climate change is known to affect the local weather patterns, resulting in changes in river flow regimes. And according to Dikanski et al., **[12]**, the scour depths can be affected and poses the risk of bridge failure.

According to Shen et al., **[13]**, local scour is the abrupt decrease in bed elevation near a pier due to erosion of bed material by the local flow structure caused by the pier. Neglecting the local scour phenomenon in the bridge pier design can result in either a huge financial cost or a high casualty rate. Briaud et al., **[14]**, there was about 1502 bridge collapsed cases due to bridge scour between 1966 and 2005 in the United States, implying that an average rate of one bridge collapse in every ten (10) days. Again, Wardhana and Hadipriono **[15]** found out that there were 500 cases of bridge structure failures between 1989 and 2000 in the United States with a common cause which was floods and the scouring process. Also, on July 9, 1981, during a debris flow event, the pier of the Chengdu–Kunming Railway Bridge located in Liziyida Gully reported failed, resulting in 130 people and 146 people reported dead or missing and injured respectively, making it the worst debris flow accident in China's highway history **[9]**.

1.2 Problem Statement

This case study area is found within Uplands, Upper Valley, and Western Highlands of Awash River Subbasins which is one of the major river flood-prone areas in part of Oromia region where the most significant part of the railway section is found **[16]**. In this section rainfall is very high, LULC changes are taking place at a high rate due to urbanizations, deforestation, changes in land drainage, and climate change; which will have a direct impact on flow variabilities and invariably on scouring depths of the critical elements (bridges/culverts) of railway infrastructure network within this area.

Also, bridge failures have occurred ever since its building started thousands of years ago **[17]** and most of these failures tend to occur both suddenly and without prior notice **[18]**. The major threats to infrastructure such as bridges, highways, buildings, etc. are large-scale floods, extreme weather fluctuations, landslides, large-scale crashes from the external environment, disruption of large waterworks, and large-scale violation of legality, such as a bomb attack **[5]**.

Because transport infrastructure is a capital asset for the development of society and a major prerequisite for an effective and productive economy, majorly characterized by long lifetimes and

high investment costs **[19]**. And railways are parts of these critical infrastructures not only for the transportation of people but also for goods and services, and network failures must be controlled as much as possible to maintain safety and to limit economic losses (**[20]**. Therefore, to maintain the common goal of constructing this railway line, assessing the flow variability and its effects on scouring depths and risks of the railway drainage structure serves as impetus and rationale for this study.

1.3 Objectives of the Study

1.3.1 Main Objective

The main objective of this study is centered on the Assessment of flow variabilities and their effects on the Scouring of bridges and culverts between Sebeta and Adama Section of Ethio – Djibouti Railway Line.

1.3.2 Specific Objectives

This research has attempted the following specific objectives

- To develop a rainfall-runoff model for the selected section (Sebeta – Adama of Ethio – Djibouti Railway Line) to investigate flow variability
- To develop a relationship between flow variability and scouring depth for slab culvert drainage structures

1.4 Research Questions

In pursuing the above objectives, the study has strived to answer the following questions:

- Is there flow variability at the selected drainage structures?
- What are the relationships between the scouring depth and flow variability at the selected drainage structures?

1.5 Research Hypothesis

- Null Hypothesis

  Ho_a: There are no flow variability and flood risks at the drainage structures

  Ho_b: Flow variabilities do not affect scouring depth and risks at the selected structures

- Alternative Hypothesis

  $H1_a$: There are flow variability flood risks at all the drainage structures

  $H1_b$: Flow variabilities have effects on scouring depth and risks at the selected structures

1.6 Significance of the Study

The bridge collapse is a very complex process resulting from the combinations of the effects of many different factors such as flooding and scouring **[21]**. Thus, this study was centered on the flow variability impact on the selected railway drainage structures within the study area concerning flooding and scouring risks. It is believed that the outcomes of this study will produce a credible, reliable source of data, and of great importance to the management of the Ethio – Djibouti Railway Line since the critical evaluation of drainage structures represents a substantial process and relevant source of information for any decision-making processes related to the strategy of bridge maintenance, repair, or reconstruction **[22]**, for the safety of both the infrastructure itself and the users without putting the activities into a halt which would affect the economic impact of railway transportation.

1.7 Scope of the Study

The study is aimed at investigating the flow variability impacts on flooding and scouring risks at the bridge piers and culverts within the Sebeta – Adama Section of Ethio – Djibouti Railway line. The scope of this study is limited to the development of a rainfall-runoff model for the selected section (Sebeta – Adama of Ethio – Djibouti Railway Line) to investigate flow variability; development of an IDF curve to estimate the design rainfall as an input to estimating the peak flows in HEC-HMS; investigation of the flood and scour risks associated with each peak flow; suggestion of mitigating measure for protecting scour risk-prone drainage structure, and develop a relationship between flow variabilities and scouring depth for slab culvert drainage structures. This is so important because drainage structure (bridges and culverts) is one of the major components of a traffic system whereby any damage to any of these components has the potential of causing loss of lives and properties **[18]**, and will directly or indirectly affect the economy of the state.

1.8 Organization of the Thesis

This section briefly outlined the content of this thesis:

Chapter 1: This section dealt with the general introduction, problem statement, and main and specific objectives of the study. It also highlights the research question which this study tried to answer within the stated scope and methodology.

Chapter 2: This section generally reviewed relevant literature with the focus on railway bridge collapse causes and mechanisms, flow variability effects, introduction to hydrological models, railway bridge hazards, bridge failure due scouring, and the importance of rainfall data are presented.

Chapter 3: This section briefly described the study area in terms of the geographical location, topographic, geological faults and features, climate, soil textures, LandUse LandCover, Elevation

of the area, railway line section, hydraulic structures within the section in consideration, data preparation and processing while the brief explanations on the materials and methods adopted are presented.

Chapter 4: This section presented the results and discussions.

Chapter 5: Here, general conclusions are made and the recommendations are suggested.

Chapter 2: LITERATURE REVIEW

2.1 Railway Hydraulic Drainage Structures

Rail transportation is a key enabler of economic growth worldwide and it consists of two main asset classes of infrastructure and rolling stock **[23]**. Reinforced concrete bridges are the backbone of bridge structures **[24]** and the effects of water must be properly managed during the different phases of the lifecycle of these infrastructures such as a railway to avoid closure or even partial destruction **[25]**. To establish the actual bridge behavior and allowing for the effects of the possible imperfections or damages of the structural members, the spatial computational models should be used for global analyses of steel railway bridges **[26]**.

2.2 Components of Hydraulic Drainage Structures

Highway hydraulic drainage structures commonly comprise hydraulic culverts and bridges.

2.2.1 Hydraulic Culverts

- Slab Culverts

Slab culverts are often referred to as open-bottom culverts because they are the structure types that have natural channel materials as the bottom. They could be cast-in-place, precast, or prefabricated structures in the rectangular or rounded top.

The slab culverts have the following advantages over other culvert types; the natural bottom material is more environmentally attractive than a traditional closed culvert, particularly for the passage of aquatic animals; they are highly considered by highway designers to be economical alternatives to short bridges, and because they are commonly prefabricated, they are more easily constructed than bridges **[27]**.

2.2.2 Bridges

Railways often involve the construction of structures, both to support the railway and its infrastructure, and to carry buildings, roads, and other forms of transport over or alongside the railway **[28]**. Railway bridges are structurally divided into three major segments which are represented in Figure 2.1.

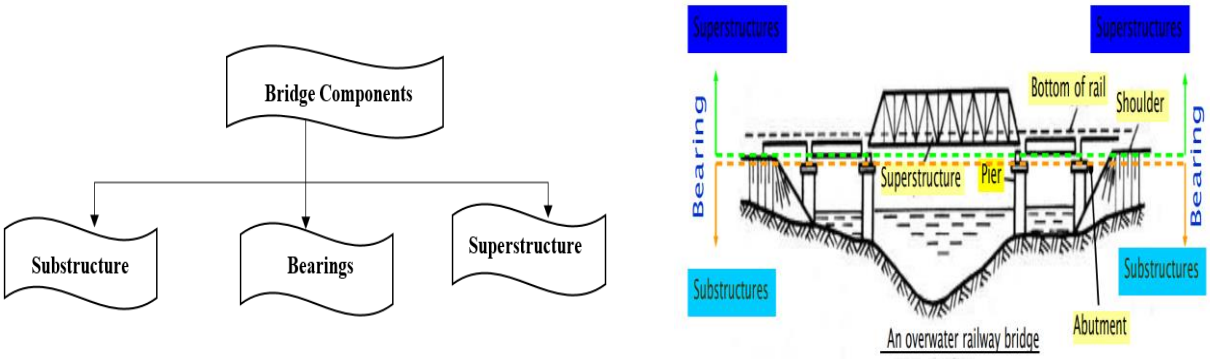

Figure 2.1: Basic Components of an Overwater Railway Bridge

2.3 Effects of Flow Variability

Some of the common effects of flows are summarized in the flow chart diagram in Figure 2.2, however, this study will be focusing only on the scouring as an effect of variable flows on the railway bridges at the selected case study area.

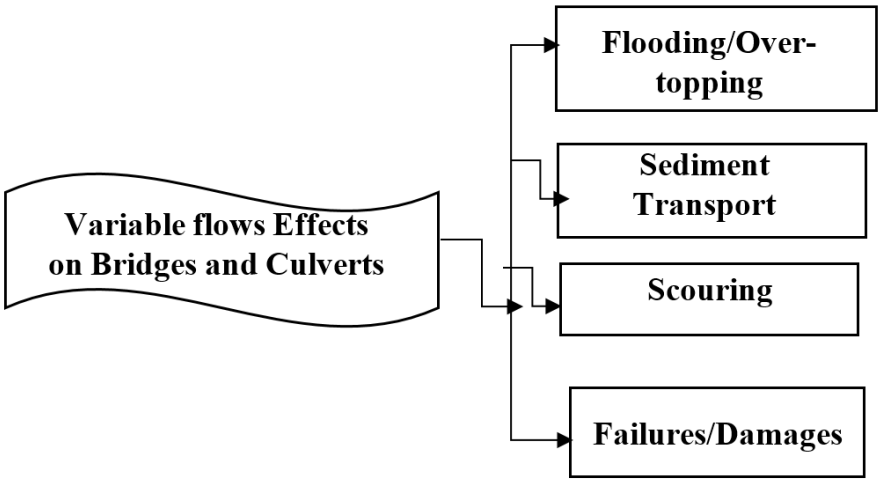

Figure 2.2: Common Effects of variable flows

2.4 Review of World Bridge Failures

Turag-Bhakurta Bridge was a 67 m long bridge constructed in 1995. It experienced two failures; a partial collapse in 1995 which was as a result of the settlement of the pier due to the 1995 flood, and a complete collapse of the structure as a result of the reduction in flood water path during the 1998 flood **[29]**.

Karnaphuli Bridge was a 920 m long road bridge constructed between 1988 and 1989 using used steel trusses donated by the Dutch government to cross over the Karnaphuli River. The failure was

as a result of a Category V super cyclone on the 29th April 1991, which hit the coastal areas of Bangladesh with up to 225 kmph accompanied by storm surges up to 6m high **[17]**.

Tay Railway Bridge collapse occurred as a result of structural failure near Dundee, Scotland on the 28th December 1879. As at that time, it was the longest railway bridge in the world at 3.5 km long. It was the worst to occur in Britain at the time in terms of both death records and damage to the infrastructure **[17]**.

I-35W Bridge is located in Minnesota and the damage occurred in 2007 which resulted in the loss of about 13 lives and 145 people severely injured **[30]** and **[31]**. Also, Tacoma Narrows best recorded and documented bridge failure in the history of bridge engineering. It was a suspension bridge and its collapse occurred near Seatle, USA, on the 7th November 1940 as a result of neglecting the dynamic forces in its design and construction phases **[17]**.

Mongolia Viaduct was a six-lane single-column-pier viaduct that collapses in the Inner Mongolia Autonomous Region in 2007 due to the passage of three overloaded trucks eccentrically on the nearside passing lane resulted in the loss of 4 lives **[21]**. Kings Bridge Melbourne (1962): It crosses over a railway, some streets, and the Yarra River in an N-S direction. The collapse occurred on the 10th of July 1962 as a result of overloading beyond the strength limits of both the I-girder and the soil conditions **[17]**.

Again, the silver bridge was constructed from 1927 to 1928 and collapsed without prior warning on the 15th December 1967 when it was crowded with heavy traffic during the evening rush hour. About 46 lives **[30]** were lost and 9 were hospitalized **[17]**. Harp Road Bridge (2007): Due to unstable bearing supports and the heavyweight of a truck, the bridge collapsed by overturning in 2007 **[21]**.

Sgt. Aubrey Cosens VC Memorial Bridge was a 106.7 m long suspended-deck steel arch bridge built in October 1960 which spans over the Montreal River. The failure occurred on the 14th January 2003, primarily as a result of fatigue fractures of three steel hanger rods under a load of transport truck during severely cold temperatures **[17]**.

Hardinge Railway Bridge is a 1.62 km long steel truss bridge, design and constructed in 1908–1915, crossing over the Padma River between Paksey and Bheramara, Pabna. Two noticeable failure events occurred within its 100 years of service. First was on the 25th September 1933 where the right guide bank was destroyed as a result of turbulent flow resulting from a flood event **[32]**, **[33]**. The second damaged occurred during the War of Liberation of Bangladesh in 1971, where one of the 18.3 m steel spans fell off as a result of a direct missile hit, and another one was blown off by explosives placed on the bridge span by the army as a part of war strategy **[33]**.

2.5 Railway Bridge Hazards

Railway bridges and tunnels are well-known most important railway infrastructures **[1]** and any deflections caused by subsidence on these facilities entail a reduction in the safety and comfort of this transportation means **[34]** and **[35]**. Railways are exposed to water-related hazards since they cross natural water-flow paths **[36]**. And according to **[37]**, between 1989 and 2000, 16 and 33% of most bridge damages were caused respectively caused by scouring and floods. Again, between the years 1960 and 1990, 60% out of 1,000 failed bridges observed in the United State, are associated with scouring **[38]**. However, the bridge failure causes are not limited to scouring and it includes deficiencies in structural and design, effects of corrosion, mistakes during construction and supervision, overloading, lack of maintenance and inspection **[18]**. These factors are classified into natural factors and human factors **[17]**.

Water has the ability to innumerable problems in civil works which can lead to the decommissioning of railway assets **[25]** and these water-related hazards can be classified into fluvial flooding, coastal flooding, groundwater flooding, and pluvial flooding when rivers flow over their banks when normally drylands are flooded by seawater, when the groundwater table level rises above the natural terrain, and when rainfall generates floods on hill slopes outside the river network respectively **[20]**. According to **[39]** floods are not only the most frequently occurring but also the costliest natural hazard throughout the world, affecting both lives and properties annually **[40]**. Generally, rivers are good transport corridors for both importation and exportation of cities' products, while the economic zone along a river is usually connected with global supply chains by a hub **[41]**. However, the railway network is liable to natural hazards and particularly to intense pluvial runoff **[20]**.

2.6 Common Causes and Mechanisms of Bridge Failures

Railway bridges as an element of rail infrastructure are heavily influenced by threats which are classified according to several factors such as those in/outside the system and those dependent and independent on human activities **[3]**. Bridge collapses usually are associated with huge economic and life losses [**[30]**; **[42]**; **[43]**]. The causes are classified into natural and human or manmade causes [**[17]**; **[30]**]. Figure 4.0 is a flow chart showing the classifications identified by **[17]**. While Table 2.1 shows the categorizations by **[30]** and **[44]** respectively.

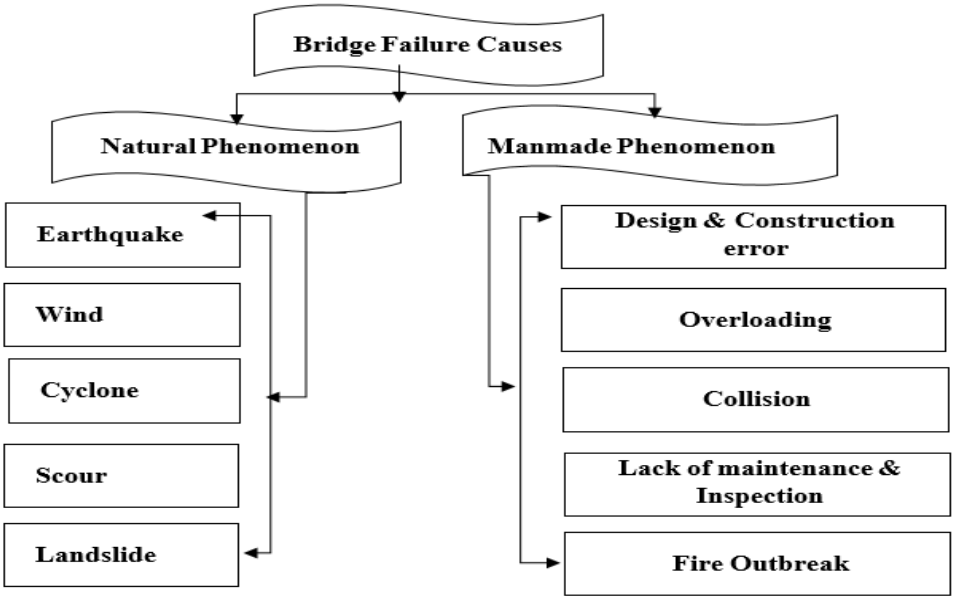

Figure 2.4: Classes of Bridge Failure Common Causes

Table 2.0.1: Most common causes for the collapse of different types of bridges [29]

Type of bridge	Most vulnerable causes
Beam bridge	Flood, scour, earthquake, collision, overloading
Masonry arch bridge	Flood, scour, overloading, earthquake
Steel arch bridge	Overloading, wind
Steel truss bridge	Overloading, fatigue
Flexible long-span bridge	Wind

2.7 Definition of Scouring

Scour is defined as erosion, excavation, and carrying away from the bed and banks along the streams and around the piers and abutments of bridges under the influence of flowing water. However, scour rates are materials-dependent. For instance, under the same condition of flowing water, loose granular soils are rapidly eroded while cohesive or cemented soils are more scour-resistant **[27]**.

2.7.1 Components of Total Scouring

There are primarily three components of total scouring, however, there are other scour types that are occurrences are situation-based as well as lateral migration of the stream that must be assessed whenever the evaluation of total scour at bridge abutments and piers are necessary.

- Long-term degradation of the river bed
- Contraction scour at the bridge
- Local scour at the piers and abutments

Local scour can be defined as the removal of materials from around piers, abutments, and embankments caused by an accelerating flow resulting from vortices induced by obstructions to the flow **[27]**. Since abutments and piers are the integral parts of bridge-like structures that often obstruct the natural flowing river resulting in scouring around them, therefore, one of the major causes of the bridge collapse is the excessive local scouring around these components during floods. Thus, is very necessary to estimate the maximum scour depth precisely around these parts taking into accounts the safety and economic considerations. **[45]**

2.7.2 Scour at Open-Bottom Culverts

Open-bottom culverts are otherwise referred to as slab culverts. This is a type of culvert without a bottom slab. It is usually constructed over a running natural water channel. Most often it is constructed for high-speed vehicles because of the absence of sharp edges as in rectangular or box culverts. In this culvert type, scour is greatest at the upstream corners of the culvert entrance and this combined the contraction and local scour effects. However, if dual slab culverts are used (i.e placed side-by-side), then the center foundation acts as a pier and must be designed to be stable for the total depth without a countermeasure **[27]**.

2.8 Review of Literatures on Bridge Failure due to Scour

Heavy precipitation is a cause of flooding which may induce phenomena such as scour, erosion, hydraulic jump, debris impact on bridge foundation [**[30]**; **[46]**; **[47]**. Bridge scour is a major among the reasons to cause bridge failure and possible serious disaster **[18]** which simply means the excavation and removal of bridge component materials such as beds and banks of rivers as a result of the erosive action of flowing water **[48]**. The bridge piers are typically among the most vulnerable structural members subjected to scour due to debris flows **[9]**. While **[37]** scoured bridge may seriously weaken the stability of piers and even the superstructure which may lead to a reduction in the load-carrying capacity of piles. Thus, the three distinct processes in which bridge scour occurs are long-term bed degradation (which occurs naturally in rivers); contraction scour (caused as a result of flow contraction at the bridge opening), and local scour at a bridge pier or abutment **[49]**.

After studying the bridge piers exposure to debris flow impact by proposing a reliability-based approach based on a nonlinear structural analysis to determine the physical vulnerability curves, incorporating relevant aleatory and epistemic uncertainties in both hazard and structure with the inclusion of a fully probabilistic framework, **[9]** assessed both the high- and low-viscosity debris flows as representative of two classes of debris flow for their different load patterns. A quantitative displacement-based damage index is defined considering the possible failure modes of the pier column which will not only address the geographical restrictions of conventional empirical debris flow vulnerability models but also provides a general approach for quantitative risk assessment in

hazard-prone areas, thereby forming a basis for subsequent engineering design or risk zoning. However, Dikanski and Hagen-Zanker **[12]** stressed that some parameters such as floodplain width and the width of abutments were found to be both subjects to high uncertainty and also very influential for the estimation of scour risk, leading to a reduction in the confidence in scouring risk assessments.

Again, after a series of experimental investigations by **[8]** on the scouring process around side-by-side bridge piers under both open flow and ice-covered flow conditions using three non-uniform natural sediments and four pairs of side-by-side bridge piers, the mechanism of incipient motion of the sediments under ice-covered conditions was found to includes the boundary shear Reynolds number, critical dimensionless shear stress, particle densimetric Froude number, grain size and roughness of ice cover, the results show their variations with shear stress. Results of this study present valuable outcomes to identify the feature of sediment motion near the scour hole under ice-covered flow conditions **[8]**. While in a similar context, **[12]** pointed out that the nature of scouring implies that a potential increase in the frequency and severity of extreme weather events will increase scour risk. In line with this, out of over 500 bridge failures categorized by **[15]** as well as **[50]** between 1989 and 2000 in the United State, bridge scour is found to be one of the major reasons.

In a study by Dikanski and Hagen-Zanker **[12]** on the climate change effects uncertainty on the bridge scour analysis as compared with other uncertainties inputs to the scour model using a sample of data on railway bridges in the UK, the results show that there are some parameters which are subject to both high uncertainties and are very influential for the scour risk estimation as compared to the ability to foresee climate change and this has led to a reduction in the scour risk assessments, however, this is in contrasts with the existing assumption that bridge elements dimensions are not associated with uncertainty. Further results indicate that data quality control, the study of model sensitivity, and assessment of other data uncertainties together with climate change uncertainty in different infrastructures globally will not only help in understanding the scale of the challenge but also to establish a coordinated system approach to the adaptation of climate change **[12]** because, during the many exploitation years, many external influences and degradation processes attack the bridge components **[22]**. Again, **[51]** stressed that flood hazard assessments are affected by several sources of uncertainties which have significant consequences on the simulation's accuracy.

2.9 Hydrological Models

This is a mathematical representation of hydrologic cycle components that simplifies real-world systems such as surface water, soil water, wetland, and groundwater, assisting in the understanding, predicting, and management of water resources in terms of flow and quality **[52]**. And the GIS

development has not only encouraged but also improved the expanded use of watershed models globally in terms of modeling process accuracy of watershed characteristics in a more practical approach. According to Cunderlik (2003) **[53]**, there are three main categorizations for the hydrologic models viz-a-viz: Lumped models, semi-distributed models, and distributed models.

2.10 Precipitation (Rainfall)

The rainfall time series dataset is an essential component of the hydrological cycle, and the accuracy of global rainfall coverage is a major necessity for improving short term, medium, and long term weather monitoring and forecasts **[54]**. Rainfall hourly data or even at smaller temporal scales have wide field applications in urban hydrology, infrastructure design including hydraulic analysis, and risk assessment of the existing structures **[55]**.

Also, the understanding of precipitation in terms of its Spatio-temporal pattern is vital for many scientific and operational applications such as hydro-climatic modeling and the forecasting of floods **[56]**. With the advent of some satellite-based rainfall products, most of the time they serve as an alternative source of data in areas where the conventional ground-based observed rainfall data are not readily available or where the availability is very inadequate **[57]**

Chapter 3: MATERIALS AND METHODS

3.1 Description of the study area

3.1.1 Study Area Location

Sebeta – Djibouti Railway line is the only railway line connecting the two counties' cities (Ethiopia and Djibouti). It covers about 30 percent of cultivated land as well as the population of Ethiopia while about 70 percent population of Djibouti **[6]**. The line has a total length of 752.7 km with double-track for the first 115km from Addis Ababa to Adama, and a single track for the remaining 600km to Djibouti with 21 stations, 61 bridges, 37 frame bridges, and 453 cross culverts along the route **[7]**. Figure 3.1 shows a map showing Addis Ababa – Djibouti Rail Line. However, this study only considers Sebeta – Adama Section which is shown in Figure 3.2.

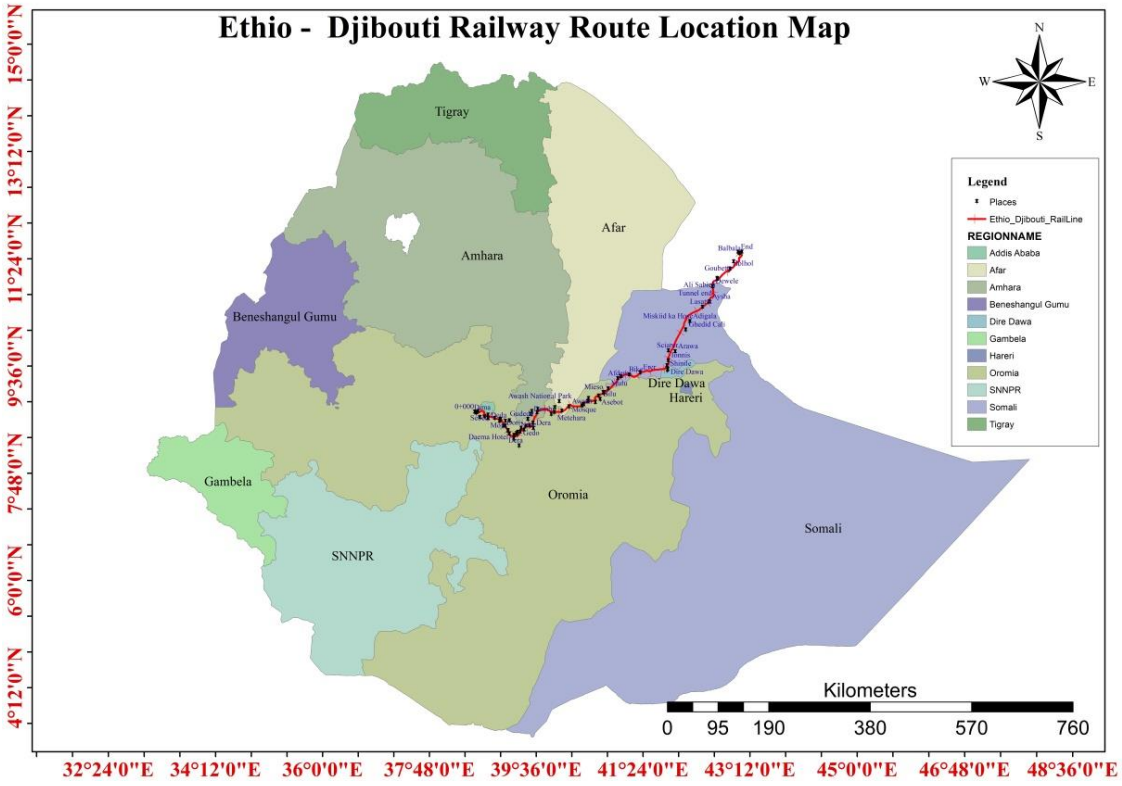

Figure 3.1: Case Study Area Map (Addis Ababa – Djibouti Railway Line)

3.1.2 Route and Alignment Location

The Sebeta – Adama Section of Ethio – Djibouti Railway line is about 115 km in length and has about 203 drainage structures in total with 168 slab culverts, 23 frame bridges, and 12 simple supported T-Beam bridges. The slab culverts range from 1.5m to 6.0m top width. This section of the Ethio-Djibouti Railway line is as shown in Figure 3.2.

However, owing to the limitations such as the DEM resolution, chosen Number of cells to define streams, and the selected number of Area Sqkm to define stream, only forty-seven drainage structures in total were able to capture after the catchment and stream network delineations. These structures also comprise 30 slab culverts, 10 simple supported T-Beam, and 7 frame bridges. Figure 3.2 and Table 3.1 show the geographical locations and the geometrical details of these structures along the route.

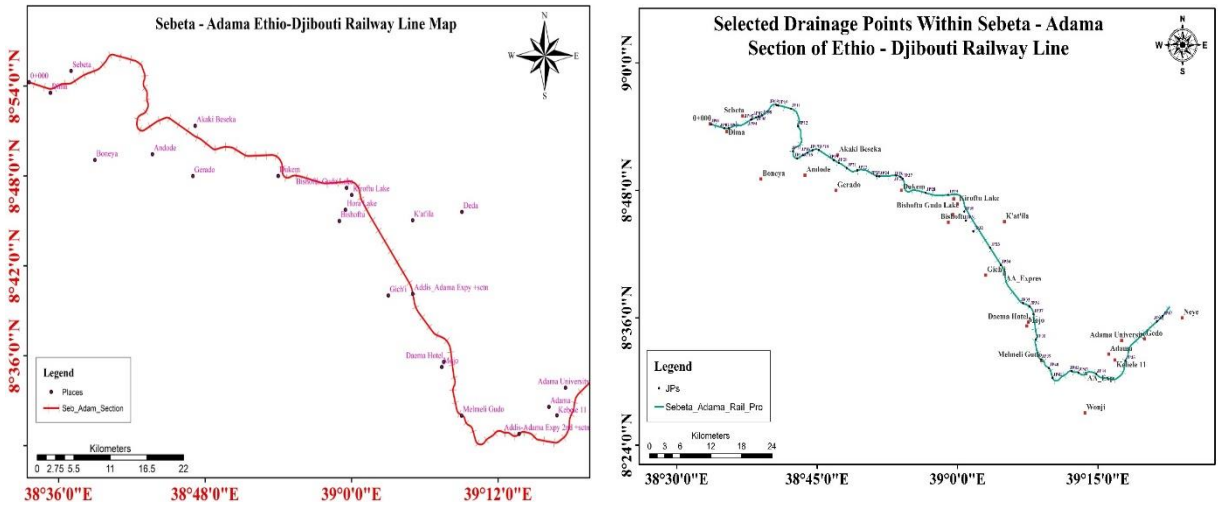

Figure 3.2: Sebeta – Adama Railway Line Section Centerline and Selected Drainage Points Map

Table 3.1: Drainage Structures' Geometrical and Geographical Details

Drainage Point	Drainage Structure	Longitude DD	Latitude DD	Location	Size
JP01	Culvert 01	38.5608	8.9038	K0+220	1-4.0m SC
JP02	Culvert 02	38.5843	8.8975	K2+650	1-6.0m SC
JP03	Culvert 03	38.5919	8.8974	K3+710	2-6.0m SC
JP04	Culvert 04	38.6318	8.9110	K9+526.07	1-5.0mSC
JP05	Culvert 05	38.6330	8.9117	K10+201.07	1-6.0M SC
JP06	Culvert 06	38.6410	8.9146	K10+761.07	1-6.0M SC
JP07	Culvert 07	38.6453	8.9159	K11+096.07	1-6.0M SC
JP08	Culvert 08	38.6511	8.9178	K11+496.07	1-3.0M SC
JP09	Culvert 09	38.6768	8.9344	K14+281.07	1-1.5M SC
JP10	Culvert 10	38.6800	8.9337	K14+983.07	1-3.0M SC
JP11	Frame Bridge 11	38.7031	8.9284	K17+24.07	1-14.0X3.5 FB
JP12	Culvert 12	38.7157	8.9009	K25+381.07	1-3.0M SC
JP13	Culvert 13	38.7068	8.8615	K26+491.07	1-3.0M SC
JP14	Culvert 14	38.7140	8.8504	K28+756.07	1-4.0M SC

JP15	Culvert 15	38.7244	8.8553	K29+942.07	1-6.0M SC
JP16	Culvert 16	38.7319	8.8595	K30+340.07	1-6.0M SC
JP17	Culvert 17	38.7412	8.8632	K30+846.07	2-6.0M SC
JP18	Culvert 18	38.7524	8.8636	K32+797.07	1-6.0M SC
JP19	frame bridge 19	38.7797	8.8478	K39+094.27	1-8.0X6.0 FB
JP20	Culvert 20	38.7885	8.8433	K39+769.27	1-1.5M SC
JP21	Culvert 21	38.8025	8.8354	K41+280.87	1-10.0M SC
JP22	Culvert 22	38.8214	8.8315	K44+0691.1	1-1.5M SC
JP23	Culvert 23	38.8559	8.8228	K47+147.7	1-3.0M SC
JP24	Culvert 24	38.8606	8.8224	K47+174.1	1-6.0m SC
JP25	Frame bridge 25	38.8902	8.8236	K50+104.1	2(1-12.0X4.5)M FB
JP26	Frame bridge 26	38.8981	8.8216	K50+659.1	2(1-12.0X4.5)M FB
JP27	Culvert 27	38.9020	8.8184	K51+674.1	1-5.0M SC
JP28	Frame bridge 28	38.9432	8.7964	K56+907.7	1-12.0X6.5M FB
JP29	Culvert 29	38.9834	8.7932	K61+400.59	2-6.0M SC
JP30	Frame bridge 30	39.0121	8.7670	K66+492.604	2(10.0X5.6)M FB
JP31	Culvert 31	39.0147	8.7529	K67+630.604	1-3.0M SC
JP32	Culvert 32	39.0281	8.7359	K70+652.66	2-6.0m SC
JP33	Culvert 33	39.0580	8.7100	K66+911.66	1-5.0M (Low) SC
JP34	Frame bridge 34	39.0772	8.6833	K91+308.46	2(1-12.0X5.5)m FB
JP35	Mojo-Adama No.1 Bridge	39.1165	8.6231	K93+941.10	2(8X32)m SSTB(No.1 DLMB)
JP36	Mojo-Adama No.2 Bridge	39.1280	8.6182	K95+962.64	2(1X32)m SSTB(No.2 DLMdB)
JP37	Mojo-Adama No.3 Bridge	39.1353	8.6057	K97+817.22	2(1X32 + 1X24 + 1X32)m SSTB(No.3 DLMdB)
JP38	Mojo-Adama No.4 Bridge	39.1398	8.5663	K100+047.26	2(1X24 + 5X32)m SSTB(No.4 DLMB)
JP39	Mojo-Adama No.5 Bridge	39.1490	8.5348	K102+007.5	2(18X32)m SSTB(No.5 DLSuperB)
JP40	Mojo-Adama No.6 Bridge	39.1629	8.5213	K105+735.11	2(1X32)m SSTB(No.6 DLMdB)
JP41	Mojo_Adama No.7 Bridge	39.1692	8.5060	K106+271.11	2(1X32)m SSTB(No.7 DLMdB)
JP42	Mojo-Adama N0.8 Bridge	39.2037	8.5163	K106+569.11	2(5X32)m SSTB(No.8 DLMB)
JP43	Mojo-Adama No.10 Bridge	39.2151	8.5140	K107+804.11	2(2X32)m SSTB(No.10 DLMdB)
JP44	Mojo-Adama No.12 Bridge	39.2472	8.5116	K111+709.21	2(27X32)m SSTB(No.12 DLMB)
JP45	Culvert 45	39.2990	8.5326	K111+097.23	1-6.0M SC
JP46	Culvert 46	39.3554	8.5944	K113+879.07	2-6.0M SC
JP47	Culvert 47	39.3651	8.6026	K115+709.21	1-3.0M SC

3.1.3 Topographic Description of the Study Area

The case study section of Ethio – Djibouti starts from $38^{0}24^{1}0^{11}$E and $9^{0}0^{1}0^{11}$N (West Shewa) and $39^{0}36^{1}0^{11}$E and $8^{0}42^{1}0^{11}$N (East Shewa) all within the Oromia region with about 115 km. It has elevation ranges between 915 – 3550 ma. s.l (West Shewa being at a higher elevation relative to

East Shewa). Again, the predominant geological features are Nc, Nn, Q, NQtb, Qb, and Qd; where the soil type is majorly Calcic aerosols, Chromic luvisols, Haptic phaeozems, and Orthic solonchaks. Also, the LULC of the area is majorly built-up areas at Sebeta and Adama while it is mostly Croplands between Bishoftu and Modjo. These are shown in Figures 3.3 – 3.6 (data source: **[58]**).

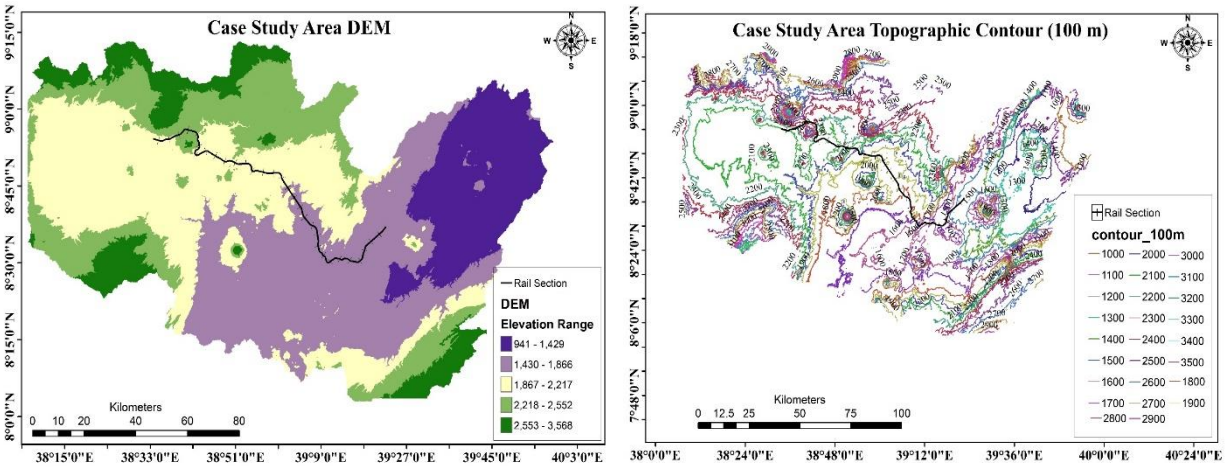

Figure 3.3: Case Study Area Digital Elevation Model [DEM] and Topographic Contour (100m) Map

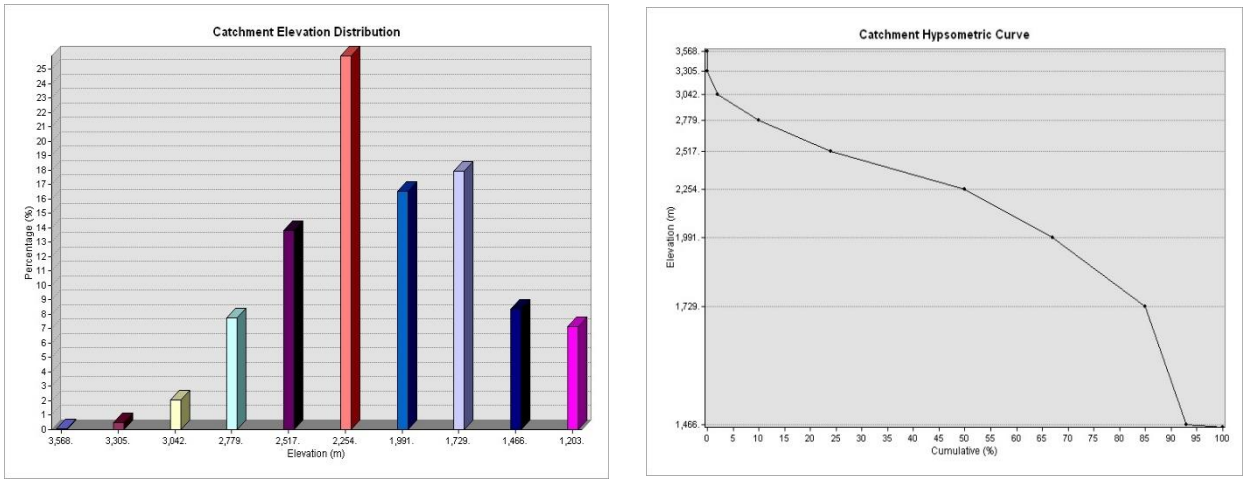

Figure 3.4: Case Study Area Elevation Distributions in Percentage (%) Shows the land area proportions that exist at the various elevations within the catchment

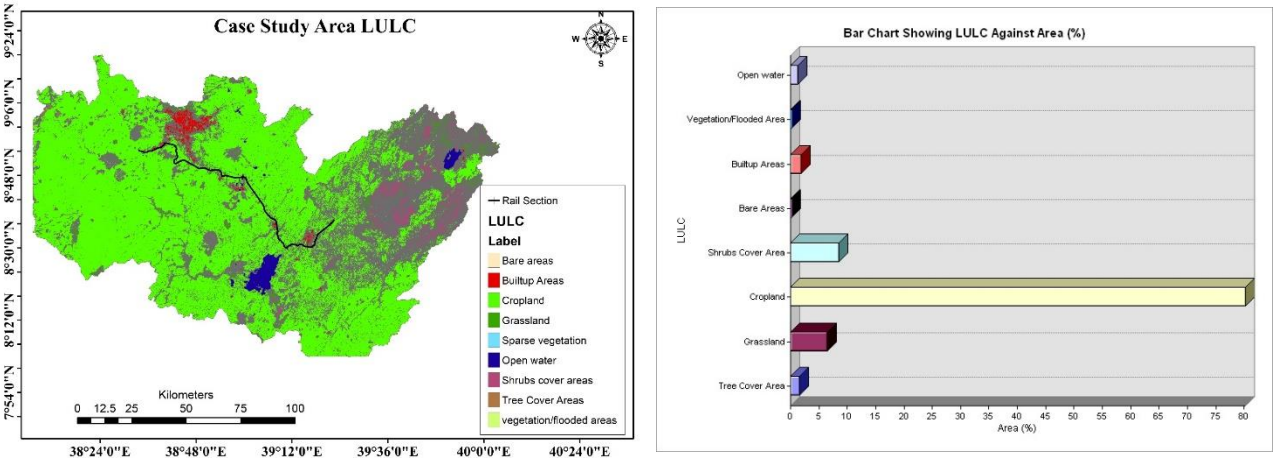

Figure 3.5: Case Study Area LULC 2020 and Graphical representation of the LC Classes Maps

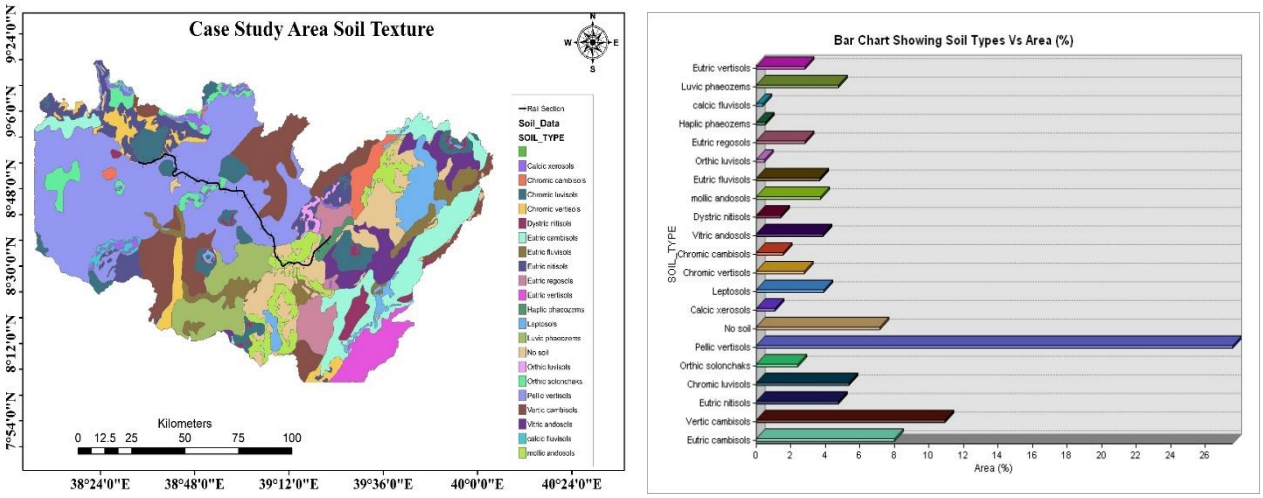

Figure 3.6: Case Study Area Soil Data Graphical Representation of Soil Data Maps

3.1.4 Climatic Description of the Study Area

Ethiopia is located in Eastern Africa with its most portion as highland and plateaus. In Ethiopia, temperatures are varied from place to place as a result of huge differences in altitudes. Generally, the country has a moderate climate. However, the rainy season is from June to September while the dry season starts from May to October every year. Again, the hottest months are March, April, and May with approximately 37^{o}C while the coolest months are usually from November to January with approximately 0^{o}C in highland areas. Also, the heaviest rainfall usually occurs in July and August. These are shown graphically in the forms of maps and bar charts as in Figures 3.7 – 3.10 which were created from the data sourced from both MoWIE and NMAoE.

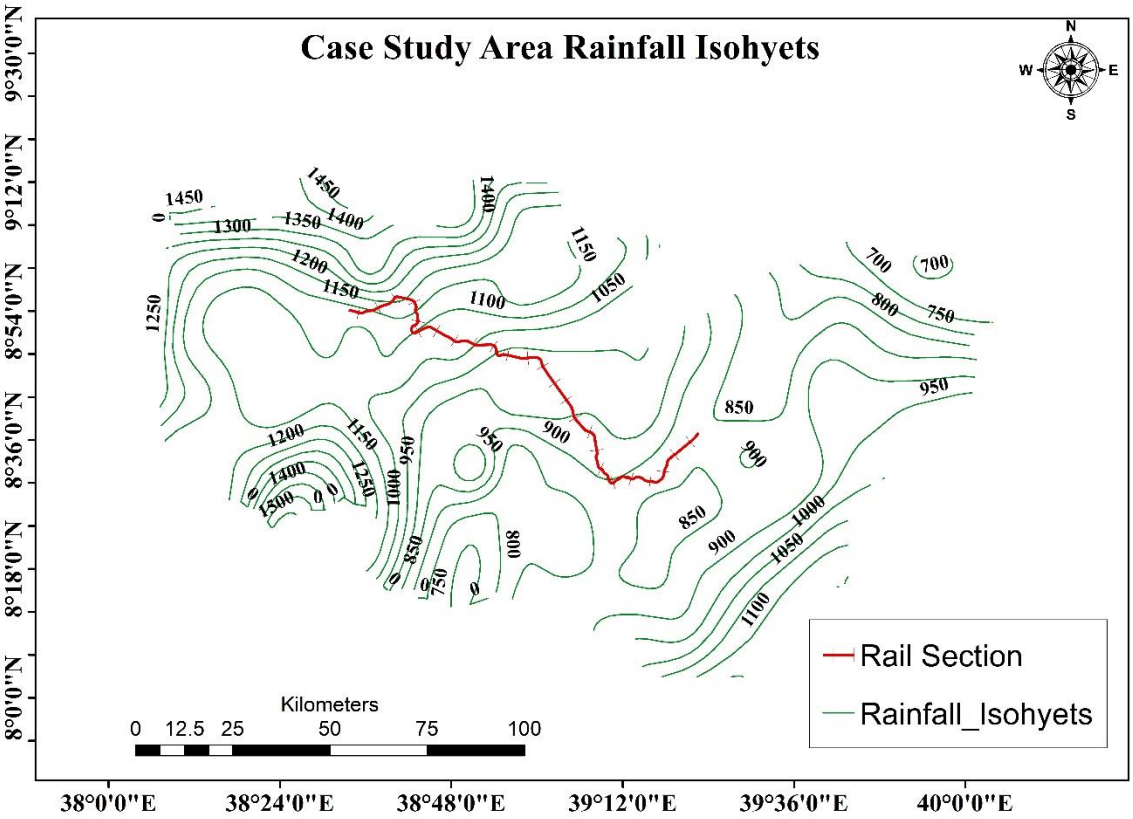

Figure 3.7: Case Study Area Rainfall Isohyets Map

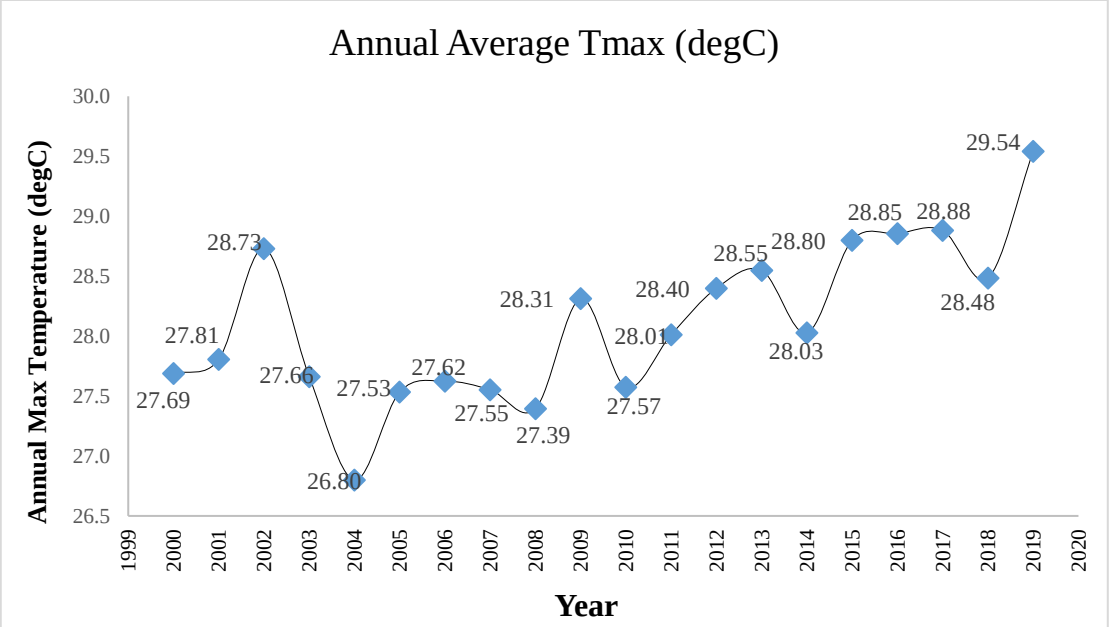

Figure 3.8: Graphical Representation of Annual Average Maximum Temperature of the Study Area

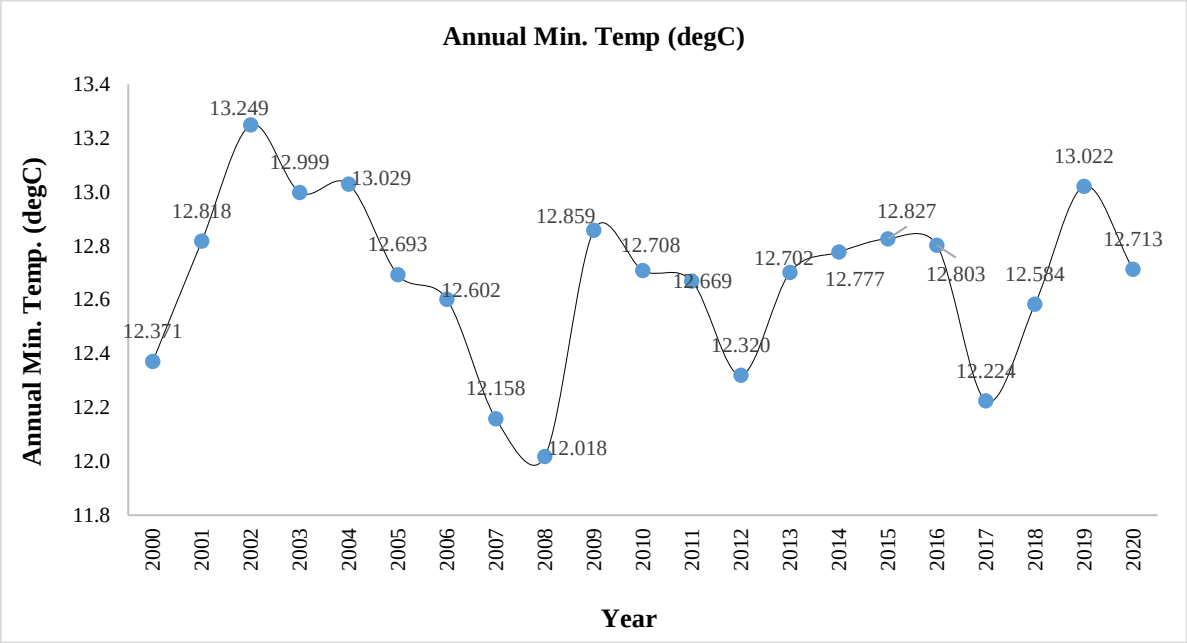

Figure 3.9: Graphical Representation of Annual Average Minimum Temperature of the Study Area

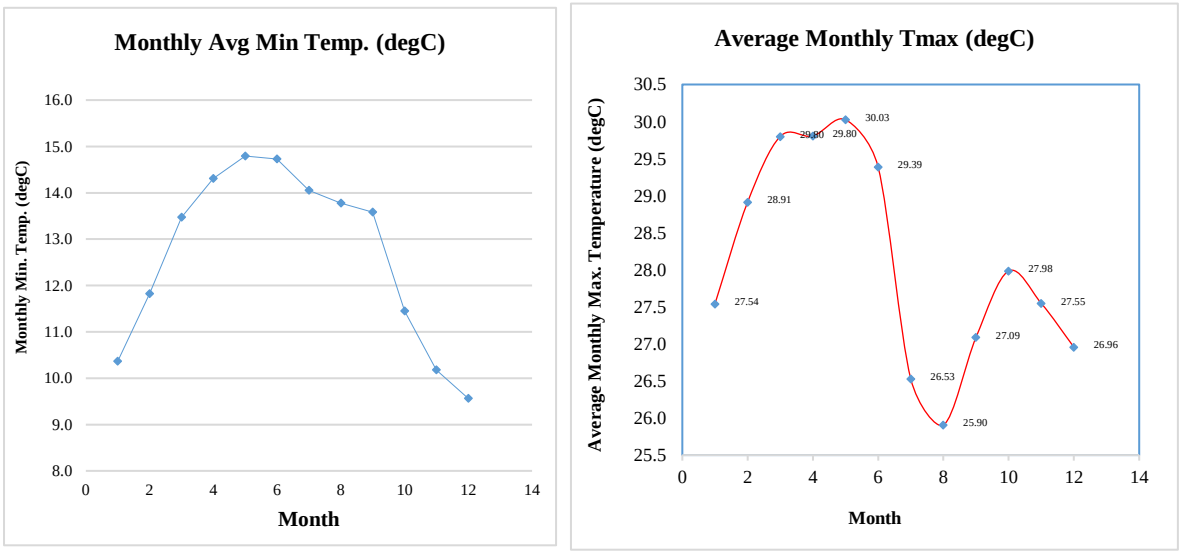

Figure 3.10: Graphical Representation of Average Monthly Min. & Max. Temperature of the Study Area

3.1.5 Geological Features Description of the Study Area

The study area is characterized by the geological features shown in Figure 3.11 which were developed from the GIS files sourced from the MoWIE. The predominant geological feature being Nn while the least is Ncb. Table 3.2 shows the description of the geological feature codes.

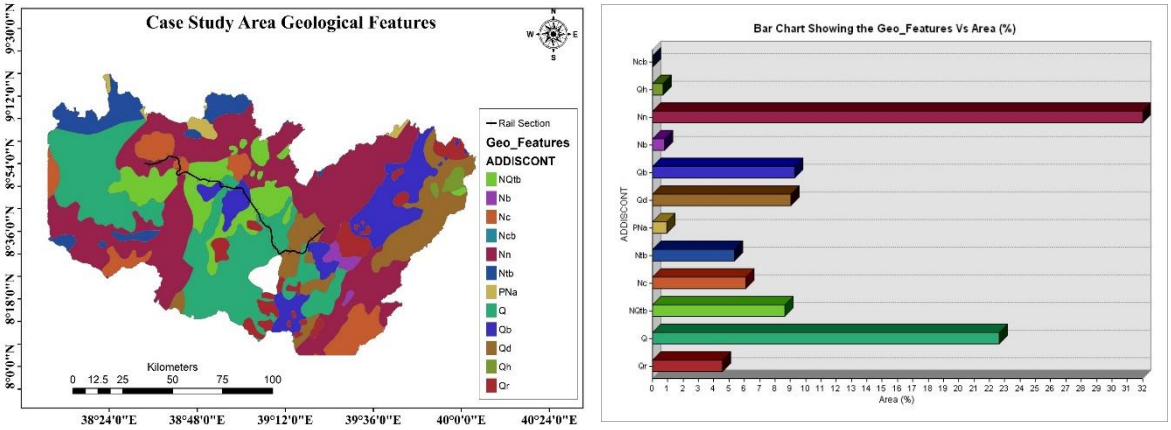

Figure 3.11: Case Study Area Geological Features Map

Table 3.2: Description of Elements in the Case Study Area Geological Features

Labels	Descriptions
NQtb	Alkaline basalt and trachyte
Nb	Mursal and Bofa basalts: Alkaline basalt
Nc	Alkaline basalt in the upper part and trachyte and trachybasalt, peralkaline rhyolites, and alkaline basalt in the lower part.
Ncb	Alkaline basalt in the upper part and trachyte and trachybasalt, peralkaline rhyolites, and alkaline basalt in the lower part
Nn	n/a
Ntb	Transitional and alkaline basalts
PNa	n/a
Q	Sand, silt, clay, diatomite, and beach sand
Qb	Plateau basalt, alkaline basalt, and trachyte
Qd	n/a
Qh	Sand, silt, clay, diatomite, and beach sand
Qr	n/a

3.1.6 Study Area Subbasins and Major River Networks

The study area is divided into two major subbasins; the uplands and upper valley subbasins. Also, there are two lakes within the selected study area; lakes Aba Samuel towards the north-western part and Koka towards the southern part of the study area as shown in Figure 3.12. Other artificial lakes which are not captured in the available data include Legedadi, Gefersa, and Dire lakes.

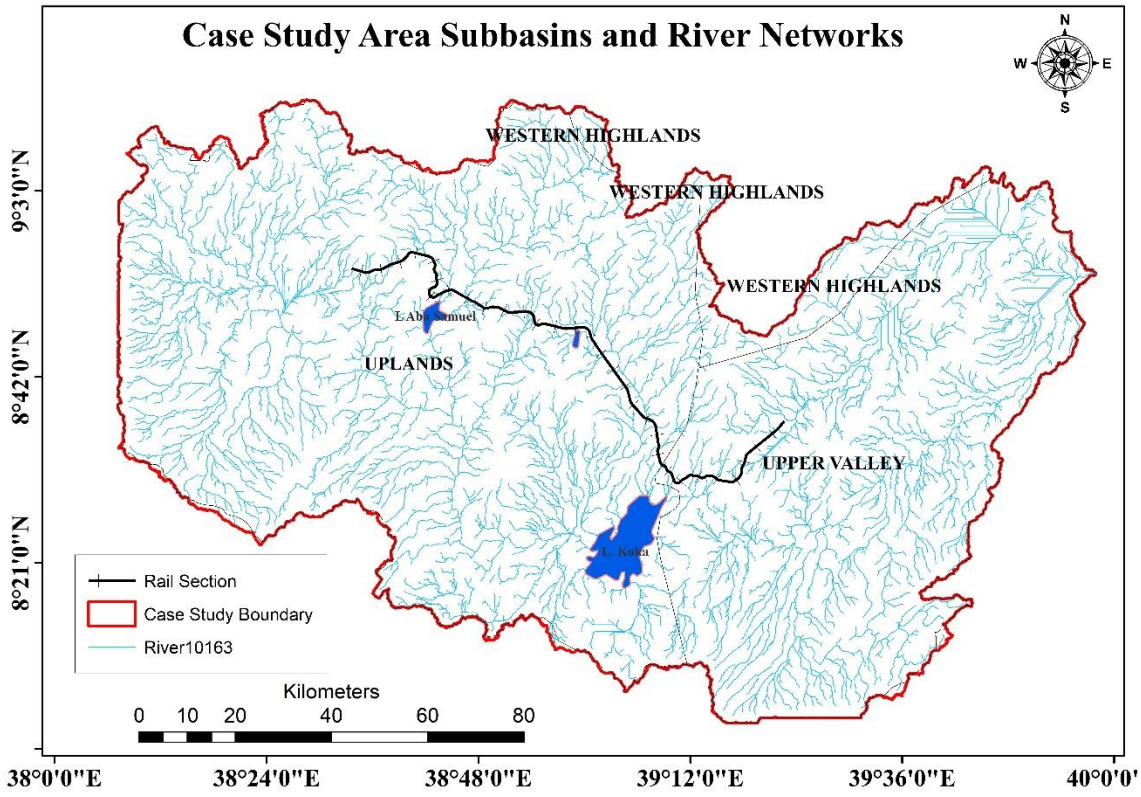

Figure 3.12: Case Study Area Subbasins and Stream Network Map

3.2 RESEARCH DESIGN

To achieve the objectives of the study, the following interrelated activities will be conducted. The detailed processes and how the data required for specific steps will be acquired are explained in the subsequent sections. As presented in Figure 3.13, the proposed methodological flow chart showing summarized processes that will be undertaken to achieve the research goal.

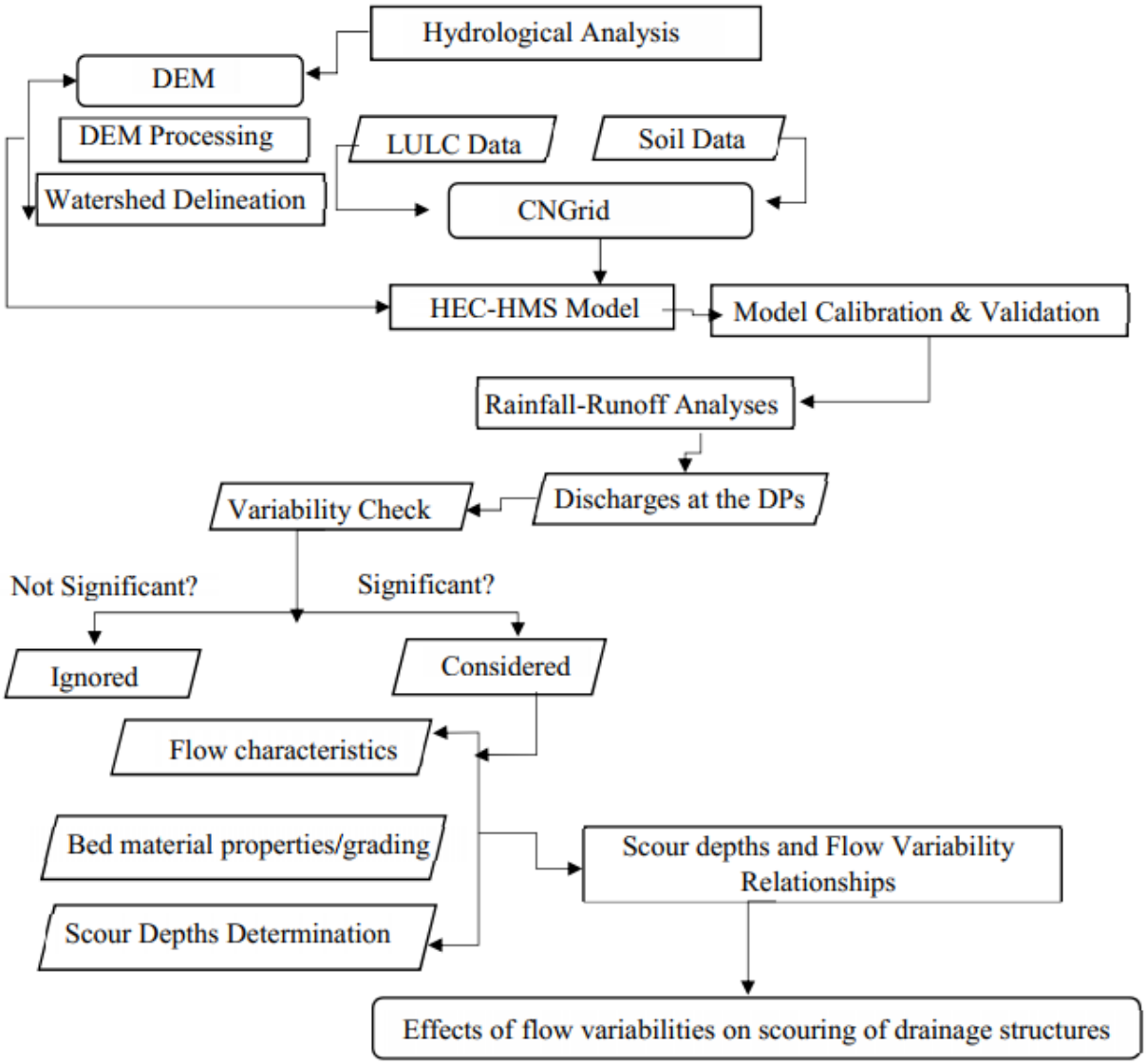

Figure 3.13: Proposed Methodological Flow Chart of the Research

3.3 Data Collection

Secondary dataset and field observations were used for this study and are classified into three major classes: spatial data and meteorological data. Spatial data (GIS shapefiles), Railroad alignments and standards (from Ethiopian Railway Corporation), Meteorological and flow datasets were collected from the relevant agencies in Ethiopia. In addition, some field measurements, inspections, and observations are to be carried out to supplement the acquired secondary dataset.

3.3.1 Spatial Data

Spatial data (GIS shapefiles) will comprise of the Digital Elevation Model (DEM) of high resolution (target is 12.5m), Rivers and lakes, LandUse data, and Soil Type data, Geographical features, Rainfall-Isohyets, Subbasins, will be sourced from the Geographical Information System Department, a unit under the Ministry of Water, Irrigation and Energy of Ethiopia, Addis Ababa.

3.3.2 Railroad Alignments and Standards

Railroad alignments and standards for the drainage structures (culverts and bridges) within the study area shall be sourced from the Ethiopian Railway Corporation, Addis Ababa, Ethiopia.

3.3.3 Hydrological and Meteorological Data

In addition to the spatial data, meteorological data for the periods of 20 years (2000 – 2019) for all the possible/available ground-based meteorological gauge stations with full data for the stated period within the uplands and the upper valley of Awash River Subbasins; sourced from the National Meteorology Agency of Ethiopia (NMAoE) for the simulation of discharge within the catchment. Also, some hydro-gauge stations within the Awash River Subbasins with full data which was sourced from the Ministry of Water, Irrigation, and Energy (MoWIE). These time-series datasets were divided into two parts, one part for the calibration and the second part for the validation of the hydrological model.

3.3.4 Ground-Based Meteorology Gauge Stations within the Catchment

There are more than fifteen (15) ground-based meteorology gauge stations within uplands and upper valley of Awash River Subbasins but the relevant to the study were selected. Therefore, Table 3.3 shows the information about their geographical locations, and catchment area, weighted areas, and the types of observed data requested from the NMAoE.

Table 3.3: The Selected Ground-Based Meteorology Gauge Stations within the Catchment with their respective geographical locations, classes, and the observed datasets

FID	Name	GH_ID	Lat	Long	Elevation	Area_Sqkm	Weight
1	Hombole	SHHOMB14	8.36817	38.77483	1743	1669.105	0.098
2	Bofa	ARBOFA44	8.47080	39.45330	1427	1625.249	0.095
3	Metehara (NMSA)$^{+}$	SHMETE12	8.85867	39.91900	944	757.399	0.044

4	Melka Jilo[+]	SHMELK33	8.89000	39.62000	1135	1492.192	0.088
5	Ayertena[+]	SHAYER23	8.98306	38.69639	2325	423.870	0.025
6	Bantuliben	SHBANT14	8.61850	38.35700	2167	1545.470	0.091
7	Debre Zeit(AF)[+]	SHDEBR42	8.73333	38.95000	1900	1602.374	0.094
8	Nazeret[+]	SHNAZE11	8.55000	39.28333	1622	782.547	0.046
9	Mojo[+]	SHMOJO13	8.60533	39.10817	1763	1099.393	0.065
10	Melkasa (IAR)[+]	SHMELK21	8.40000	39.31667	1540	817.370	0.048
11	Huruta[+]	ARHURU13	8.14200	39.34220	2044	1219.917	0.072
12	Teji	SHTEJI14	8.83330	38.36667	2091	1035.888	0.061
13	Sebeta[+]	SHSEBE23	8.92000	38.63000	2220	771.786	0.045
14	Kality[+]	SHKALI13	8.93333	38.76683	2186	1134.563	0.067
15	Addis Alem[+]	SHADDI33	9.04200	38.38333	2372	1053.381	0.062

[+] Indicated the stations that recorded both rainfall and temperature data

Again, Figure 3.14 is a Thiessen Polygon Map developed from Table 3.3 in ArcGIS 10.4 which was used to estimate the catchment rainfall using the observed data from the surrounding gauge stations.

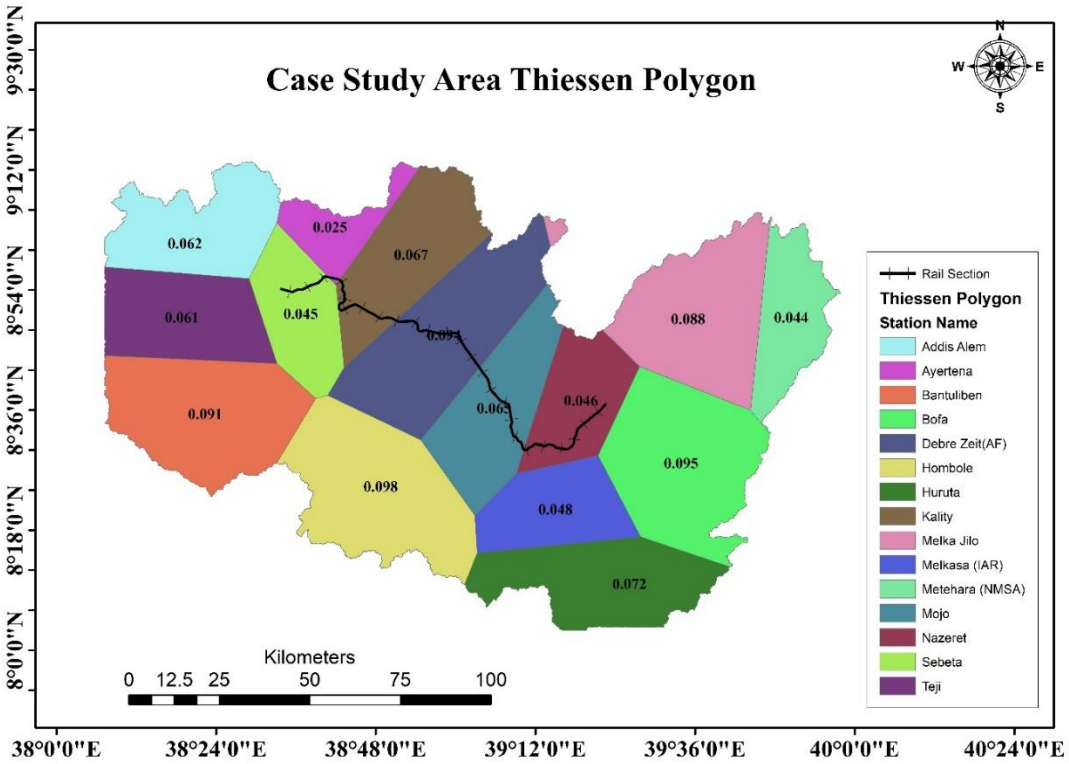

Figure 3.14: Rainfall Thiessen Polygon Map of the Catchment Ground-Based Met Stations

3.4 Data Processing and Analysis

Data processing and analyses shall be divided into three major steps:

i. Hydrological Analysis
ii. Statistical Analyses of Discharges
iii. Establishing the Relationships between the flow variabilities and Scouring

3.4.1 Hydrological Analysis

The software used for processing the spatial data is ESRI ArcGIS 10.4, alongside the Arc Hydro Tool and HEC-GeoHMS extensions for terrain and catchment processing, and delineation. While an HEC-HMS model was developed for simulating the hydrological processes within this catchment using the rainfall datasets for the meteorological gauge stations within and surrounding the catchment. The results of these processes give the estimated discharges (m^3/s) at the selected drainage points.

3.4.2 Data Preparation

Rainfall is an important part of the hydrological cycle and is one of the first steps in any hydrological and meteorological study for accessing the reliability of the data. However, as a result of any or combination of the following; damaged measuring instruments, measurement errors and geographical paucity of data (data gaps) or changes to instrumentation over time, a change in the measurement site, a change in data collectors, the measurement irregularity, or severe changes in tropical zone climate, precipitation data are frequently incomplete **[59]**.

3.4.3 Estimating the Missing Rainfall

Due to the above reasons, there are three (3) commonly used techniques for estimating the missing data:

- Linear Regression Method, (LR):

For estimation of data at a station with a similar condition, LR is the most suitable method. This is often carried out by initially calculating the correlation coefficients between the target station and each of the neighboring stations, followed by ranking. Thus, the missing data are determined by a linear regression equation with the station that has the highest correlation coefficient.

- Arithmetic Mean Method, (AM):

AM is the simplest and most widely used of estimating the missing meteorological data. However, it is only applicable if and only if the normal yearly precipitation around the gauges are less than 10% of the normal yearly precipitations at station X and the gauges are uniformly distributed. It is often estimated using the following expression in equation 3.1:

$$\mathbf{Px} = \frac{\mathbf{1}}{\mathbf{m}}(\mathbf{P1} + \mathbf{P2} + \mathbf{P3} + \cdots + \mathbf{Pm}) \qquad \textbf{Eq. (3.1)}$$

Where

P_x is the estimated magnitude of the missing data

$P_{1\text{-}m}$ is the values of the neighboring gauge stations' precipitation values

- Normal ratio method

This is method is most suitable for estimating the missing precipitation of gauge under consideration provided that the surrounding gauging stations have the normal annual precipitations greater than 10% of the gauge under consideration. This is estimated using the expression in equation 3.2.

$$\mathbf{Px} = \frac{\mathbf{Nx}}{\mathbf{m}}\left(\frac{\mathbf{P1}}{\mathbf{N1}} + \frac{\mathbf{P2}}{\mathbf{N2}} + \frac{\mathbf{P3}}{\mathbf{N3}} + \cdots + \frac{\mathbf{Pm}}{\mathbf{Nm}}\right) \qquad \textbf{Eq. (3.2)}$$

Where

P_i is the rainfall values at the surrounding rain gauges

N_x is the Normal annual precipitation of missing data station

N_i Normal annual precipitation of the surrounding stations

M is the number of surrounding stations excluding the station under consideration

Therefore, the choice of any of these methods depends on the nature of the precipitation dataset to be sourced from NMAoE.

3.4.4 Data Consistency Check

Data consistency is one of the basic analyses needed to be carried out on rainfall data recorded in any meteorological gauge stations before it could be used as an input for simulating the hydrological process in a model. The consistencies of the rainfall dataset in all the meteorological gauge stations were checked using the double mass curve method; some stations were consistent while others with inconsistencies were corrected before further process. Figure 3.15 shows the original and adjusted double mass curves for Bofa meteorological gauge station. DMCs for other gauge stations are shown in Appendix A.

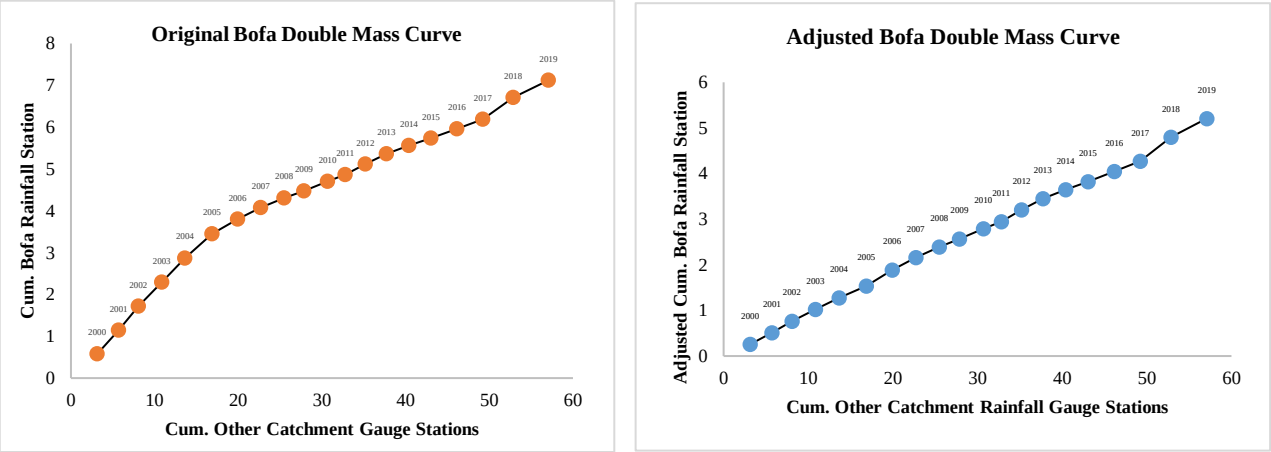

Figure 3.15: Original and the Adjusted Bofa Rainfall Dataset Double Mass Curves

3.4.5 Selected Ground-Based Hydro - Gauge Stations within the Catchment

Out of about twelve (12) Hydrometric Gauge Stations within the uplands and upper valley of Awash River Subbasins as shown in Figure 3.16, only three (3) stations were selected for model calibration and validation not only because they are connected to the area of interest but also they have full data record. These gauge stations are enclosed using square boxes as shown in Figure 3.16. Again, Figures 3.17 and 3.18 were plotted using the time-series data sourced from the MoWIE for the selected stations.

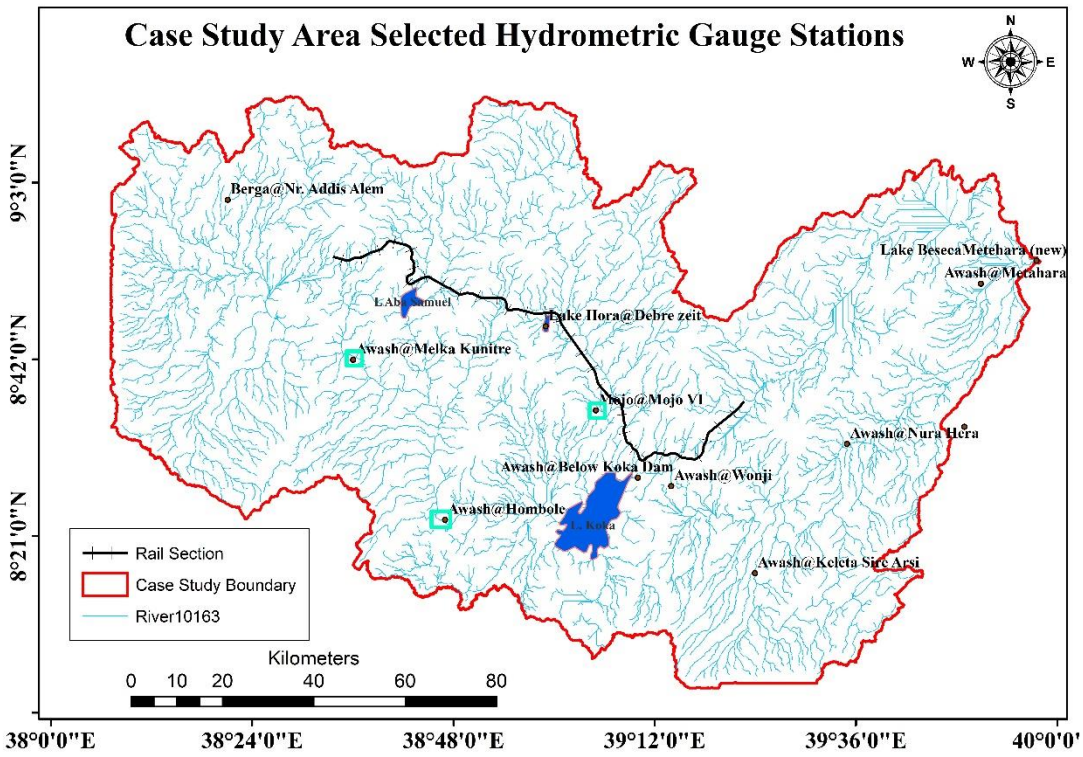

Figure 3.16: The Selected Ground-Based Hydro-Gauge Stations and their Locations within the Study Area

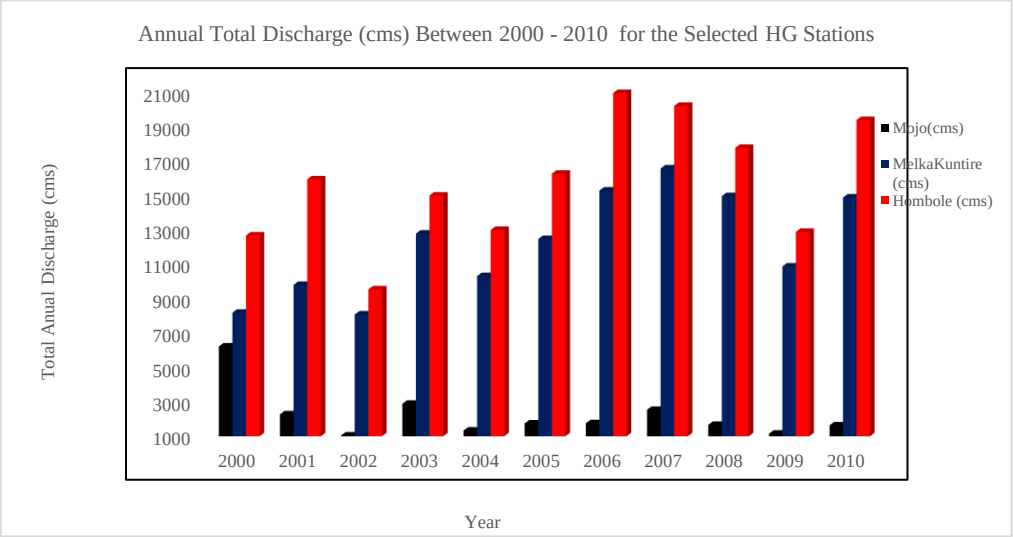

Figure 3.17: Graphical Representation of the Annual Total Discharge (cms) the Selected Ground-Based Hydro-Gauge Stations and their Locations within the Study Area

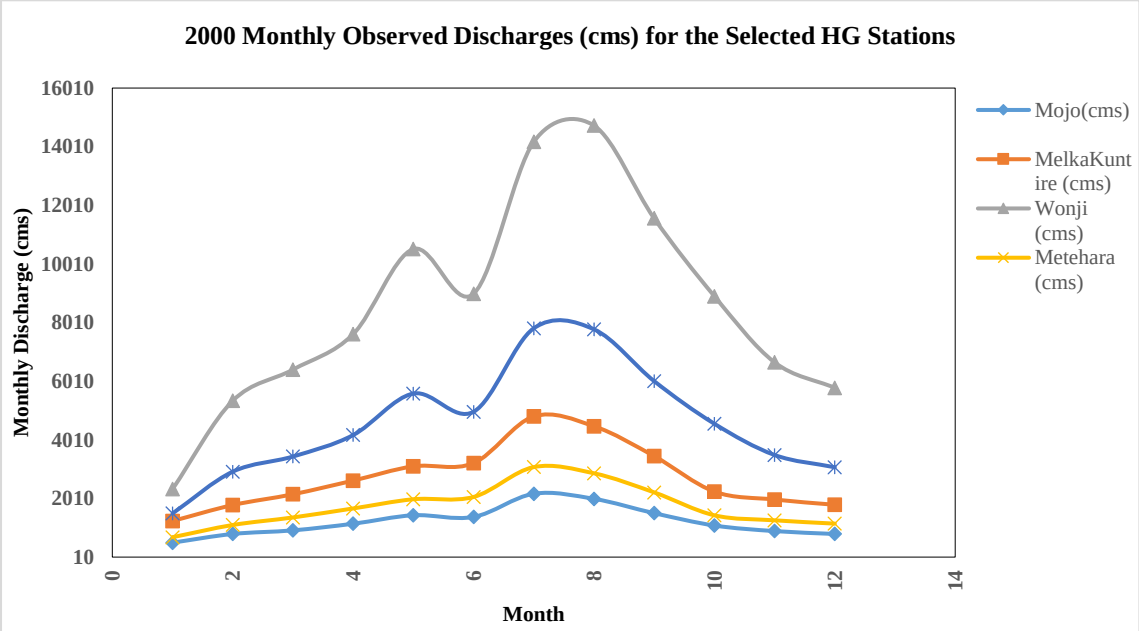

Figure 3.18: Graphical Representation of the Year 2000 Monthly Total Discharge (cms) for the Selected Ground-Based Hydro-Gauge Stations and their Locations within the Study Area

3.5 Criteria for Model Selection

The selection of the best and appropriate model is an essential part of any research work. Most often it is difficult to determine the relative pros and cons of models proposed for operational use. However, the choice of a model for a specific hydrological scenario has implications in water resources planning, development, and management. The following are the criteria commonly used by researchers/hydrologists for models selection **[60]**:

- Purpose of the model

- Availability of input data
- Prices and availability of the model
- The model structure
- The lengths of the records of the various types of data;
- The availability and size of computers for both the development and operation of the model
- The ability of the model to be updated based on current hydro-meteorological conditions

The selection of modeling software is often made on much more realistic grounds. Of the most important factors often considered in selecting the software for hydrologic modeling is the potential user's familiarity with the techniques employed by the software in addition to the techniques applied by the users' knowledge to produce more realistic results **[61]**. Therefore, the HEC-HMS model was selected based on the above criteria.

3.6 Model Calibration and Performance Check

This study divided the flow dataset sourced from the department of hydrology, Ministry of Water, Irrigation, and Electricity of Ethiopia, into two (2) sections. Section A contains time-series datasets from the years 2005 to 2010, for the hydrologic model calibration while Section B contains the datasets from the year 2011 to 2014 for the model validation. Again, this study considered only the hydro-gauge stations that are relevant to the case study area and whose full flow datasets are available.

Most of the time, the performance of a model must be evaluated on the extent of its accuracy, consistency, and adaptability **[59]**. So, this research evaluated the performance of the hydrologic model using the following efficiency measure techniques: Nash and Sutcliffe Efficiency criteria (NSE), Coefficient of Determination R^2, and Percent Bias.

- Nash-Sutcliffe Efficiency, NSE:

The Nash and Sutcliffe Efficiency (NSE) is a measure of efficiency that relates the goodness-of-fit of the model to the variance of measured data. NSE can range from -∞ to 1 and an efficiency of 1 indicates a perfect match between observed and simulated discharges. NSE values between 0.9 and 1 indicate that the model performs excellently while values between 0.6 and 0.8 indicate the model performs well **[62]**.

The NSE is defined by equation 3.3:

$$\mathbf{NSE} = \mathbf{1} - \frac{\sum_{\mathbf{i=1}}^{\mathbf{n}} (\mathbf{OBS} - \mathbf{SIM})^{\mathbf{2}}}{\sum_{\mathbf{i=1}}^{\mathbf{n}} (\mathbf{OBS} - \overline{\mathbf{OBS}})\mathbf{\hat{}2}} \qquad \textbf{Eq. (3.3)}$$

Where

OBS = Measured or Observed Flows (m^3/s)

SIM = Simulated or Modelled Flows (m^3/s)

OBS= Average of measured flows (m^3/s)

n = Number of Observations or Dataset

- Coefficient of Determination, R^2:

The coefficient of determination, R^2, can be determined as the square of the coefficient of correlation, R, as shown in equation 3.4:

$$\mathbf{r = \frac{\sum_{i=1}^{n} (OBS - \overline{OBS}) * (SIM - \overline{SIM})}{\sqrt{\sum_{i=1}^{n} (OBS - \overline{OBS})\text{^}2 * (SIM - \overline{SIM})\text{^}2}}} \qquad \textbf{Eq. (3.4)}$$

$R^2 = r^2$; R ranges from 0 to 1.0

Where;

r = Coefficient of correlation

R^2 = Coefficient of determination

OBS = Observed flows, m^3/s

SIM = Simulated flows, m^3/s

- Percent Bias, PBIAS:

The PBIAS is defined as the change in observed and computed volumes divided by the observed volume, measured in percentage (%). It is estimated as in equation 3.5:

$$\mathbf{PBIAS = \left[\frac{SIMV - OBSV}{OBSV}\right] * 100} \qquad \textbf{Eq. (3.5)}$$

SIMV = Simulated Volume (m^3)

OBSV = Observed Volume (m^3)

Thus, the statistically acceptable range of PBIAS for the surface runoff model is – or +20%.

3.7 Drainage Structures Selection Criteria

Upon estimating the daily discharges for the predetermined period (2000-2019) at each drainage structure within the selected railway line section, this study uses the following criteria to select the structures for further considerations:

i. Group the drainage points into the numbers of major sub-catchments within the study area i.e. Melka Kuntire, Hombole, Mojo, and others
ii. Determine how each daily time-series at each drainage point are far from each other and their respective mean discharges using their respective coefficient of variance
iii. Categorize the hydraulic structures at each drainage points into two categories i.e. bridges and culverts

Selection is, therefore, based on the hydraulic structures with a large coefficient of variance which comprises bridges and culverts for further analyses.

3.8 Flow Variability Check

The flow variability was checked by calculating the coefficient of variance for the daily flows estimated for each drainage structure. This coefficient of variance was calculated using equation 3.6:

$$\mathbf{CoV = \frac{Stdev}{Mean}} \qquad \textbf{Eq. (3.6)}$$

Where;

CoV = Coefficient of Variance

Mean = Mean of the daily flow

Stdev = Standard deviation of the daily flow

3.9 Flood Storm Frequency Analysis

To estimate the peak flows at the outlets of the selected drainage structures based on the variability check results, this research developed a rainfall intensity – duration frequency to estimate the design rainfall (mm) at different return periods which was used as input data in HEC-HMS to determine the peak flows at the selected drainage points.

3.9.1 Peak Annual Rainfall Estimation

The peak daily rainfall magnitudes were selected for each year which represented the annual peak rainfall values. The result is shown in Table 3.4

Table 3.4: Estimated Annual Peak Rainfall (mm)

Year	Annual Peak Rainfall (mm)	Year	Annual Peak Rainfall (mm)
2000	41.323	2010	40.705
2001	50.677	2011	42.431
2002	52.225	2012	46.055
2003	59.861	2013	42.815
2004	53.601	2014	33.489
2005	48.204	2015	35.279
2006	59.691	2016	73.327
2007	57.433	2017	45.526
2008	57.652	2018	35.239
2009	46.455	2019	32.228

3.9.2 Determination of Goodness-of-fit

The peak annual rainfall magnitudes were subjected to statistical analyses to determine the best probability distribution that best fit the trends in the magnitudes. This research uses EasyFit software, selected about seven (7) different probability distributions while Kolmogorov, Anderson Darling, and Chi-Squared were selected for ranking the best distribution as shown in the summary Table 3.5. Thus, Gen. Extreme Value probability distribution with the probability distribution curve shown in Figure 19 was selected for the estimation of design rainfall magnitudes at different return periods.

Table 3.5: Summary Table for the Goodness of Fit Used for Ranking Distributions

Goodness of Fit - Summary

#	Distribution	Kolmogorov Smirnov		Anderson Darling		Chi-Squared	
		Statistic	Rank	Statistic	Rank	Statistic	Rank
3	Gen. Extreme Value	0.08827	1	0.18473	1	0.24563	4
2	Chi-Squared (2P)	0.09961	2	0.22379	5	0.34864	6
4	Log-Pearson 3	0.10009	3	0.19583	2	0.21786	3
5	Lognormal	0.10472	4	0.20709	3	0.24886	5
9	Weibull (3P)	0.10805	5	0.28385	7	0.17593	1
6	Lognormal (3P)	0.10812	6	0.22348	4	0.20143	2
1	Chi-Squared	0.10837	7	0.25787	6	0.35901	7
8	Weibull	0.1265	8	0.47764	8	0.72413	8
7	Power Function	0.38556	9	4.695	9	8.0001	9

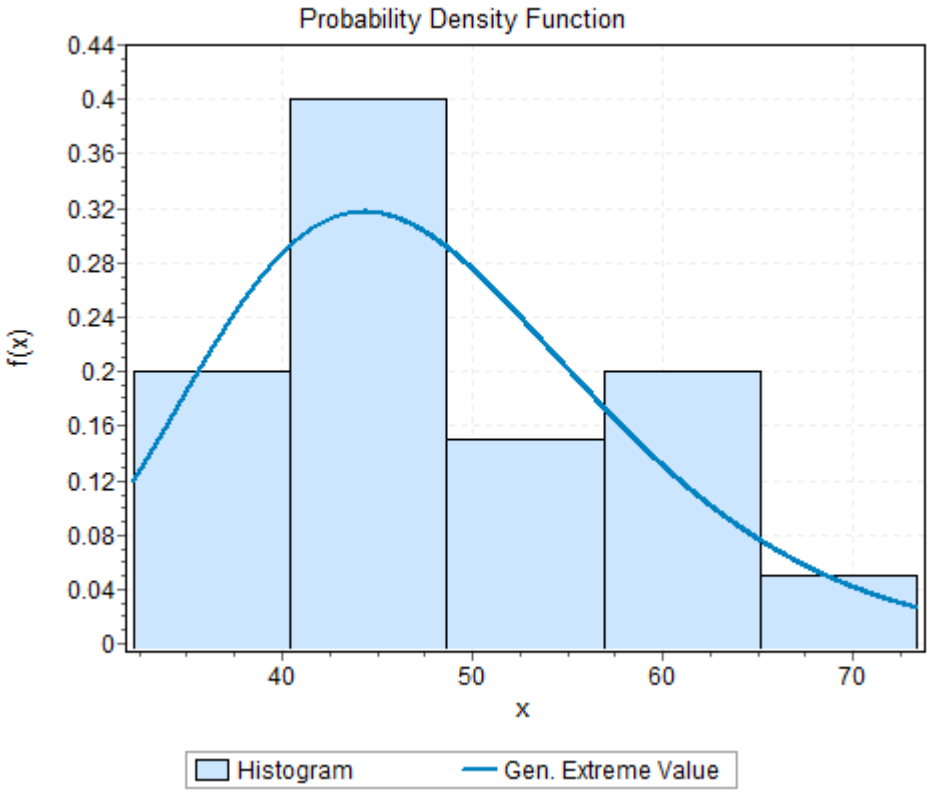

Figure 3.19: Probability Distribution Curve for Gen. Extreme Value

3.10 Flow Variability - Scouring Depths Relationship Development

To achieve this (developing some relationships between the daily flow variabilities on the scouring depths at the railway bridge piers and culverts), the methodological flow chart in Figure 3.20 was used.

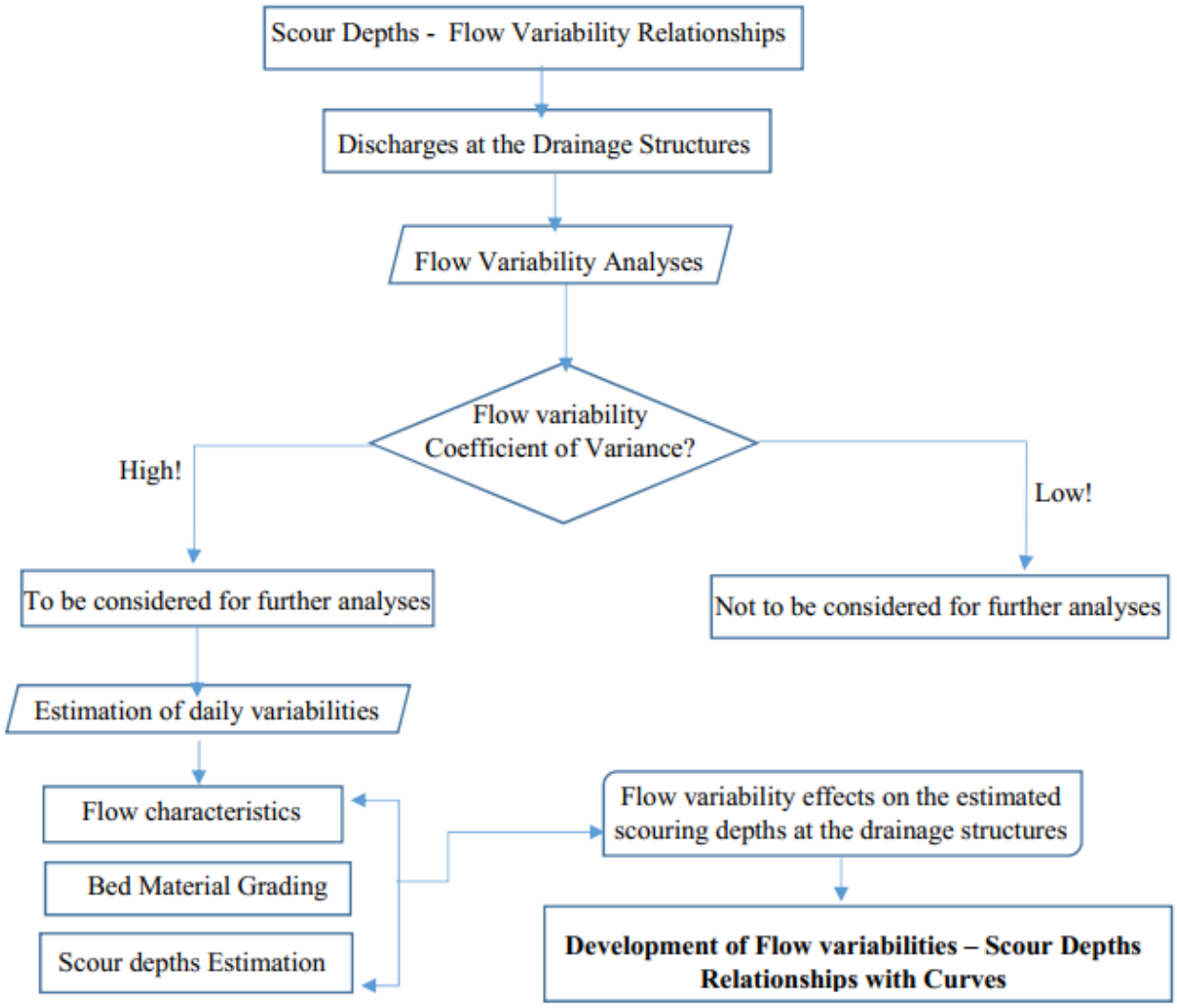

Figure 3.20: Variable flows – Scouring Relationships Procedures

3.10.1 Estimation of Scour Depth

There are two major drainage structures identified within the selected section, these are:

- Open-Bottom Culverts (Slab culverts)
- Bridges

Therefore, different approaches are available for the estimation of scour depths for each of the drainage structure types. These are explained as follows:

3.10.2 Open-Bottom Culverts (Slab Culverts)

Slab culverts are culvert types with natural channel materials as the bottom. They can be cast-in-situ, precast, or prefabricated in rectangular shape or rounded top in shape. For these structure types, scour is greatest at the upstream corners of the culvert entrance and this accounts for both contraction and local scour phenomena. Figure 3.28 shows a typical example of slab or open-bottom culverts **[27]**.

Figure 3.21: Typical example of an Open-Bottom Culvert with rounded top

To estimate the scour depth for an open-bottom culvert under the clear-water condition the equations 3.7 and 3.8 are used respectively for with wing wall cases and without wing wall cases **[27]**:

With wing wall case:

$$\mathbf{Ymax = K * Qb^{0.28} * \left(\frac{Q}{B * Dm^{\frac{1}{3}}} \right)^{0.26}} \qquad \textbf{Eq. (3.7)}$$

Without wing wall case:

$$\mathbf{Ymax = K * Qb^{0.12} * \left(\frac{Q}{B * Dm^{\frac{1}{3}}} \right)^{0.60}} \qquad \textbf{Eq. (3.8)}$$

$Y_s = Y_{max} - Y_o$

Where;

K = 1.16

Y_{max} = flow depth at culvert entrance corner including contraction and local scour (m)

Q_b = Flow blocked by road embankment on one side of the culvert (m^3/s)

B = Culvert width (m)

D_m = Median diameter of the bed material (D_{50}) (m)

Y_s = Scour depth at the culvert entrance corner (m)

Y_o = Flow depth (m)

Q = flow through the culvert (m^3/s)

3.10.3 Scour around Bridge Piers

Bridge Pier is one of the substructure parts of a railway bridge which is characterized by its type, dimensions, and shape. Generally, local scour at bridge piers is a function of channel material characteristics, flow behaviors, bed stability, and pier and footing geometry. A Bridge pier could be referred to as a simple pier if it comprises of a single shaft, column, or multiple columns exposed to the flow or as a complex pier if the pier, footing, or pile cap, and piles are all exposed to the flow **[27]**. Figure 3.22 shows a typical definition sketch for scour around pier while equations 3.9 and 3.10 described the HEC-18 pier scour formula for estimating the scour depth for both live-bed and clear-water conditions.

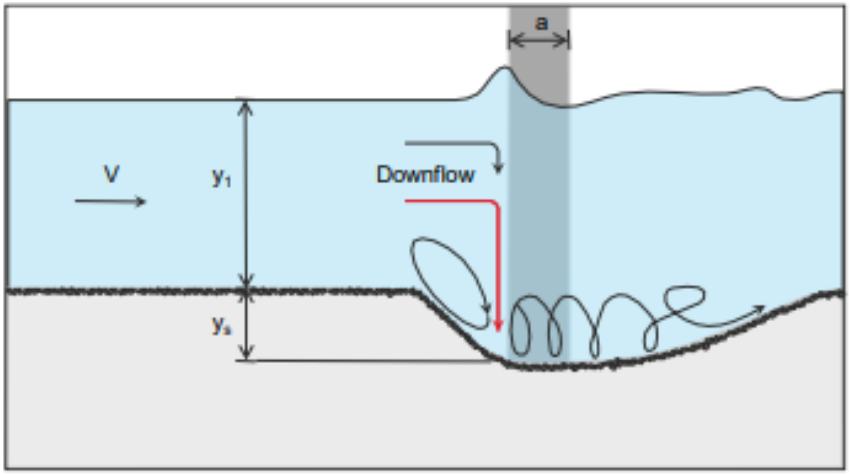

Figure 3.22: Typical example of Pier Scour Sketch [27]

$$\frac{Ys}{Yo} = 2.0ABC\left(\frac{w}{Yo}\right)^{0.65} Fr^{0.43} \qquad \textbf{Eq. (3.9)}$$

$$\frac{Ys}{w} = 2.0ABC\left(\frac{Yo}{w}\right)^{0.35} Fr^{0.43} \qquad \textbf{Eq. (3.10)}$$

Where;

w = pier width (m)

A = pier nose shape correction factor

B = angle of attack of flow correction factor

C = bed condition correction factor

Fr = Froude Number = $V/(gYo)^{0.5}$

Y_s = Scour depth (m)

Y_o = Flow depth upstream of the pier (m)

g = acceleration of gravity ($9.81 m/s^2$)

V = flow velocity upstream of the pier (m/s)

As a general rule of thumb, for round nose piers with the angle of attack being zero, the maximum scour depth is checked using the limits below as recommended in **[27]**:

$Y_s \leq (2.4*w)$ for $Fr \leq 0.8$

$Y_s \leq (3.0*w)$ for $Fr > 0.8$

- Correction factor for pier nose shape (A)

This value can be selected in Table 3.6 as recommended in the HEC-18 formula for estimating scour depth at the pier.

Table 3.6: Correction Factor, A, for Pier Nose Shape [27]

The shape of Pier Nose	A
Square nose	**1.1**
Round nose	**1.0**
Circular cylinder	**1.0**
Group of cylinders	**1.0**
Sharp nose	**0.9**

- Correction factor for the angle of attack of flow (B)

As recommended in **[27]**, this factor B can be calculated using the following expression in equation 3.11:

$$\mathbf{B = \left(\cos\theta + \frac{L}{a}\sin\theta\right)^{0.65}} \qquad \textbf{Eq. (3.11)}$$

Where;

L = Length of Pier (m)

a = Width of Pier (m)

However, it is recommended to adopt 12.0 if L/a > 12 as in equation 10 **[27]** as illustrated in Figure 3.23:

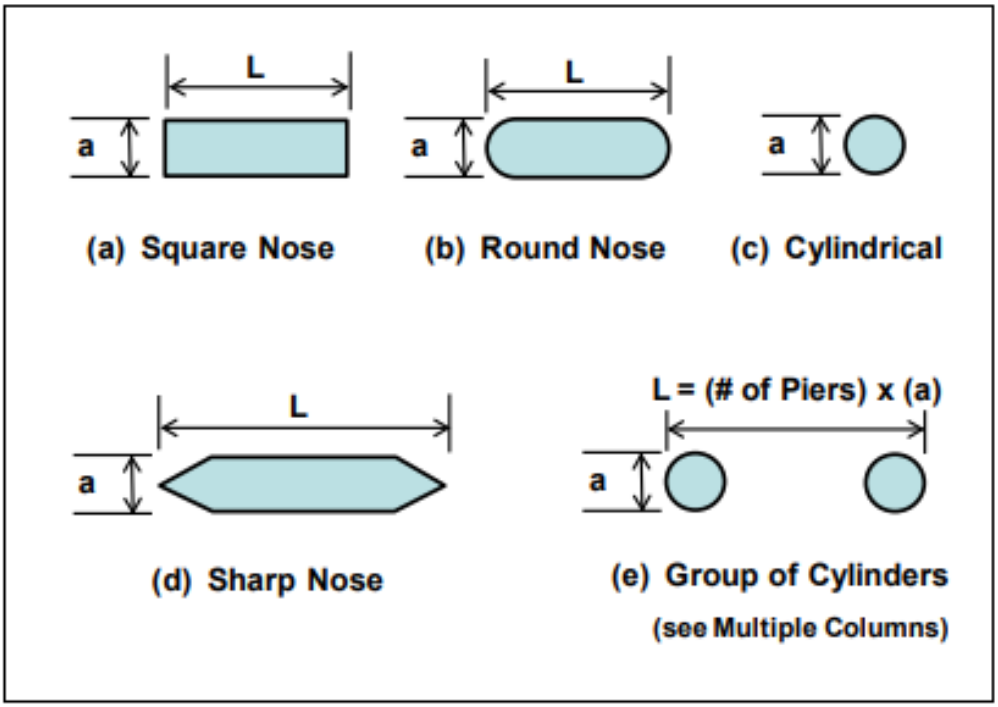

Figure 3.23: Commonly used pier shapes [27]

- Bed condition Correction Factor (C)

There are five (5) types of bed conditions available in the HEC-18 formula with different correction factors. These are presented in Table 3.7:

Table 3.7: Bed Conditions and their corresponding correction factors C [27]

Bed Condition	Dune Height	C
Clear-Water Scour	**N/A**	**1.1**
Plane bed and Antidune flow	**N/A**	**1.1**
Small Dunes	**10 > H >= 2**	**1.1**
Medium Dunes	**30 > H >= 10**	**1.2 to 1.1**
Large Dunes	**H >= 30**	**1.3**

3.10.4 Particle Size Distribution

Particle size distribution curves at the selected drainage structures are plotted using the data extracted from the subgrade soil test reports sourced from the Ethiopian Railway Corporation. These curves are used to estimate the particle size diameters equivalent to D_{50} which are among the basic data required for estimating scour depth. An example of how the median diameter of bed particle size is shown in Figure 3.24.

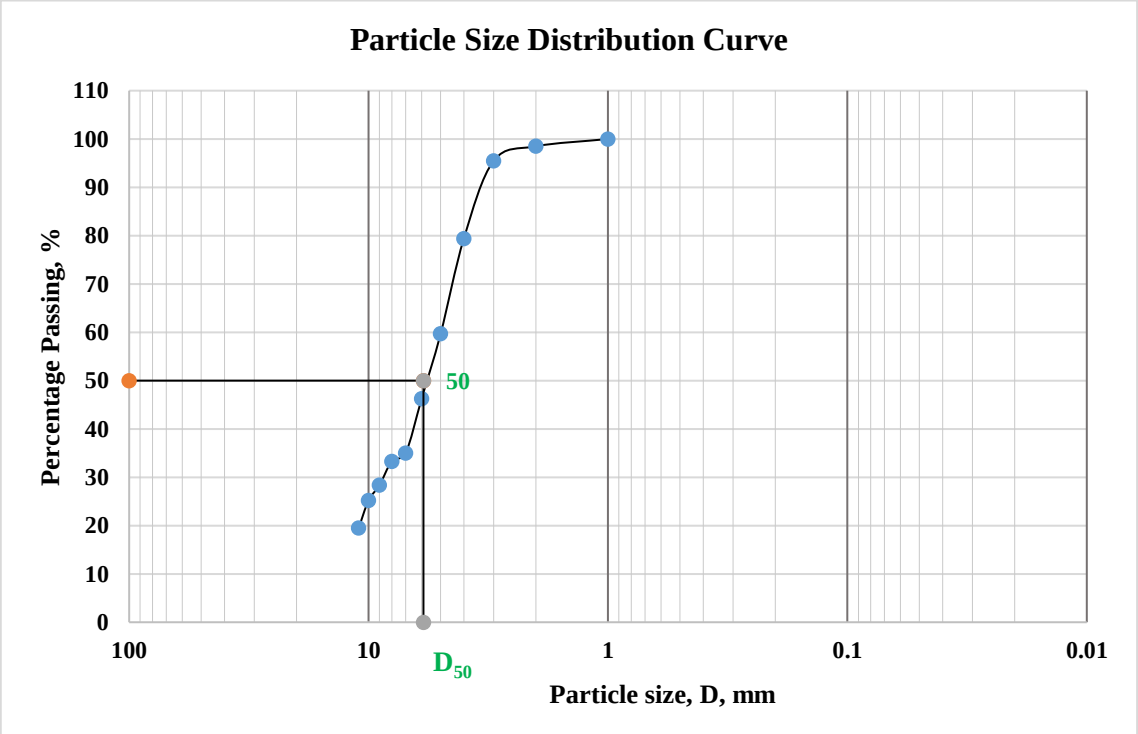

Figure 3.24: An example of Particle Size Distribution Curve for Estimating D_{50} (mm)

3.10.5 Manning's Roughness Coefficient, (n)

To determine the manning's roughness coefficients for the channels at drainage structure locations, the Stickler formula expressed in equation 3.12 was used:

$$\mathbf{n = 0.0132 * \left(D50^{\frac{1}{6}}\right)} \qquad \textbf{Eq. (3.12)}$$

3.11 Flow Characteristics Estimation

The flow characteristics are estimated using the following expressions in equations 3.13 – 3.17:

- Discharge, Q, m^3/s:

The magnitudes of the discharge can be determined using manning's equation:

$$\mathbf{Q = AV} \qquad \textbf{Eq. (3.13)}$$

$$\mathbf{Q} = \frac{\mathbf{1}}{\mathbf{n}} * \mathbf{a}\mathbf{R}^{\frac{\mathbf{2}}{\mathbf{3}}}\mathbf{S}^{\frac{\mathbf{1}}{\mathbf{2}}} \qquad \textbf{Eq. (3.14)}$$

$$\mathbf{R} = \left(\mathbf{V} * \frac{\mathbf{n}}{\mathbf{S}^{\frac{\mathbf{1}}{\mathbf{2}}}}\right)^{\mathbf{3/2}} \qquad \textbf{Eq. (3.15)}$$

$$\mathbf{S} = \left(\mathbf{V} * \frac{\mathbf{n}}{\mathbf{R}^{\frac{\mathbf{2}}{\mathbf{3}}}}\right)^{\mathbf{2}} \qquad \textbf{Eq. (3.16)}$$

- Normal Flow Velocity, m/s

$$\mathbf{Vn} = \frac{\mathbf{1}}{\mathbf{n}}\mathbf{R}^{\mathbf{2/3}}\mathbf{S}^{\mathbf{1/2}} \qquad \textbf{Eq. (3.17)}$$

Where;

V = flow velocity, m/s

a = Area of flow, m^2

R = Hydraulic radius, (m) = a/P

P = Wetted Perimeter, (m)

S = Hydraulic slope in (m/m)

n = Manning's coefficient of roughness.

- Critical Velocity, Vc (m/s)

Is the velocity at which cohesionless particles such as sands and gravels begin to move. It can be estimated using the expression in equation 3.18:

$$\mathbf{Vc} = \mathbf{Ku} * \mathbf{y}^{\frac{\mathbf{1}}{\mathbf{6}}} * \mathbf{d}^{\frac{\mathbf{1}}{\mathbf{3}}} \qquad \textbf{Eq. (3.18)}$$

Where;

y = Flow depth, m

d = Grain size of the particles, usually D_{50}

K_u = 6.19

- Critical Depth, Yc, (m)

Critical depth, Yc, can be determined by finding the depth at critical flow, i.e when the Froude number equals 1. This is shown in equation 3.19:

$$\mathbf{Yc = \frac{v^2}{g}} \qquad \textbf{Eq. (3.19)}$$

By substituting Fr = 1.0 into equation 3.20:

$$\mathbf{Fr = \frac{v}{\sqrt{gY}}} \qquad \textbf{Eq. (3.20)}$$

Where;

Y_c = Critical Depth, (m)

g = Acceleration due to gravity, 9.81 m/s^2

Fr = Froude Number; Fr = 1.0 for critical flow

3.12 Riprap Diameter Estimation

As recommended in HEC-18, the median stone diameter (m) requires for protecting the bed materials around a bridge pier can be estimated using the expression in equation 3.21:

$$D_{50} = 0.692[KV^2]/[(S_s\text{-}1)*2G] \qquad \textbf{Eq. (3.21)}$$

Where;

D_{50} = Median stone diameter (m)

K = Correction factor for pier shape; 1.5 for rounded-nose piers and 1.7 for rectangular piers

V = Velocity at pier (m/s)

S_s = Specific gravity of riprap material (usually 2.65)

G = acceleration due to gravity (9.81 m/s^2)

Chapter 4: RESULTS AND DISCUSSIONS

4.1 Hydrological Model Setup

The hydrological model (HEC-HMS) was developed in ArcGIS 10.4 using HEC-GeoHMS and Arc Hydro Tools extensions for catchment and river delineation and location of drainage points as shown in Figure 4.1 following the steps-by-steps processes in the methodological flow chart of this study.

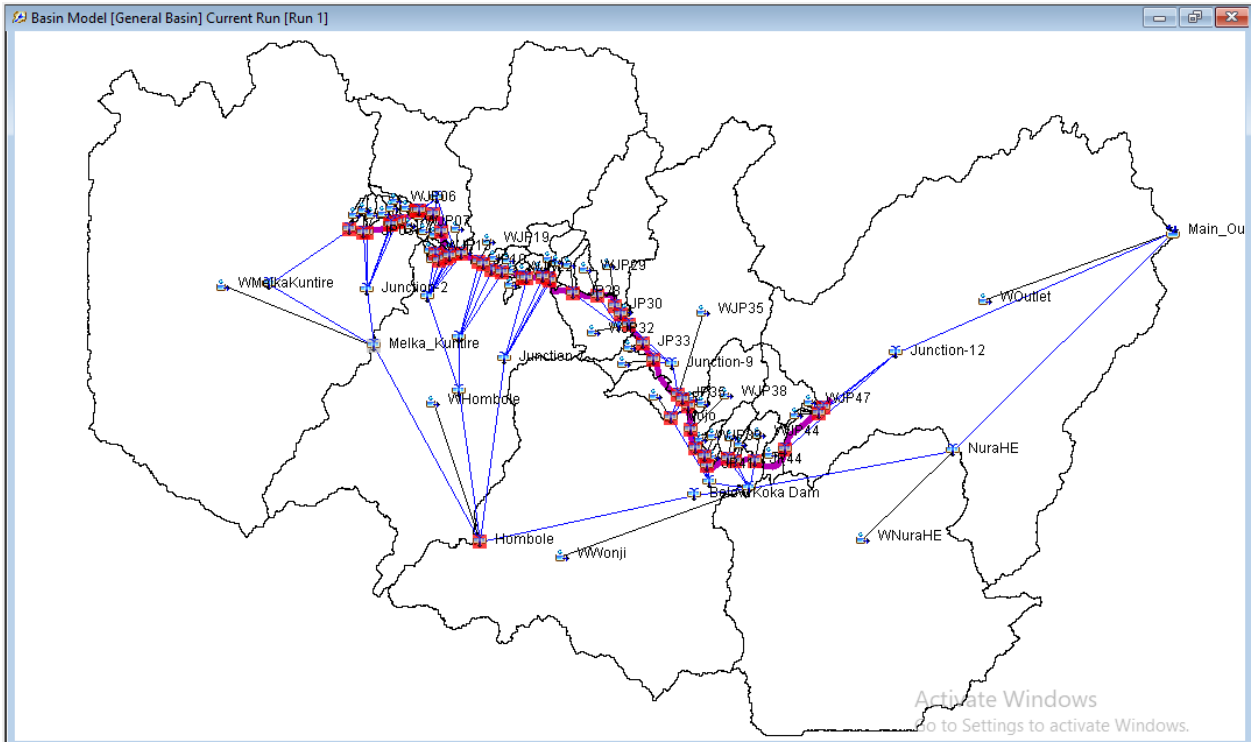

Figure 4.1: HEC-HMS Model Setup

In this model, the whole catchment considered is 17,030.00 km^2 in size with a total number of 6 sub-major catchments. Again, each drainage point (i.e. drainage structure locations) has a sub-catchment as shown in Table 4.1.

Table 4.1: Hydrologic Elements and their respective catchment areas (km2)

Hydrologic Element	Area (sqkm)	Slope (m/m)	Hydrologic Element	Area (sqkm)	Slope (m/m)	Hydrologic Element	Area (sqkm)	Slope (m/m)
WJP01	4.6	0.0468	WJP10	2.5	0.0104	WJP19	90.9	0.0039
WJP02	5.1	0.0684	WJP11	7.8	0.0024	WJP20	7.2	0.0011
WJP03	10.4	0.0379	WJP12	3.2	0.0308	WJP21	17.7	0.0072
WJP04	9.1	0.0449	WJP13	3.3	0.1144	WJP22	3.8	0.0069
WJP05	7.5	0.0490	WJP14	5.7	0.0401	WJP23	7.8	0.0089
WJP06	18.5	0.0352	WJP15	4.8	0.0206	WJP24	15.6	0.0226
WJP07	9.6	0.0053	WJP16	3.7	0.0134	WJP25	25.2	0.0159

WJP08	6.9	0.0262	WJP17	352.9	0.0029	WJP26	35.6	0.0229
WJP09	7.1	0.0104	WJP18	4.0	0.0114			

Hydrologic Element	Area (sqkm)	Slope (m/m)	Hydrologic Element	Area (sqkm)	Slope (m/m)	Hydrologic Element	Area (sqkm)	Slope (m/m)
WJP27	22.5	0.0204	WJP36	8.5	0.0049	WJP45	23.8	0.0112
WJP28	25.6	0.0197	WJP37	133.8	0.0144	WJP46	4.2	0.0385
WJP29	125.5	0.0107	WJP38	3.2	0.0210	WJP47	83.1	0.0087
WJP30	301.8	0.0036	WJP39	13.6	0.0050	WMelkaKuntire	4456.0	
WJP31	130.0	0.0007	WJP40	5.5	0.0264	WMojo	1264.4	
WJP32	468.7	0.0013	WJP41	38.6	0.0271	WHombole	7656.0	
WJP33	33.3	0.0007	WJP42	37.0	0.0239			
WJP34	875.9	0.0031	WJP43	6.0	0.0137			
WJP35	1382.1	0.0049	WJP44	29.2	0.0335			

4.1.1 Model Calibration and Performance Check

This section dealt with model calibration, validation, and how well the model simulated the previous flows and predict the future flows. For this study, simulating the hydrological processes within the study area the routing method used is the Muskingum method and the Muskingum constant K ranges from 26.11 to 56.55 (hr^{-1}), SCS Runoff Curve Number as the loss method with values ranging from 85 to 88, and SCS Unit Hydrograph Lag Time as the Transform method with values ranging from 9.07 to 340.93 minutes. These are shown in Appendix B.

4.1.1.1 Model Calibration

The model was calibrated using the ground-based observed discharges at the three hydrometric gauge stations (Melka Kuntire, Hombole, and Mojo HG Stations) and the results are as shown in Figures 4.2 – 4.4. This was carried out using some portion of the time-series dataset for the selected hydrometric stations from the year 2005 to 2014. This period is selected because of the availability of a full data record with few missing data.

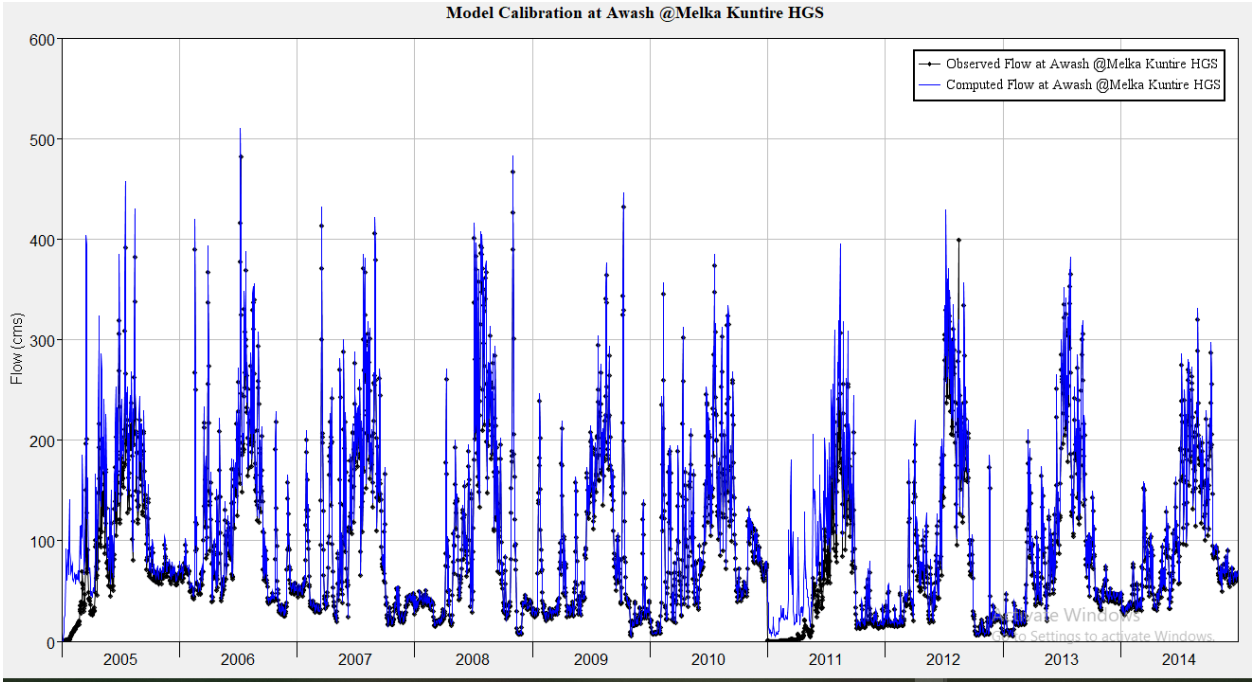

Figure 4.2: Model Calibration Result at Melka Kuntire HG Station

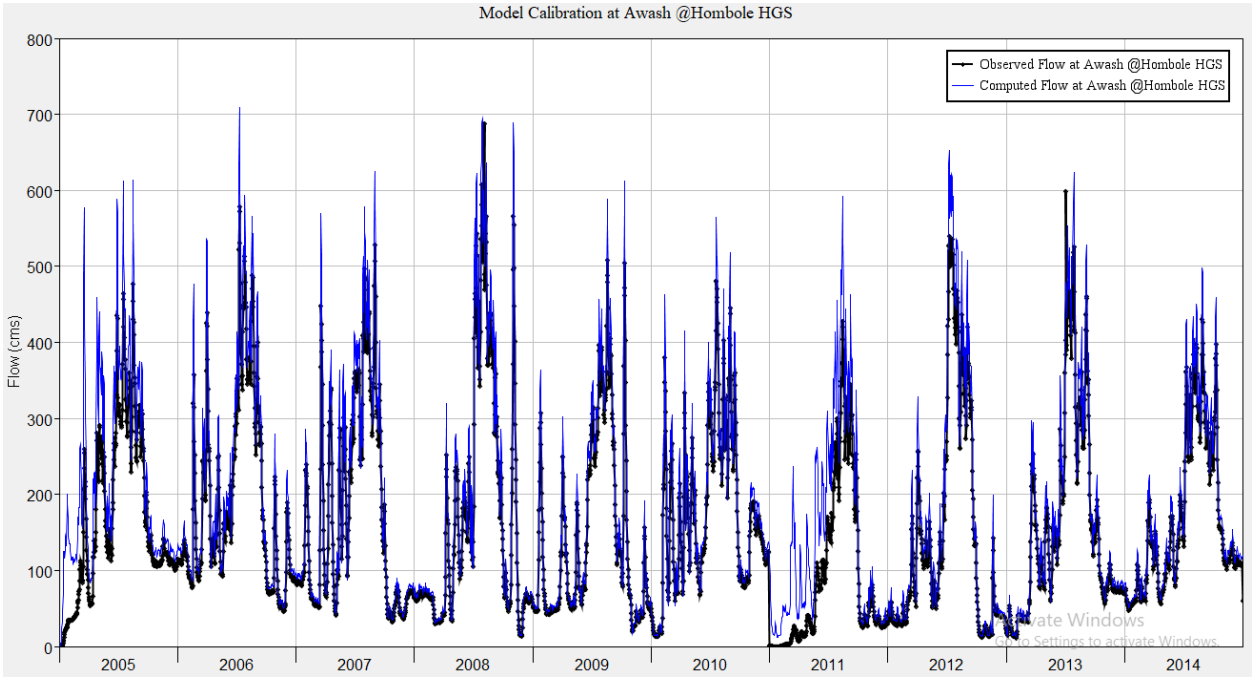

Figure 4.3: Model Calibration Result at Hombole HG Station

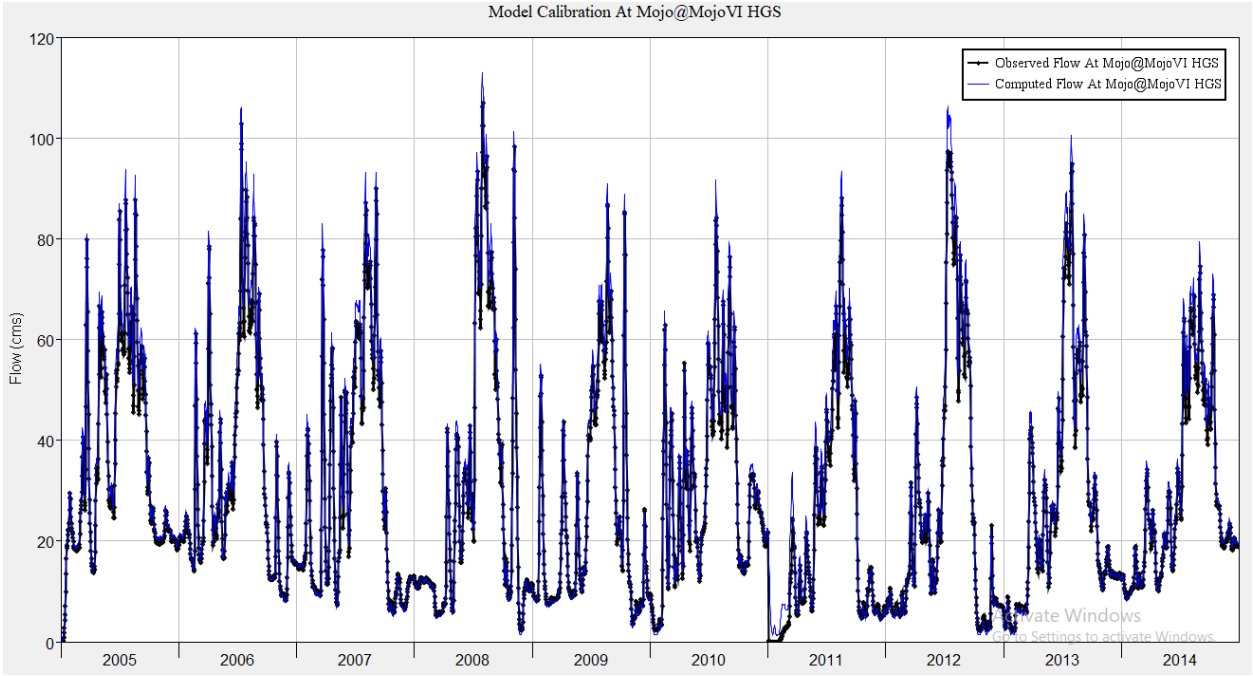

Figure 4.4: Model Calibration Result at Mojo HG Station

4.1.1.2 Model Performance Check

4.1.1.2.1 NSE and PBIAS

The performance of the model was checked using two statistical approaches; the Nash and Sutcliffe Efficiency (NSE) and the Percentage Bias. The results are as shown in Figures 4.5 – 4.7 for Melka Kuntire, Hombole, and Mojo HG stations respectively.

The Nash-Sutcliffe Efficiency (NSE) are 0.938, 0.892, and 0.942 while the Percentage Bias are 10.54%, 16.38%, and 6.11% for Melka Kuntire, Hombole, and Mojo HG Stations respectively which are within the statistically acceptable range of NSE > 0.5, and PBIAS = $\pm$ 20% for surface runoff model calibration and validation. The overall performance shows that the model calibration is very good.

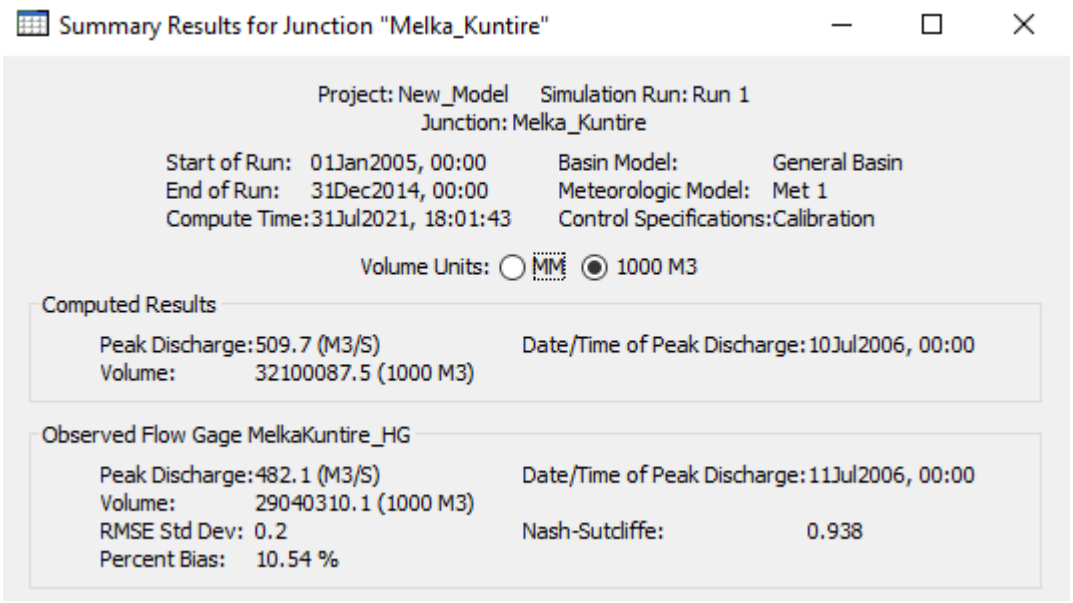

Figure 4.5: Model Calibration Performance Result at Melka Kuntire HG Station

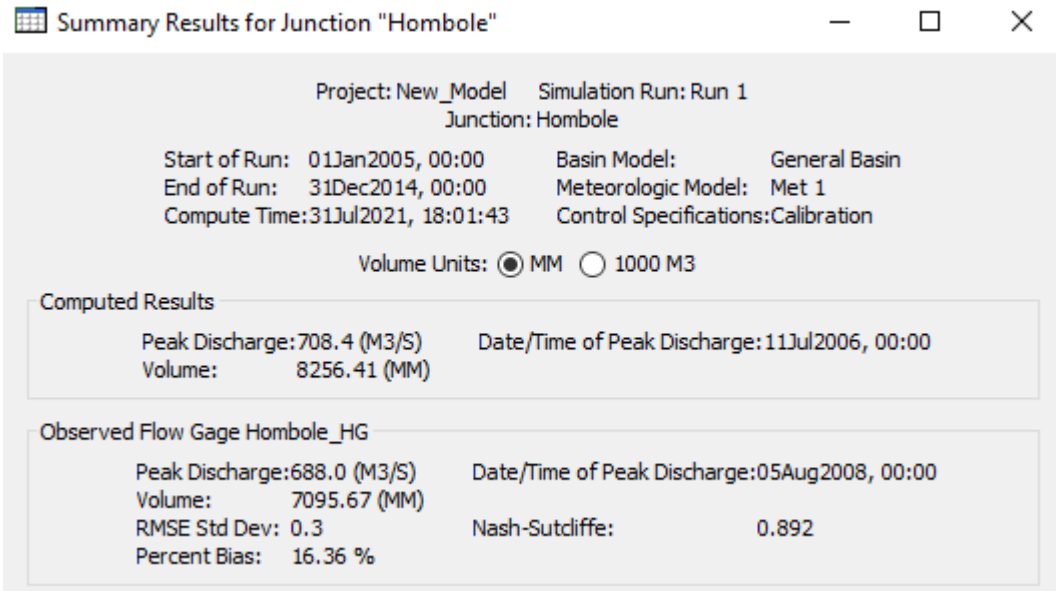

Figure 4.6: Model Calibration Performance Result at Hombole HG Station

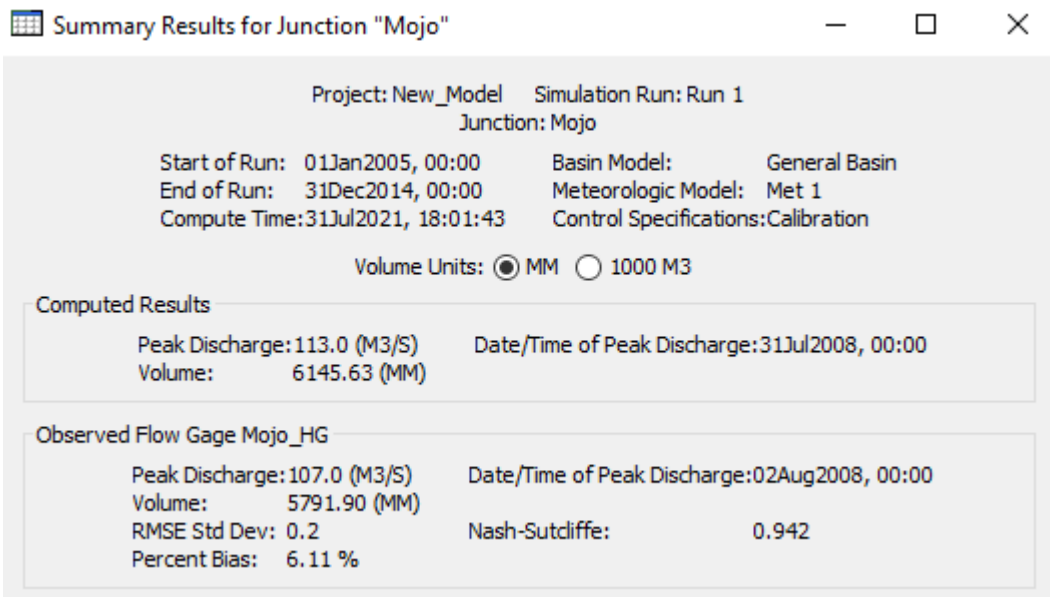

Figure 4.7: Model Calibration Performance Result at Mojo HG Station

4.1.1.2.2 Coefficient of Determination, R^2

For model calibration and validation at each selected hydrometric gauge station, the coefficient of determination (R^2) is determined using scatter plots of the computed against the observed discharges for the calibration and validation periods of 2005 – 2010 and 2011 – 2014 respectively. The plots are shown in Figures 4.8 – 4.10 for Melka Kuntire, Hombole, and Mojo HG Stations respectively. Therefore, a summarized result of the model performance check is tabulated in Table 4.2.

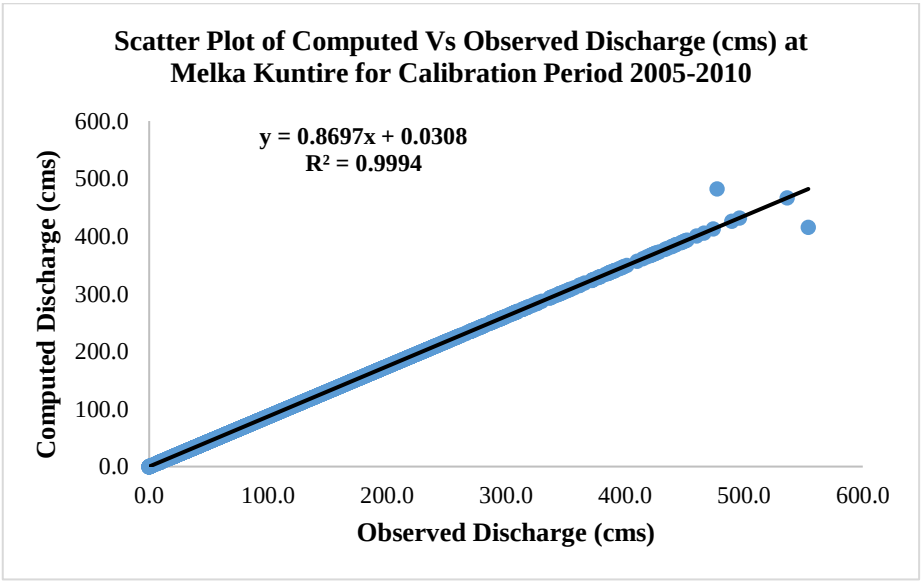

Figure 4.8: Performance Analysis Using Scatter Plot for Model Calibration at Melka Kuntire HG Station

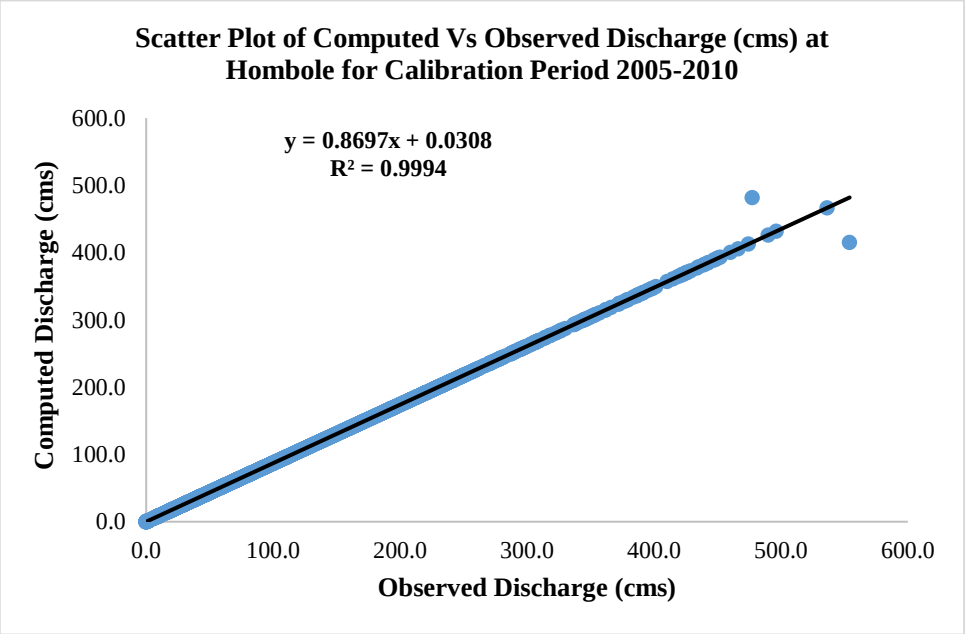

Figure 4.9: Performance Analysis Using Scatter Plot for Model Calibration at Hombole HG Station

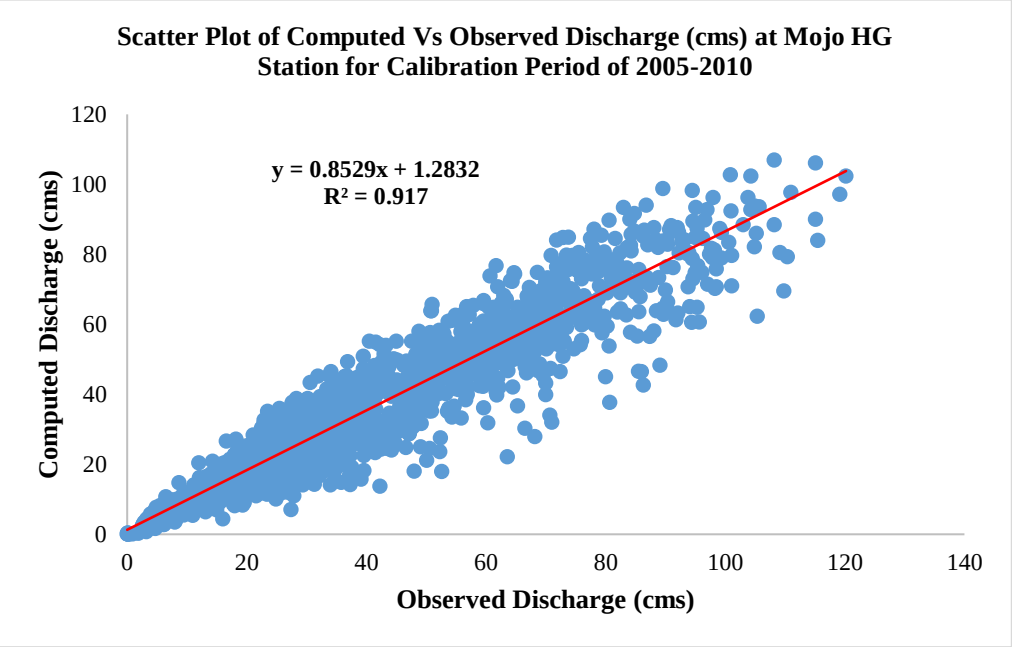

Figure 4.10: Performance Analysis Using Scatter Plot for Model Calibration at Mojo HG Station

Table 4.2: Summary of Model Performance Check Using NSE, PBIAS, and R2 Statistical Methods

HG Station	Calibration Period	2005 -2010	Validation Period	2011 - 2014
Melka Kuntire HG Station	NSE	0.938	NSE	0.951
	PBIAS %	10.54%	PBIAS %	14.94%
	R^2	0.9994	R^2	0.9979
	Overall: Very Good		Overall: Very Good	
Hombole HG Station	NSE	0.892	NSE	0.938

	PBIAS %	16.36%	PBIAS %	16.28%
	R^2	0.9994	R^2	0.9976
	Overall: Very Good		Overall: Very Good	
Mojo HG Station	NSE	0.942	NSE	0.921
	PBIAS %	6.11%	PBIAS %	12.34%
	R^2	0.917	R^2	0.9617
	Overall: Very Good		Overall: Very Good	

4.2 Daily Flow Results at Each Drainage Structure

There are about forty-seven (47) drainage structures (both culverts and bridges) identified within the selected reach based on the resolution of the spatial data used for watershed and stream network delineation. For each drainage structure, twenty (20) years of flows have been estimated by modeling and simulating the hydrological processes within the catchment's study area. Therefore, Figures 4.11 and 4.12 show the flow patterns per every four (4) years from the year 2000 to 2007 for the structure at JP01. See the Appendix C for other JPs.

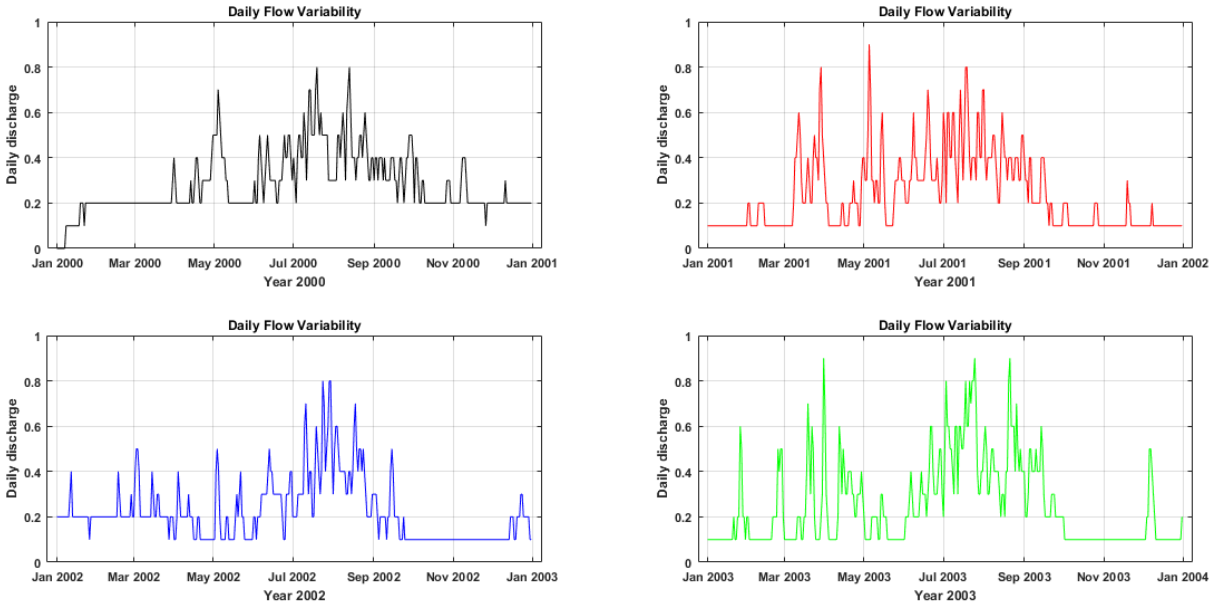

Figure 4.11: Daily Flows (cms) for the Year 2000-2003 at JP01

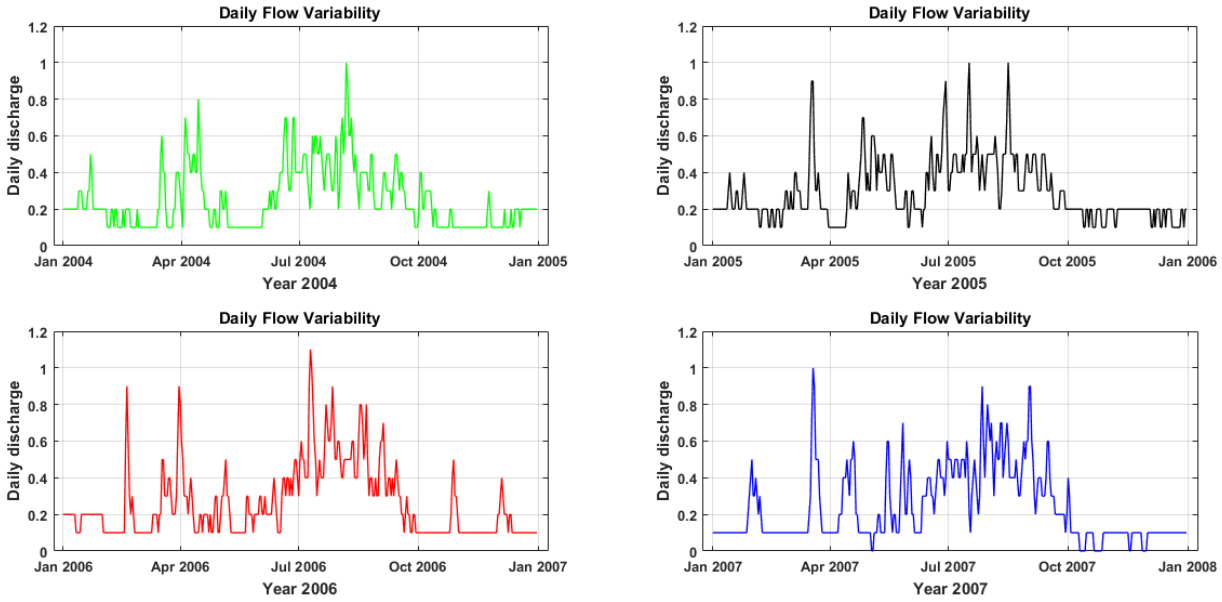

Figure 4.12: Daily Flows (cms) for the Year 2004-2007 at JP01

4.3 Daily Flow Variability

To determine the flow variabilities, this study performed the descriptive test on IBM SPSS version 25 for the computed flows at the selected drainage structures. The results are as shown in Tables 4.3 – 4.5. Where Group 1, Group 2, and Group 3 indicate all the hydrologic elements within Melka Kuntire, Hombole, and Mojo with Other catchments respectively.

Table 4.3: Group 1 Descriptive Statistic Results

	Mean	Std. Deviation	Variance	CoV
JP 01	0.2444	0.17893	0.032	0.732
JP 02	0.2016	0.14806	0.022	0.734
JP 03	0.4125	0.29490	0.087	0.715
JP 04	0.4309	0.30940	0.096	0.718
JP 05	0.3284	0.23426	0.055	0.713
JP 06	1.1250	0.77459	0.600	0.688
JP 07	0.5295	0.37931	0.144	0.716

Table 4.4: Group 2 Descriptive Statistic Results

Label	Mean	Std. Deviation	Variance	CoV	Label	Mean	Std. Deviation	Variance	CoV
JP 08	0.1969	0.14506	0.021	0.737	JP 18	0.1158	0.08775	0.008	0.758
JP 09	0.2023	0.14239	0.020	0.704	JP 19	25.9063	18.50901	342.583	0.714
JP 10	0.0621	0.06416	0.004	1.034	JP 20	0.2034	0.14958	0.022	0.735

JP 11	0.2199	0.16113	0.026	0.733	JP 21	0.5045	0.36207	0.131	0.718
JP 12	0.0877	0.07729	0.006	0.881	JP 22	0.1104	0.08505	0.007	0.770
JP 13	0.0904	0.07826	0.006	0.866	JP 23	0.2778	0.20272	0.041	0.730
JP 14	0.164	0.1198	0.014	0.730	JP 24	0.557	0.37461	0.140	0.673
JP 15	0.1302	0.09563	0.009	0.735	JP 25	0.3475	0.24814	0.062	0.714
JP 16	0.1053	0.08352	0.007	0.793	JP 26	1.0147	0.72353	0.523	0.713
JP 17	10.0874	7.11986	50.692	0.706	JP 27	0.6386	0.45863	0.210	0.718

Table 4.5: Group 3 Descriptive Statistic Results

Label	Mean	Std. Deviation	Variance	CoV	Label	Mean	Std. Deviation	Variance	CoV
JP 28	0.7293	0.52157	0.272	0.715	JP 38	0.0877	0.0773	0.006	0.881
JP 29	8.1514	5.82366	33.915	0.714	JP 39	38.7346	27.67331	765.812	0.714
JP 30	0.1029	0.08286	0.007	0.806	JP 40	0.158	0.1151	0.013	0.729
JP 31	2.6208	1.87268	3.507	0.715	JP 41	1.0985	0.78554	0.617	0.715
JP 32	11.8463	7.8168	61.102	0.66	JP 42	0.1721	0.12559	0.016	0.73
JP 33	0.9502	0.67822	0.46	0.714	JP 43	1.0549	0.75266	0.567	0.714
JP 34	19.2719	13.769	189.585	0.714	JP 44	0.8317	0.59482	0.354	0.715
JP 35	32.1737	20.7509	430.6	0.645	JP 45	0.6788	0.48691	0.237	0.717
JP 36	0.2422	0.17735	0.031	0.732	JP 46	0.1221	0.09095	0.008	0.745
JP 37	3.5283	2.52078	6.354	0.714	JP 47	2.3674	1.69299	2.866	0.715

Since the coefficient of variance is very high for all the junction points (ranges from 0.645 to 1.034) as shown in Tables 4.3 – 4.5, it can be concluded that there are flow variabilities to all the drainage structures within the selected reach.

4.4 Design Rainfall Estimation

This study uses the Gen. Extreme Value (GEV) to estimate the design rainfall magnitudes at different return periods for different durations. The rainfall–duration frequency and rainfall intensity–duration frequency tables and curves were developed and the results were presented in Table 4.6, Figure 4.13, and Table 4.7, Figure 4.14 respectively. The rainfall magnitudes corresponding to 24hrs were used as input in HEC-HMS for estimating the peak flows.

Table 4.6: Rainfall (mm) Vs Return Periods at Different Durations

Duration (minutes)	Rainfall (mm) vs Return Period							
	2 yrs	5 yrs	10 yrs	25 yrs	50 yrs	100 yrs	200 yrs	500 yrs
5	6.96	8.37	9.31	10.48	11.36	12.23	13.09	14.23
15	10.04	12.07	13.42	15.12	16.38	17.63	18.88	20.53
60	15.94	19.17	21.30	24.00	26.00	27.99	29.97	32.58
120	20.08	24.15	26.84	30.24	32.76	35.27	37.76	41.05
180	22.99	27.64	30.72	34.62	37.51	40.37	43.23	47.00
360	28.97	34.83	38.71	43.62	47.25	50.87	54.46	59.21
720	36.49	43.88	48.77	54.95	59.54	64.09	68.62	74.60

1440	45.98	55.29	61.45	69.23	75.01	80.74	86.46	93.99

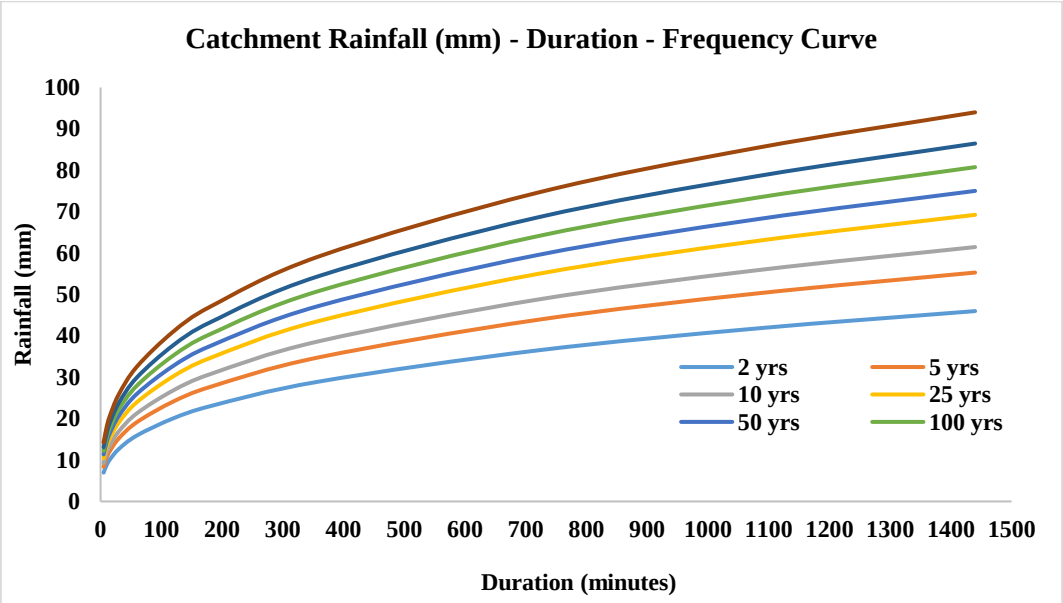

Figure 4.13: Catchment Rainfall (mm) – Duration Frequency Curve

Table 4.7: Rainfall Intensity (mm/hr) Vs Return Periods at Different Durations

Duration (Minutes)	Rainfall intensity (mm/hr) vs Return Period							
	2 yrs	5 yrs	10 yrs	25 yrs	50 yrs	100 yrs	200 yrs	500 yrs
5	83.55	100.46	111.66	125.81	136.30	146.72	157.10	170.79
15	40.17	48.30	53.68	60.48	65.53	70.54	75.53	82.11
60	15.94	19.17	21.30	24.00	26.00	27.99	29.97	32.58
120	10.04	12.07	13.42	15.12	16.38	17.63	18.88	20.53
180	7.66	9.21	10.24	11.54	12.50	13.46	14.41	15.67
360	4.83	5.80	6.45	7.27	7.88	8.48	9.08	9.87
720	3.04	3.66	4.06	4.58	4.96	5.34	5.72	6.22
1440	**1.92**	**2.30**	**2.56**	**2.88**	**3.13**	**3.36**	**3.60**	**3.92**

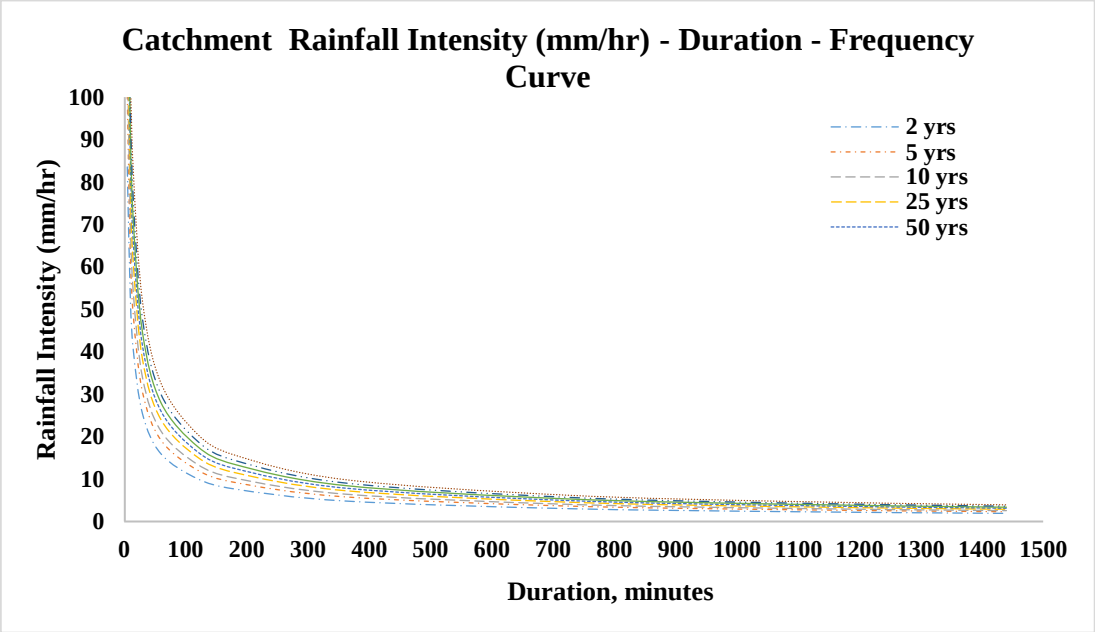

Figure 4.14: Catchment Rainfall Intensity (mm/hr) – Duration Frequency Curve

4.5 Flood Frequency Analysis

The peak flows at the outlets of the selected drainage structures based on the variability check results, this research developed a rainfall intensity – duration frequency to estimate the design rainfall (mm) at different return periods which was used as input data in HEC-HMS to determine the peak flows at the selected drainage points. The results are shown in Table 4.8

Table 4.8: The Estimated Peak Flows at Different Return Periods at the Drainage Locations

Drainage Points	JP01	JP02	JP03	JP04	JP05	JP06	JP07	JP08	JP09	JP10	JP11	JP12
Area (km^2)	4.6	5.1	10.4	9.1	7.5	18.5	9.6	6.9	7.1	2.5	7.8	3.2
Qp_2yrs (cms)	13.80	14.30	28.90	26.60	17.80	19.80	25.60	16.60	1.30	6.90	17.60	10.80
Qp_5yrs (cms)	19.10	19.80	39.70	36.70	24.60	27.40	35.40	23.10	1.80	9.50	24.80	15.00
Qp_10yrs (cms)	22.60	23.50	47.20	43.50	29.20	32.60	42.10	27.50	2.10	11.30	29.90	17.80
Qp_25yrs (cms)	27.20	28.30	56.80	52.30	35.20	39.20	50.70	33.30	2.60	13.70	36.40	21.50
Qp_50yrs (cms)	30.70	32.00	64.00	59.00	39.70	44.20	57.20	37.60	2.90	15.40	41.30	24.20
Qp_100yrs (cms)	34.20	35.60	71.30	65.60	44.10	49.20	63.70	41.90	3.30	17.20	46.30	27.00
Qp_200yrs (cms)	37.70	39.20	78.60	72.30	48.60	54.30	70.20	46.30	3.60	19.00	51.30	29.70
Qp_500yrs (cms)	42.30	44.10	88.20	81.10	54.60	60.90	78.80	52.10	4.10	21.30	57.90	33.40
Drainage Points	JP13	JP14	JP15	JP16	JP17	JP18	JP19	JP20	JP21	JP22	JP23	JP24
Area (km^2)	3.3	5.7	4.8	3.7	352.9	4	90.9	7.2	17.7	3.8	7.8	15.6
Qp_2yrs (cms)	10.30	17.00	11.20	8.70	52.90	9.40	52.02	13.40	27.00	11.50	17.00	21.90
Qp_5yrs (cms)	14.80	23.90	15.90	12.00	73.08	13.00	71.98	18.50	37.60	15.80	23.40	30.30
Qp_10yrs (cms)	17.90	28.70	19.10	14.30	86.94	15.40	85.75	22.10	44.90	18.80	27.90	36.10
Qp_25yrs (cms)	22.00	35.00	23.20	17.30	104.88	18.60	103.63	26.60	54.30	22.60	33.60	43.60
Qp_50yrs (cms)	25.10	39.70	26.40	19.50	118.44	20.90	117.14	30.10	61.40	25.50	37.90	49.20
Qp_100yrs (cms)	28.20	44.50	29.50	21.70	132.04	23.30	130.72	33.60	68.50	28.40	42.20	54.80
Qp_200yrs (cms)	31.40	49.40	32.70	24.00	145.68	25.70	144.38	37.00	75.60	31.30	46.50	60.40
Qp_500yrs (cms)	35.60	55.80	36.90	26.90	163.84	28.90	162.59	41.70	85.10	35.10	52.20	67.90

Drainage Points	JP25	JP26	JP27	JP28	JP29	JP30	JP31	JP32	JP33	JP34	JP35	JP36
A (km^2)	25.2	35.6	22.5	25.6	125.53	301.8	130	468.7	33.3	875.9	1382.1	8.5
Qp_2yrs (cms)	44.27	43.60	3.91	37.40	44.20	48.50	8.00	65.24	3.70	17.60	147.00	15.70
Qp_5yrs (cms)	61.37	60.20	5.47	51.80	61.20	67.00	11.02	90.15	5.10	24.80	201.00	21.80
Qp_10yrs (cms)	73.15	71.60	6.54	61.60	72.88	79.00	13.09	107.27	6.07	29.90	238.50	25.90
Qp_25yrs (cms)	88.16	86.30	7.93	74.30	88.03	95.50	15.79	129.43	7.31	36.40	286.50	31.20
Qp_50yrs (cms)	99.56	97.40	8.97	83.90	99.48	107.50	17.81	146.12	8.25	41.30	322.50	35.20
Qp_100yrs (cms)	110.96	108.50	10.03	93.50	110.98	119.50	19.82	162.87	9.20	46.30	358.50	39.20
Qp_200yrs (cms)	122.36	119.70	11.08	103.20	122.51	131.50	21.84	179.67	10.14	51.30	394.50	43.20
Qp_500yrs (cms)	137.56	134.50	12.48	116.10	137.85	147.50	24.49	201.93	11.40	57.90	442.50	48.60

Drainage Points	JP37	JP38	JP39	JP40	JP41	JP42	JP43	JP44	JP45	JP46	JP47
Area (km^2)	133.8	3.2	13.6	5.5	38.6	37	6	29.2	23.84	4.2	83.1
Qp_2yrs (cms)	14.23	10.10	24.90	4.44	12.90	55.00	13.30	46.30	7.24	7.10	3.56
Qp_5yrs (cms)	19.80	14.10	34.40	6.12	18.03	75.80	18.40	64.00	10.10	9.90	5.19
Qp_10yrs (cms)	23.62	16.70	41.00	7.29	21.55	90.00	21.80	76.20	12.08	11.80	6.33
Qp_25yrs (cms)	28.57	20.20	49.40	8.76	26.10	108.30	26.30	91.90	14.62	14.20	7.85
Qp_50yrs (cms)	32.29	22.80	55.70	9.90	29.53	122.10	29.60	103.80	16.54	16.00	8.99
Qp_100yrs (cms)	36.04	25.40	62.10	11.01	32.98	135.90	33.00	115.60	18.46	17.90	10.15
Qp_200yrs (cms)	39.79	28.00	68.50	12.12	36.45	149.70	36.30	127.50	20.40	19.70	11.33
Qp_500yrs (cms)	44.78	31.50	76.90	13.62	41.05	168.10	40.80	143.30	22.96	22.10	12.90

4.6 Flood Risk Check

This study assessed the drainage structures that are prone to flooding by comparing the estimated peak flows at 100 years return period with the design flow magnitudes at the same return period extracted from the design documents sourced from ERC. The results of the comparison are presented in Table 4.9.

Table 4.9: Comparison between the Estimated and the Design Peak Flows at 100 years Return Periods at the Drainage Locations

Drainage	Q_{100} Design (cms)	Q_{100} Estimated (cms)	Rmrk	Drainage	Q100 Design (cms)	Q100 Estimated (cms)	Rmrk	Drainage	Q100 Design (cms)	Q100 Estimated (cms)	Rmrk
1	47.75	34.20	*	17	106.90	132.04	**	33	8.20	9.20	**
2	65.55	35.60	*	18	28.58	23.30	*	34	NS	46.30	ND
3	128.30	71.30	*	19	98.00	130.72	**	35	535.00	358.50	*
4	57.80	65.60	**	20	NS	33.60	ND	36	27.60	39.20	**
5	71.00	44.10	*	21	NS	68.50	ND	37	34.30	36.04	**
6	63.00	49.20	*	22	3.90	28.40	**	38	13.20	25.40	*
7	63.00	63.70	*	23	24.28	42.20	**	39	45.20	62.10	**
8	13.15	41.90	**	24	23.40	54.80	**	40	8.53	11.01	**
9	12.60	3.30	*	25	186.20	110.96	*	41	21.30	32.98	**

10	7.37	17.20	**	26	174.00	108.50	*	42	178.90	135.90	*
11	NS	46.30	ND	27	10.50	10.30	*	43	46.00	33.00	*
12	18.16	27.00	**	28	159.50	93.50	*	44	NS	115.60	ND
13	21.00	28.20	**	29	109.96	111.98	**	45	13.10	18.46	**
14	48.00	44.50	*	30	273.30	119.50	*	46	18.88	17.90	**
15	54.00	29.50	*	31	8.20	19.82	**	47	5.40	10.15	**
16	52.00	21.70	*	32	141.40	162.87	**				

*** Not prone to flood risk; **prone to flood risk; ND: Not Determined**

As shown in Table 4.9, about 40% of the drainage structures identified in the study area are likely to experience flooding once every 100 years. However, due to insufficient data regarding the probability distribution that was used to estimate the design flows as extracted from the document, this study, therefore, could not ascertain the outcome of this flood risk investigation.

4.7 Flow Variability's Effects on Scour Depth

Having confirmed that there is flow variability to all the selected drainage structures within the selected section with their high coefficient of variances, this section, therefore, investigated the effects of flow variability on the scouring depth and developed relationships between these two variables for all the drainage structures.

4.7.1 Estimation of Scour Depth

This section is divided into two sub-section with each section dealing separately with slab (open-bottom) culverts and bridge piers. The parameters required are determined in the following sub-sections.

4.7.2 Particle Size Distribution Curves

The following figures are plotted from the subgrade soil test report data sourced from ERC. For the soil test report at JP01 and JP02 locations, the extracted results are tabulated in Table 4.10 while others are in Appendix D. These are used to estimate the D_{50} values at each drainage point for the determination of scour depth. The plotted Particle size distribution curves for soil report data near JP03 and JP12 are shown in Figures 4.15 and 4.16 respectively, for other drainage structure locations are found in Appendix D. Therefore, Table 4.11 summarizes the results of D_{50} for all the drainage structure locations.

Table 4.10: Extracted Soil Test Report near the Culvert 01 and Culvert 02 Locations

Mileage culvert 01	DK0+220	Mileage Culvert 02	DK2+650
Report Date	1/9/2015	Report Date	30/05/2014
Digging Depth	1.9 m	Digging Depth	2.0 m
Sieve Sizes (mm)	Particle Size Passing (%)	Sieve Sizes (mm)	Particle Size Passing (%)

<200	100	<200	100
<60	74.2	<60	44.2
<40	51.2	<40	27.3
<20	38.2	<20	10.9
<10	27.6	<10	5.4
<5	14.5	<5	3.2
<2	6.1	<2	1.8
<1	5.3	<1	1.6
<0.5	3.9	<0.5	1
<0.25	2.8	<0.25	0.8
<0.075	1.8	<0.075	0.3
Uniformity Coefficient Cu	16.05	Uniformity Coefficient Cu	3.42
Coefficient of Curvature Cc	0.9	Coefficient of Curvature Cc	1.57
Particle Density (g/cm^3)	2.51	Particle Density (g/cm^3)	2.61
Sample Description	Grayish yellow, granular Bad Graded Coarse	Sample Description	Grayish yellow, granular
Name of the soil	Breccia	Name of the soil	Bad Graded crushed stone
Group of the Filling Material	B	Group of the Filling Material	B
Conclusion	Meets the design requirements	Conclusion	Meets the design requirements

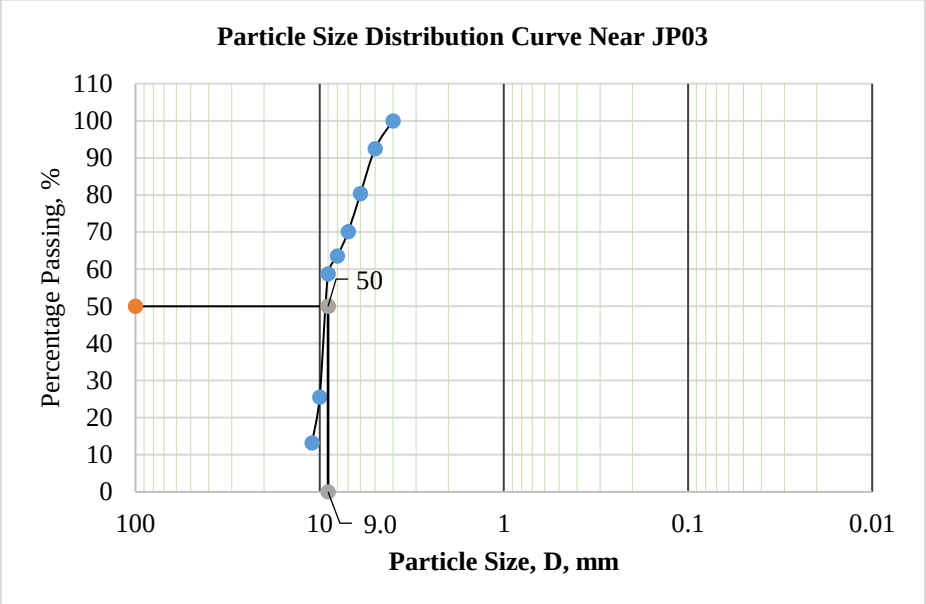

Figure 4.15: Particle Size Distribution Curve for the Subgrade Data at JP03

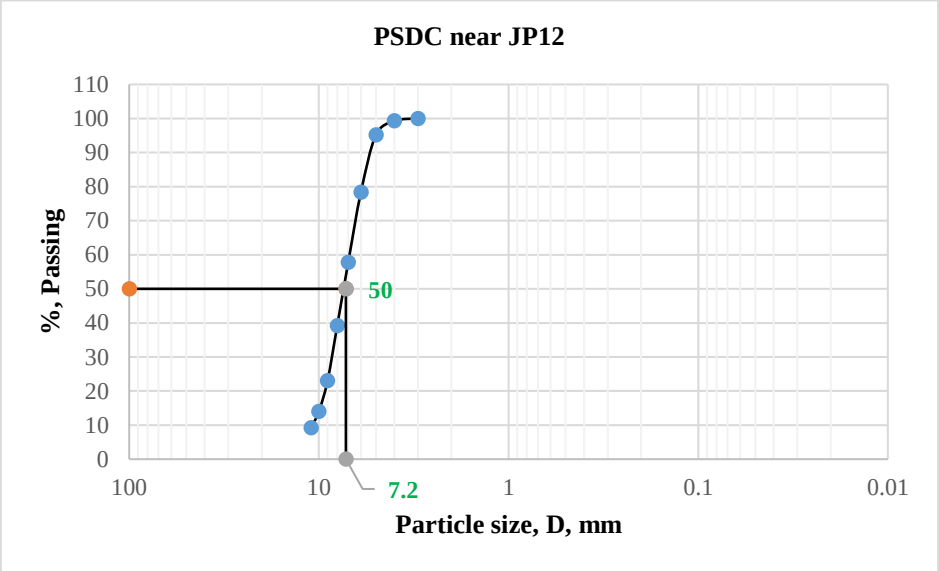

Figure 4.16: Particle Size Distribution Curve for the Subgrade Data at JP12

Table 4.11: Summary table of the Median Particle Size (D50) for the soil materials near the structure locations

Locations	D_{50} (mm)	Locations	D_{50} (mm)	Locations	D_{50} (mm)	Locations	D_{50} (mm)
JP01	7.50	**JP13**	6.31	**JP25**	7.20	**JP37**	6.10
JP02	6.90	**JP14**	9.85	**JP26**	6.30	**JP38**	6.01
JP03	9.00	**JP15**	9.01	**JP27**	7.50	**JP39**	8.10
JP04	6.25	**JP16**	8.00	**JP28**	6.20	**JP40**	9.02
JP05	6.00	**JP17**	6.30	**JP29**	5.90	**JP41**	6.40
JP06	6.90	**JP18**	11.00	**JP30**	6.10	**JP42**	6.40
JP07	6.50	**JP19**	8.50	**JP31**	6.50	**JP43**	6.40
JP08	7.00	**JP20**	9.00	**JP32**	6.05	**JP44**	6.10
JP09	6.10	**JP21**	6.95	**JP33**	7.10	**JP45**	6.10
JP10	5.90	**JP22**	6.71	**JP34**	10.30	**JP46**	10.30
JP11	5.70	**JP23**	7.30	**JP35**	10.00	**JP47**	10.50
JP12	7.20	**JP24**	6.80	**JP36**	5.98		

4.7.3 Manning's Roughness Values (n)

The manning's roughness coefficients for the channels at drainage structure locations are presented in Table 4.12:

Table 4.12: Estimated Manning's coefficients at the drainage structure locations

Locations	D_{50}(mm)	$n = 0.0132(D50)^{1/6}$	Locations	D_{50}(mm)	$n = 0.0132(D50)^{1/6}$
JP01	7.50	0.01650	**JP25**	7.20	0.01584
JP02	6.90	0.01518	**JP26**	6.30	0.01386
JP03	9.00	0.01980	**JP27**	7.50	0.01650
JP04	6.25	0.01375	**JP28**	6.20	0.01364

JP05	6.00	0.01320	**JP29**	5.90	0.01298
JP06	6.90	0.01518	**JP30**	6.10	0.01342
JP07	6.50	0.01430	**JP31**	6.50	0.01430
JP08	7.00	0.01540	**JP32**	6.05	0.01331
JP09	6.10	0.01342	**JP33**	7.10	0.01562
JP10	5.90	0.01298	**JP34**	10.30	0.02266
JP11	5.70	0.01254	**JP35**	10.00	0.02200
JP12	7.20	0.01584	**JP36**	5.98	0.01316
JP13	6.31	0.01388	**JP37**	6.10	0.01342
JP14	9.85	0.02167	**JP38**	6.01	0.01322
JP15	9.01	0.01982	**JP39**	8.10	0.01782
JP16	8.00	0.01760	**JP40**	9.02	0.01984
JP17	6.30	0.01386	**JP41**	6.40	0.01408
JP18	11.00	0.02420	**JP42**	6.40	0.01408
JP19	8.50	0.01870	**JP43**	6.40	0.01408
JP20	9.00	0.01980	**JP44**	6.10	0.01342
JP21	6.95	0.01529	**JP45**	6.10	0.01342
JP22	6.71	0.01476	**JP46**	10.30	0.02266
JP23	7.30	0.01606	**JP47**	10.50	0.02310
JP24	6.80	0.01496			

4.7.4 The angle of Attack (θ) and Correction Factor "B"

The angle of attack (θ) is one of the basic parameters for the estimation of scour depth around bridge piers. The angle of attack of the flow direction to the pier location is directly measured from the as-built drawings of each bridge section. The samples of the sourced drawing are shown in Appendix E. The results are summarized in Table 4.13.

Table 4.13: Summary table for the angles of attack and the correction factor "B"

Label	θ	$B=(\cos\theta + (L/a)*\sin\theta)^{0.65}$
JP11	64.47	2.29
JP19	54.60	1.40
JP25	61.43	2.18
JP26	106.50	1.90
JP28	105.27	1.45
JP30	126.67	0.94
JP34	115.69	1.16
JP35	102.60	0.99
JP36	121.87	0.48
JP37	96.27	1.99
JP38	84.05	2.62
JP39	95.21	2.04
JP40	84.05	2.62
JP41	64.47	2.29
JP42	54.60	1.40
JP43	61.43	2.18

JP44	106.50	1.90	

4.7.5 Bridge Piers Scour Depth

This study exclusively focused on bridge piers of the bridge sections within the selected section. So, to determine the bridge pier scour depth using the HEC-18 formula as expressed in equation 3.9, Tables 4.14 - 4.16 show the values of each component parameter. Figure 4.17 is a representation of bridge piers which was snapped during one of the site visitations by the researcher. All the piers within the selected section are rounded noses and constructed on pile foundations with varied dimensions.

Figure 4.17: Railway bridge piers snapped during site-visitation

Table 4.14: Input parameters values at each Pier Location for HEC-18 formula

Label	Structure	θ	L/a	$B = (\cos\theta + L/a\sin\theta)^{0.65}$
JP35	Mojo-Adama No.1 Bridge	64.47	3.50	2.29
JP36	Mojo-Adama No.2 Bridge	54.60	1.36	1.40
JP37	Mojo-Adama No.3 Bridge	61.43	3.22	2.18
JP38	Mojo-Adama No.4 Bridge	106.50	3.10	1.90
JP39	Mojo-Adama No.5 Bridge	126.67	1.87	0.94

JP40	Mojo-Adama No.6 Bridge	102.60	1.23	0.99
JP41	Mojo_Adama No.7 Bridge	121.87	1.00	0.48
JP42	Mojo-Adama N0.8 Bridge	96.27	3.00	1.99
JP43	Mojo-Adama No.10 Bridge	95.21	3.10	2.04
JP44	Mojo-Adama No.12 Bridge	84.05	4.33	2.62

Table 4.15: Input parameters values at each Pier Location for HEC-18 formula

Locations	Pier #	Pier Length (L), m	Pier width (w), m	Foundation depth (m), m	Channel width (m)	L/w
JP35	#6	8.4	2.4	30	8.78	3.5
JP36	#0	7.8	5.75	38	2.02	1.36
JP37	#1	8.7	2.7	11	13.51	3.22
JP38	#2	9.0	2.9	32	5.21	3.1
JP39	#6	10.1	5.4	41.5	5.53	1.87
JP40	#1	8.0	6.5	29	13.49	1.23
JP41	#1	8.0	8.0	41	3.9	1.0
JP42	#2	10.2	3.4	27	3.2	3.0
JP43	#1	9.0	2.9	39	2.21	3.1
JP44	#4	7.8	1.8	30	2.7	4.33

Table 4.16: Input parameters values at each Pier Location for HEC-18 formula

Bridge Piers Location	A (Round Nose)	B (θ)	C (Clear-water scour)
#6	1.0	2.29	1.1
#0	1.0	1.40	1.1
#1	1.0	2.18	1.1
#2	1.0	1.90	1.1
#5	1.0	1.45	1.1
#6	1.0	0.94	1.1
#8	1.0	1.16	1.1
#1	1.0	0.99	1.1
#1	1.0	0.48	1.1
#2	1.0	1.99	1.1
#4	1.0	2.62	1.1
#1	1.0	2.04	1.1
#4	1.0	2.62	1.1

Therefore, substituting the values in Table 4.16 into equation 3.9 for each bridge pier, their corresponding scours depths and flow characteristics are presented in Tables 4.17 and 4.18 for bridge piers at K93+921.63 and K95+965.11 corresponding to JP35 and JP36 respectively while Table 4.19 gives the summary for other bridge piers. Other results are in Appendix F.

Table 4.17: Mojo-Adama No. 1 Simple Supported T Beam Bridge; Location: K93+921.63; Size: 2(8x32)m No.1 DLMB

JP35

T(yrs)	Peak Q(cms)	Yo(m)	Vn(m/s)	A(m^2)	Yc (m)	Vc (m/s)	Vc/Vn	Fr	Ys/Yo	Ys (m)	Risk FPR = Ys/fd	Risk (%)
2	147	3.42	4.914	29.915	9.590	9.699	1.974	0.848	2.111	7.218	0.241	24.1
5	201	4.31	5.334	37.683	17.930	13.263	2.486	0.821	1.791	7.714	0.257	25.7
10	238.5	4.90	5.563	42.873	25.245	15.737	2.829	0.802	1.631	7.993	0.266	26.6
25	286.5	5.64	5.805	49.354	36.429	18.904	3.257	0.780	1.471	8.297	0.277	27.7
50	322.5	6.19	5.959	54.120	46.159	21.279	3.571	0.765	1.373	8.496	0.283	28.3
100	358.5	6.72	6.094	58.828	57.039	23.655	3.882	0.750	1.290	8.675	0.289	28.9
200	394.5	7.26	6.214	63.486	69.070	26.030	4.189	0.737	1.218	8.839	0.295	29.5
500	442.5	7.96	6.356	69.619	86.900	29.197	4.594	0.719	1.136	9.037	0.301	30.1

Table 4.18: Mojo-Adama No. 3 Simple Supported T Beam Bridge; Location: K95+965.11; Size: 2(1x32)m No.6 DLMdB

JP36

T(yrs)	Peak Q(cms)	Yo(m)	Vn(m/s)	A(m^2)	Yc (m)	Vc (m/s)	Vc/Vn	Fr	Ys/Yo	Ys (m)	Risk FPR = Ys/fd	Risk (%)
2	15.7	1.444	4.18	3.755	1.239	3.486	0.834	1.111	2.538	3.665	0.096	9.6
5	21.8	1.861	4.51	4.838	2.389	4.841	1.074	1.055	2.104	3.916	0.103	10.3
10	25.9	2.133	4.67	5.546	3.372	5.751	1.232	1.021	1.899	4.051	0.107	10.7
25	31.2	2.478	4.84	6.444	4.893	6.928	1.431	0.982	1.694	4.199	0.110	11.0
50	35.2	2.735	4.95	7.111	6.228	7.816	1.579	0.956	1.571	4.295	0.113	11.3
100	39.2	2.990	5.04	7.775	7.724	8.705	1.726	0.931	1.466	4.382	0.115	11.5
200	43.2	3.243	5.12	8.433	9.381	9.593	1.873	0.908	1.376	4.461	0.117	11.7
500	48.6	3.582	5.22	9.314	11.872	10.792	2.068	0.880	1.272	4.557	0.120	12.0

Table 4.19: Summary of the estimated peak flows at different return periods for the selected Simply Supported Bridge Locations

		Scour Risk (%) vs Return Period							
Drainage Points	**Drainage Area (km2)**	**2**	**5**	**10**	**25**	**50**	**100**	**200**	**500**
JP35	1382.10	24.06	25.71	26.64	27.66	28.32	28.92	29.46	30.12
JP36	8.50	9.64	10.31	10.66	11.05	11.30	11.53	11.74	11.99
JP37	133.80	48.37	52.40	54.65	57.20	58.89	60.43	61.86	63.59
JP38	3.20	14.24	15.45	16.09	16.85	17.34	17.79	18.21	18.72
JP39	13.60	5.47	5.88	6.11	6.37	6.53	6.68	6.82	6.99
JP40	5.50	7.74	8.31	8.63	8.98	9.21	9.42	9.61	9.84
JP41	38.60	2.68	2.91	3.04	3.19	3.29	3.38	3.46	3.56
JP42	37.00	26.62	28.62	29.72	30.95	31.75	32.49	33.16	33.97
JP43	6.00	14.03	15.09	15.66	16.31	16.73	17.12	17.47	17.90
JP44	29.20	31.83	34.30	35.69	37.22	38.24	39.16	40.01	41.03

From Table 4.19, it is seen that the maximum associated risks for the piers at JP35 to JP44 have been estimated to about 30.12%, 11.99%, 63.59%, 18.72%, 6.99%, 9.84%, 3.56%, 33.97%, 17.90%, and 41.03% respectively. Thus, JP37 and JP41 are with the highest and the least scour risks respectively.

4.7.6 Frame Bridge Scour Depth

This sub-section summarizes the estimated scour depth results at the frame bridge locations. Tables 4.20 and 4.21 show the results for the JP11 and JP34 while Table 4.22 summarizes the estimated scour depth (m) at the other frame bridge locations.

Table 4.20: Frame Bridge; Location: K17+024.07; Size: 1-14.0x3.5m

JP11										
T(yrs)	Peak Q(cms)	Yo(m)	Vn(m/s)	A(m^2)	Yc (m)	Vc (m/s)	Vc/Vn	Fr	Ymax (m)	Ys (m)
2	17.6	0.751	2.823	6.235	0.164	1.270	0.450	1.040	1.412	0.661
5	24.8	0.929	3.188	7.779	0.327	1.790	0.561	1.056	1.699	0.770
10	29.9	1.044	3.402	8.789	0.475	2.158	0.634	1.063	1.879	0.835
25	36.4	1.181	3.639	10.003	0.703	2.627	0.722	1.069	2.090	0.909
50	41.3	1.278	3.797	10.877	0.906	2.981	0.785	1.072	2.238	0.960
100	46.3	1.373	3.945	11.736	1.138	3.341	0.847	1.075	2.380	1.007
200	51.3	1.464	4.081	12.570	1.397	3.702	0.907	1.077	2.516	1.052
500	57.9	1.58	4.246	13.636	1.780	4.179	0.984	1.078	2.685	1.105

Table 4.21: Frame Bridge; Location: K91+308.46; Size: 2(1-12.0x5.5)m

JP34										
T(yrs)	Peak Q(cms)	Yo(m)	Vn(m/s)	A(m^2)	Yc (m)	Vc (m/s)	Vc/Vn	Fr	Ymax (m)	Ys (m)
2	17.6	0.751	2.823	6.235	0.164	1.270	0.450	1.040	1.412	0.661
5	24.8	0.929	3.188	7.779	0.327	1.790	0.561	1.056	1.699	0.770
10	29.9	1.044	3.402	8.789	0.475	2.158	0.634	1.063	1.879	0.835
25	36.4	1.181	3.639	10.003	0.703	2.627	0.722	1.069	2.090	0.909
50	41.3	1.278	3.797	10.877	0.906	2.981	0.785	1.072	2.238	0.960
100	46.3	1.373	3.945	11.736	1.138	3.341	0.847	1.075	2.380	1.007
200	51.3	1.464	4.081	12.570	1.397	3.702	0.907	1.077	2.516	1.052
500	57.9	1.58	4.246	13.636	1.780	4.179	0.984	1.078	2.685	1.105

Table 4.22: Summary of the estimated scour depths (m) at different return periods for the selected Frame Bridge Locations

		Scour Depth (m) Vs Return Period							
Drainage Points	**Drainage Area (km^2)**	**2**	**5**	**10**	**25**	**50**	**100**	**200**	**500**
JP11	7.8	0.66	0.77	0.84	0.91	0.96	1.01	1.05	1.11
JP19	90.9	0.50	0.53	0.54	0.55	0.55	0.56	0.56	0.56
JP25	25.2	1.21	1.43	1.57	1.73	1.84	1.95	2.05	2.18
JP26	35.6	1.33	1.57	1.72	1.90	2.02	2.14	2.25	2.39
JP28	25.6	1.36	1.61	1.76	1.94	2.06	2.18	2.29	2.43
JP30	301.8	1.19	1.40	1.52	1.68	1.78	1.88	1.97	2.09
JP34	875.9	0.66	0.77	0.84	0.91	0.96	1.01	1.05	1.11

From the summary results in Table 4.22, it is seen that the frame bridges at the location JP28 and JP19 have the highest and the lowest estimated scour depth (m) respectively; ranging from 0.5m – 0.56m and 1.36m – 2.43m for 2yrs – 500yrs return periods respectively.

4.7.7 Slab Culvert Scour Depth

This sub-section highlights the scour depth results for the open-bottom culverts portion of the hydraulic structures within the selected section of the Ethio – Djibouti Railway Line using equation 3.7. The results are tabulated in Tables 4.23 and 4.24 for JP07 and JP09. Others are in Appendix F. Table 4.25 gives the summary of the estimated scour depths at different return periods for all the selected slab box culverts.

Table 4.23: Structure Type: Slab Culvert; Location: K11+096.07; Size: 6.0m x 5.0m; Culvert Length: 28.74m

JP07										
T(yrs)	Peak Q(cms)	Yo(m)	Vn(m/s)	A(m^2)	Yc (m)	Vc (m/s)	Vc/Vn	Fr	Ymax (m)	Ys (m)
2	25.6	0.996	4.284	5.976	0.619	2.463	0.575	1.371	1.800	0.804
5	35.4	1.239	4.763	7.432	1.183	3.406	0.715	1.366	2.144	0.905
10	42.1	1.394	5.032	8.366	1.673	4.051	0.805	1.361	2.355	0.961
25	50.7	1.586	5.329	9.514	2.426	4.879	0.915	1.351	2.603	1.017
50	57.2	1.725	5.526	10.351	3.088	5.504	0.996	1.343	2.779	1.054
100	63.7	1.861	5.704	11.168	3.830	6.130	1.075	1.335	2.945	1.084
200	70.2	1.995	5.866	11.967	4.651	6.755	1.152	1.326	3.104	1.109
500	78.8	2.167	6.061	13.001	5.861	7.583	1.251	1.315	3.303	1.136

Table 4.24: Structure Type: Slab Culvert; Location: K14+281.07; Size: 3.0m x 3.5m; Culvert Length: 15.8m

JP09										
T(yrs)	Peak Q(cms)	Yo(m)	Vn(m/s)	A(m^2)	Yc (m)	Vc (m/s)	Vc/Vn	Fr	Ymax (m)	Ys (m)
2	1.3	0.184	2.35	0.553	0.006	0.250	0.106	1.751	0.438	0.254
5	1.8	0.226	2.65	0.679	0.012	0.346	0.131	1.781	0.523	0.297
10	2.1	0.249	2.81	0.748	0.017	0.404	0.144	1.795	0.568	0.319
25	2.6	0.286	3.03	0.858	0.026	0.500	0.165	1.810	0.637	0.351
50	2.9	0.307	3.15	0.920	0.032	0.558	0.177	1.816	0.676	0.369
100	3.3	0.333	3.30	1.000	0.041	0.635	0.192	1.826	0.725	0.392
200	3.6	0.353	3.40	1.058	0.049	0.693	0.204	1.828	0.760	0.407
500	4.1	0.384	3.56	1.152	0.063	0.789	0.222	1.834	0.815	0.431

Table 4.25: Summary of the estimated scour depths (m) at different return periods for the selected slab culverts Locations

Drainage Points	**Drainage Area (km^2)**	**Scour Depth (m) vs Return Period (cms)**							
		2	**5**	**10**	**25**	**50**	**100**	**200**	**500**
JP01	4.60	0.880	1.026	1.110	1.207	1.275	1.337	1.396	1.466
JP02	5.10	1.123	1.327	1.449	1.594	1.698	1.792	1.882	1.998
JP03	10.40	1.052	1.217	1.316	1.428	1.503	1.574	1.639	1.719
JP04	9.10	1.366	1.600	1.737	1.897	2.010	2.112	2.211	2.332
JP05	7.50	1.143	1.349	1.471	1.618	1.718	1.811	1.902	2.016
JP06	18.50	1.066	1.252	1.363	1.491	1.580	1.664	1.744	1.841
JP07	9.60	0.804	0.905	0.961	1.017	1.054	1.084	1.109	1.136
JP08	6.90	0.879	0.998	1.062	1.130	1.172	1.208	1.240	1.273
JP09	7.10	0.254	0.297	0.319	0.351	0.369	0.392	0.407	0.431
JP10	2.50	0.547	0.621	0.663	0.709	0.738	0.764	0.787	0.812
JP12	3.20	0.732	0.841	0.901	0.969	1.012	1.052	1.087	1.129
JP13	3.30	0.993	1.190	1.308	1.447	1.543	1.633	1.719	1.826

JP14	5.70	0.723	0.829	0.887	0.951	0.991	1.026	1.057	1.092
JP15	4.80	0.585	0.688	0.747	0.813	0.860	0.901	0.941	0.989
JP16	3.70	0.520	0.603	0.653	0.710	0.748	0.784	0.818	0.858
JP17	352.90	1.078	1.235	1.325	1.426	1.494	1.555	1.611	1.676
JP18	4.00	0.238	0.240	0.235	0.222	0.209	0.194	0.176	0.150
JP21	17.70	0.780	0.863	0.902	0.939	0.958	0.970	0.977	0.979
JP23	7.80	0.434	0.416	0.389	0.341	0.297	0.247	0.193	0.113
JP24	15.60	0.941	1.046	1.099	1.150	1.178	1.198	1.212	1.222
JP27	22.50	0.348	0.385	0.402	0.418	0.426	0.431	0.433	0.434
JP29	125.53	1.413	1.663	1.813	1.989	2.112	2.227	2.337	2.474
JP45	23.84	0.661	0.779	0.850	0.932	0.990	1.042	1.093	1.155
JP46	4.20	0.478	0.558	0.605	0.658	0.693	0.728	0.760	0.799

4.7.8 Scour Depth Comparisons

This sub-section compares the estimated scour depth (m) and scour risks (%) for the selected drainage structures using the design flow magnitudes extracted from the design document sourced from ERC and the estimated peak flow magnitudes both at 100 years return period. The results are presented in Tables 4.26, 4.27, and 4.28 for the slab culverts, frame bridges, the bridge piers respectively.

Table 4.26: Comparison between the estimated scour depths (m) at different slab culverts Locations for 100 years return period

Drainage	**Q_{100} Design (cms)**	**Q_{100} estimated (cms)**	**Ys Q_{100}_Design (m)**	**Ys Q_{100} estimated (m)**
1	47.75	34.20	1.543**	1.337
2	65.55	35.60	2.112**	1.557
3	128.30	71.30	1.988**	1.574
4	57.80	65.60	1.990	2.112**
5	71.00	44.10	2.296**	1.811
6	63.00	49.20	1.871**	1.664
7	63.00	63.70	1.080	1.084**
8	13.15	41.90	0.800	1.208**
9	12.60	3.30	0.676**	0.392
10	7.37	17.20	0.562	0.764**
12	18.16	27.00	0.908	1.052**
13	21.00	28.20	1.414	1.633**
14	48.00	44.50	1.049**	1.026
15	54.00	29.50	1.148**	0.901
16	52.00	21.70	1.108**	0.784
17	106.90	132.04	1.437	1.555**
18	28.58	23.30	0.152	0.194**
21	NS	68.50	ND	0.970
23	24.28	42.20	0.411**	0.247
24	23.40	54.80	0.962	1.198**
27	10.50	10.30	0.491**	0.490
29	109.96	111.98	2.218	2.238**
45	13.10	18.46	0.768	0.888**
46	18.88	17.90	0.746**	0.728

**Higher scour depth values relative to other; ND: Not Determined; NS: Not Stated

Table 4.27: Comparison between the estimated scour depths (m) at different Frame Bridge Locations for 100 years return period

Drainage	Q_{100} Design (cms)	Q_{100} estimated (cms)	Ys_Design (m)	Ys_Estimated (m)
11	NS	46.30	ND	1.010
19	98.00	130.72*	0.803	0.822**
25	186.20*	110.96	2.546	1.949
26	174.00*	108.50	2.737**	2.138
28	159.50*	93.50	2.807**	2.153
30	273.30*	119.50	2.843**	1.878
34	NS	46.30	ND	0.272

* Higher peak value; **higher scour depth values relative to other; ND: Not Determined; NS: Not Stated

Table 4.28: Comparison between the estimated scour depths (m) at different Bridge Pier Locations for 100 years return period

Drainage	Q_{100} Design (cms)	Q_{100} estimated (cms)	Risk_Design (%)	Risk_Estimated (%)
35	535.00*	358.50	31.22**	28.92
36	27.60	39.20*	10.79	11.53**
37	34.30	36.04*	59.73	60.43**
38	13.20	25.40*	15.13	17.71**
39	45.20	62.10*	6.29	6.73**
40	8.53	11.01*	8.93	9.42**
41	21.30	32.98*	3.03	3.38**
42	178.90*	135.90	30.97**	29.24
43	46.00*	33.00	19.04**	17.92
44	NS	115.60	ND	41.52

* Higher peak value; **higher pier scour risk relative to other; ND: Not Determined; NS: Not Stated

From Table 4.28, it is observed that the bridge pier at location K97+817.22 has the highest scour risk of about 60.43% while the bridge pier at location K106+271.0 has the least scour risk of about 3.38%. Thus, the bed materials around the bridge pier at location K97+817.22 need to be protected with riprap with the diameter designed as follows.

4.7.9 Riprap Material Size Determination

Since the scour risk around the bridge at location K97+817.22 seems to be high (about 60.43%), this study proposed the use of riprap for protecting the surface of the bed material, and the median stone diameter was estimated using Equation 4.21. The result is shown as follows;

$D_{50} = 0.692[KV^2]/ [(S_s-1)*2G]$

K = 1.5 (rounded-nose pier)

V_1 = 7.03 m/s (for the estimated Q_{100})

V_2 = 6.914 m/s (for the designed Q_{100})

S_s = 2.65

$G = 9.81\ m/s^2$

For the estimated Q_{100}

$D_{50} = 0.692*[1.5*7.03^2]/[(2.65 – 1)*2*9.81]$

$D_{50} = 1.58$ m

For the designed Q_{100}

$D_{50} = 0.692*[1.5*6.914^2]/[(2.65 – 1)*2*9.81]$

$D_{50} = 1.53$ m

4.8 Relation Equation Development

There are three different structure types identified within the study, however, an equation that shows the relationships between the flow variability and the scour depths was generated only for sab culvert structure type using the linear regression model. To generate these representative equations, this study used both univariate and multiple linear regression methods as demonstrated in the following sub-sections.

4.8.1 Slab Culverts

The variables used are the estimated and the design peak flows at 100 years return period (flow variability) and the estimated scour depths at all the identified locations. Of the 30 slab culverts, 17 were used for generating equations while the remaining 13 were used for validations as shown in Tables 4.29 – 4.31. Also, two trials were performed for each scenario.

Table 4.29: Regression Statistics for the Slab Culverts

Regression Statistics				
	Design Q_{100}		Estimated Q_{100}	
	1st Trial	2nd Trial	1st Trial	2nd Trial
Multiple R	0.663	0.694	0.552	0.758
R Square	0.439	0.482	0.305	0.575
Adjusted R Square	0.402	0.447	0.258	0.555
Standard Error	0.467	0.449	0.441	0.418
Observations	17	17	17	17

From Table 4.29, the results of R^2 and adjusted R^2 indicated that about 50% and above of the dependent variables (Scour depths) are explained by the independent variables (peak flows) for the slab culverts.

Table 4.30: ANOVA Output for the Slab Culverts

ANOVA										
		df	SS_1	SS_2	MS_1	MS_2	F_1	F_2	*sig.* $_1$	*sig.* $_2$
Design Q_{100}	Regression	1	2.57	4.96	2.57	4.96	11.75	28.40	0.004	0.000
	Residual	15	3.28	3.67	0.22	0.17				
	Total	16	5.84	8.63						
Estimated Q_{100}	Regression	1	1.28	2.82	1.28	2.82	6.57	13.95	0.022	0.002
	Residual	15	2.92	3.03	0.19	0.20				
	Total	16	4.20	5.84						

The results of ANOVA for all the structure types as shown in Table 4.30 are statistically significant, sig. < 0.05 and 0.01 at 95%, and 99% confidence intervals respectively, indicating the suitability of the linear regression model for establishing the relationships between the peak flows (independent variable) and the scour depths (dependent variable).

Table 4.31: Multiple Regression Coefficients for the Slab Culverts

		Coefficients	*SError*	*t Stat*	*P-value*
Design Q_{100}	Intercept	0.690	0.212	3.25	0.0054
	Q(cms)	0.012	0.004	3.43	0.0037
	Intercept	-0.622	0.527	-1.18	0.0256
	LnQ	0.524	0.140	3.73	0.0020
Estimated Q_{100}	Intercept	0.797	0.195	4.08	0.0010
	Q(cms)	0.097	0.004	2.56	0.0216
	Intercept	0.568	0.148	3.84	0.0009
	Q (cms)	0.014	0.003	5.33	0.0000

As shown in Table 4.31, in all the cases the results are statistically significant. Indicating the suitability of the univariate linear regression model for the establishment of the relationships between the dependent and independent variables for the slab culverts. Therefore, Table 4.32 summarizes the general equations for both scenarios of 100 years peak flows for the slab culverts.

Also, the performances of these equations were checked by calculating the Nash-Sutcliff Efficiency (NSE) and the coefficient of determination (R^2).

Table 4.32: Equation Evaluation Results for the Slab Culverts

	Trial	Equation	NSE	R^2
Design Q_{100}	1	Ys = 0.69 + 0.0122Q	**0.77**	**0.90**
	2	Ys = -0.622 + 0.524LnQ	0.73	0.81
Estimated Q_{100}	1	Ys = 0.797 + 0.097Q	0.49	0.73
	2	Ys = 0.568 + 0.014Q	**0.82**	**0.83**

This follows that the scour depths can be estimated using equations 4.1 and 4.2 for when the peak flows (from the design document or estimated) at 100 years return period are available.

$$\mathbf{Ys = 0.69 + 0.0122Q} \qquad \textbf{Eq. (4.1)}$$

$$\mathbf{Ys = 0.568 + 0.014Q} \qquad \textbf{Eq. (4.2)}$$

Where;

Y_s = Scour depth (m)

Q = Peak Flow variability (Q_{100}), (m^3/s)

Ln = Natural Log

Chapter 5: CONCLUSIONS AND RECOMMENDATIONS

5.1 Conclusions

In line with the goal of this study which was to investigate the flow variability and its effects on scouring at the bridge piers and culverts within the Sebeta – Adama Section of the Ethio – Djibouti Railway Line, the following conclusions can be made:

The hydrological processes in the study area are well simulated and capable of predicting future flows as the overall performance of the model is excellent. This is seen when the calculated NSE, the PBIAS, and the R^2 are respectively > 0.5, < $\pm$ 20%, and approaching + 1.0 which are within the statistically acceptable range for surface runoff model calibration.

This study also concludes from the results that there is flow variability in all the selected drainage structures since the coefficient of variance is very high for all the junction points (ranges from 0.645 to 1.034).

The study has also developed Rainfall (mm) Duration Frequency and Rainfall Intensity (mm/hr) – Duration Frequency Curves for the selected catchment which could also supplement an existing one in the ERA 2013 manual.

The results of the comparison between the estimated peak flows and the designed peak flow extracted from the design documents, Q_{100} (m^3/s), show that about 40% of the drainage structure are likely to experience flooding once every 100 years. However, this could only be true if and only if the probability distribution used for peak flow estimation is the same as that used for the design of peak flows in the document.

The results of scour depth comparison for all the structure types indicated that the flow variability (in peak flows) has an effect on scouring depths and it varies at different return periods.

Also, this study has attempted to estimate the median stone size for riprap materials as a mitigating measure to ameliorate the high risk of scouring (about 60%) estimated around a pier at bridge location K97+817.22 (Mojo-Adama No.3 Bridge). This value was found to be about 1.58 m.

Thereafter, this study has generated some relationship equations for the slab culverts and was evaluated by calculating the NSE and R^2. The results show that NSE and R^2 are (0.77, 0.90) and (0.82, 0.83) for scenario 1 (Estimated Q_{100}) and scenario 2 (Design Q_{100}) respectively.

5.2 Recommendations

Within the scope, the results and discussions, and the conclusions of this study, therefore, the following recommendations are suggested:

This study recommends the developed IDF curve specifically for the catchment considered in this research as a supplement to an existing IDF curve in ERA 2013 manual for subsequent studies. Also, that flood protection measures be put in place to ameliorate any flooding effects especially at the drainage structures prone to flooding as identified in this study.

This study again recommends that the bed materials around the bridge pier located at K97+817.22 be protected to mitigate the scouring risk as estimated in this research. In addition to this, there are other flow variability effects such as sediment transport, backwater effect, flooding, etc, this study also suggests that as a form of research gap that other researchers can investigate it.

This study, therefore, recommends the use of the scour depth equations generated in other areas provided that the information about the flow variabilities are available to estimate the scour depths at other slab culverts along the Ethio – Djibouti Railway Line.

REFERENCES

[1] Z. Dvorak, M. Luskova, D. Rehak and S. Slivkova, "Criticality Assessment of Railway Bridges. In Gopalakrishnan K., Prentkovskis O., Jackiva I., Junevicius R. (eds)," in *TRANSBALTICA XI: Transportation Science and Technology. TRANSBALTICA 2019. Lecture Notes in Intelligent Transportation and Infrastructure.*, Cham., 2020.

[2] L. Hofreiter, K. Boc, S. Jangl, T. Lovecek, V. Mach, M. Seidl, P. Selinger, and A. Velas, Protection of critical transport infrastructure objects. Monograph 1st edn, Zilina: EDIS University of Zilina, 2013.

[3] Z. Dvorak, M. Cizlak, B. Leitner, R. Sousek and E. Sventekova, Risk Management in Rail Transport, Monograph. 1st edn., Pardubice: Institute of Jan Perner, 2010.

[4] B. M. Nikola, J. P. Zdenka, P. P. Andrey, M. L. Luka and V. Z. Andrey, "Management of Stresses in the Rails on Railway Bridges," *FEM Transactions*, pp. 636-643, 2018.

[5] MICR, "Threat analysis for the Czech Republic: Final Report.," Approved by Resolution of the Government of the Czech Republic of 27 April, 2016, no. 369, 9 pp., Czech Republic, 2015.

[6] D. R. Mohapatra, "An Economic Analysis of Djibouti - Ethiopia Railway Project," *European Academic Research*, pp. 11376 - 11400, 2016.

[7] A. Taju, "Ethio-Djibouti Railway Line Modernization Project," Pandit Deendayal Petroleum University, School of Technology, Ethiopia, 2020.

[8] M. R. Namaee and J. Sui, "Effects of ice cover on the incipient motion of bed material and shear stress around side-by-side bridge piers," *Cold Regions Science and Technology*, pp. 1 - 14, 2019.

[9] Y. Shuaixing, H. Siming, D. Yu, L. Wei, W. Dongpo and S. Fei, "A reliability-based approach for the impact vulnerability assessment of brdige piers subjected to debris flows," *Engineering Geology*, pp. 1 - 14, 2020.

[10] P. F. Lagasse, L. W. Zevenbergen and L. G. Girard, Countermeasures to Protect Bridge Piers from Scour, Washington D. C: Transportation Research Board, 2007.

[11] J. Thornes, M. Rennie, H. Marsden and L. Chapman, Climate Risk Assessment for the Transport Sector, Defra, 2012.

[12] H. Dikanski, B. Imam and A. Hagen-Zanker, "Effects of uncertain asset stock data on the assessment of climate change risks: A case study of bridge scour in the UK," *Structural Safety*, pp. 1-12, 2018.

[13] H. Shen, V. Schneider and S. Karaki, "Local scour around bridge piers," *J. Hydraul. Div.*, pp. 1919-1940, 1969.

[14] J. I. Briaud, P. Gardoni and C. Yao, Bridge scour. Geotech, News: BiTech Publishers Ltd, 2006.

[15] K. Wardhana and F. C. Hadipriono, "Analysis of recent bridge failures in the United States," *J. Perform. Constr. Facil.*, pp. 144 - 150, 2003.

[16] A. Keno, "Flood Risk Mapping (Casse Study of Ketar Watershed Ziway-Dugda Woreda, Ethiopia," Addis Ababa University, Addis Ababa, 2020.

[17] J. R. Choudhury and A. Hasnat, "Bridge collapses around the world: Causes and mechanisms," in *Joint Conference on Advances in Bridge Engineerng-III*, Bangladesh, 2015.

[18] C.-W. Feng, H.-Y. Huang and S.-H. Ju, "Integrating Finite Element Method with GAs to Estimate the Scour Depth of Bridge," *LACSIT International Journal of Engineering and Technology.*, pp. 2-5, 2013.

[19] Z. Kalantari, S. C. Santos Ferreira, J. A. Koutsouris, A. Ahlmer, A. Cerda and G. Destouni, "Assessing flood probability for transportation infrastructure based on catchment characteristics, sediment connectivity and remotely sensed soil moisture," *Science of the Total Environment*, pp. 393-406, 2019.

[20] L.-R. Lagadec, L. Moulin, I. Braud, C. Blandine and P. Breil, "A surface runoff mapping method for optimzing risk assessment on railways," *Safety Science*, pp. 253-267, 2018.

[21] W. Xiong, C. S. Cai, B. Kong and J. Ye, "Overtuning-Collapse Modeling and Safety Assessment for Bridges Supported by Single-Column Piers," *J. Bridge Eng.*, pp. 2-14, 2017.

[22] J. Vican, J. Gocal, J. Odrobinak and P. Kotes, "Analysis of existing steel railway bridges. Procedia Engineering," in *9th International Conference "Bridges in Danube Basin 2016", BDB 2016*, Danube, 2016a.

[23] F. Dinmohammadi, B. Alkali, M. Shafiee, C. Berenguer and A. Labib, "Risk Evaluation of Railway Rolling Stock Failures Using FMECA Technique: A Case Study of Passenger Door System," *Urban Rail Transit*, pp. 128-145, 2016.

[24] K. Liu, K. Hou, Z. Fei, R. Shi and S. Wang, "Field Test and Numerical Analysis of In-Service Railwat Bridge," *Advances in Materials Science and Engineering*, pp. 1-16, 2020.

[25] R. Sanudo, M. Miranda, C. Garcia and D. Garcia-Sanchez, "Drainage in railways," *Construction and Building Materials*, pp. 391-412, 2019.

[26] J. Vican, J. Gocal, J. Odrobinak and P. Kotes, "Existing Steel Railway Bridges Evaluation," *Civil and Environmental Engineering*, pp. 103-110, 2016b.

[27] HEC-18, Evaluating Scour at Bridges Fifth Edition, US: U.S. Department of Transportation Federal Highway Administration, 2012.

[28] F. C. Bonnett, Practical Railway Engineering, London: Imperial College Press, 1996.

[29] S. K. Bala, M. M. Hoque and S. M. U. Ahmed, "Failure of Bridge Due to Flood in Bangladesh - a Case Study.," *UAP Journal of Civil and Environmental Engineering*, pp. 38-44, 2005.

[30] L. Deng, W. Wang and Y. Yu, "State-of-the-Art Review on the Causes and Mechanisms of Bridge Collapse," *J. Perform. Constr. Facil.*, pp. 2-14, 2015.

[31] B. J. Feldman, "The collapse of the I-35 W Bridge in Minneapolis," *Phys. Teacher*, pp. 541-542, 2010.

[32] G. Warrier, "Restoration of Hardinge Bridge in Bangladesh," in *ICE Proceeding*, Bangladesh, 1977.

[33] A. Ghoshal, "Saga of Hundred Years of Hardinge Bridge. In A. F. M. S. Amin, Y. Okui, & A. R. Bhuiyan (Eds.)," in *Joint Conference on Advances on Bridge Engineering-III.*, Bangladesh, 2015.

[34] J. P. Gourc, P. Villard and H. Giraud, "Full scale experimentation of discountinuous subsidence for railway and motorway embankments. In: Barends, -F.B.J., Lindenberg, J., Luger, H.J., de Quelerij, L., Verruijt, A. (Eds.),," in *Proceedings of the Twelfth European Conference on Soil Mechanics and Geotechnical Engineering; Geotechnical Engineering for Transportation Infrastructure; Theory and Practice, Planning and Design, Construction and Maintenance.*, Rotterdam, 1999.

[35] J. Guerrero, F. Gutierrez, J. Bonachea and P. Lucha, "A sinkhole susceptibility zonation based on paleokarst analysis along a stretch of the Madrid-Barcelona high-speed railway built over gypsum-and salt-bearing evaporites (NE Spain)," *Engineering Geology*, pp. 62-73, 2008.

[36] B. Chazelle, L. Lambert and C. P. Capoccioni, "Railway vulnerability in case of extremes floods. Knowledge and risk management," *La Houille Blanche*, pp. 48-54, 2014.

[37] W. Xiong, B. Kong, P. Tang and J. Ye, "Vibration-Based Identification for the Presence of Scouring of Cable-Stayed Bridges," *J. Aerosp. Eng.*, pp. 2-17, 2018.

[38] A. M. Shirole and R. C. Holt, "Planning for a comprehensive bridge safety assurance program," *Transp. Res. Rec.* , pp. 137-142, 1991.

[39] S. P. Simonovic, "Managing flood risk, reliability and vulnerability (Editorial).," *J. Flood Risk Manage. 2 (4), https://doi.org/10.1111/j/1753-318X.2009.01040.x,* pp. 230-231, 2009.

[40] A. Perrone, A. Inam, R. Albano, J. Adamowski and A. Sole, "A participatory system dynamics modeling approach to facilitate collaborative flood risk management: A case study in the Bradano River (Italy)," *Journal of Hydrology,* pp. 1-16, 2020.

[41] R. Zhang, C. Huang and X. Feng, "Empty container repositioning with foldable containers in a river transport network considering the limitations of bridge heights," *Transportation Research Part A,* pp. 197-213, 2020.

[42] A. C. Estes and D. M. Frangopol, "Bridge lifetime system reliability under multiple limit states," *J. Bridge Eng.,* pp. 523-528, 2001.

[43] K. H. LeBeau and S. J. Wadia-Fascetti, "Fault tree analysis of Schoharie Creek Bridge collapse," *J. Perform. Constr. Facil.,* pp. 320-326, 2007.

[44] J. Scheer, Failed Bridges: Case Studies, Causes and Consequences, Germany: Ernst & Sohn, 2010.

[45] M. M. Rahman and A. M. Haque, "Local Scour Estimation at Bridge Site: Modification and Application of Lacey Formula," *International Journal of Sediment Research.* , vol. Vol. 18., no. No.4, pp. 333-339, 2003.

[46] J. Witzany, T. Cejka and R. Zigler, "Failure resistance of historic stone bridge structure of Charles Bridge. II: Susceptibility to floods.," *J. Perform. Constr. Facil.,* pp. 83-91, 2008.

[47] J. H. Hong, Y. M. Chiew, J. Y. Lu, J. S. Lai and Y. B. Lin, "Houfeng bridge failure in Taiwan," *J. Hydraul. Eng.,* pp. 186-198, 2012.

[48] L. Hamill, Bridge hydraulics, London: E. & F. N. Spon., 1999.

[49] L. Arneson, L. Zevenbergen, P. Lagasse and P. Clopper, Evaluating Scour at Bridges. Fifth ed., USA: Department of Transportation, Federal Highway Administration, 2012.

[50] M. V. Biezma and F. Schanack, "Collapse of Steel Briges," *Journal of Performance of Constructed Facilities,* pp. 398-405, 2007.

[51] P. Costabile and F. Macchione, "Enhancing river model set-up for 2-D dynamic flood modelling," *Environmental Modelling & Software,* pp. 89-107, 2015.

[52] G. Tewele, Hydrological Modelling in Ungauged Catchment (In Case Suluh), Tigray. A Thesis In Hydraulic Engineering, Addis, Ababa: Addis Ababa University, 2017.

[53] Cunderlik, "Hydrologic Model Selection for the CFCAS project: Assessment of Water Resources Risk and Vulnerability to Changing Climate Conditions," 2003.

[54] M. S. Shrestha, Bias_Adjustment of Satellite-Based Rainfall Estimates over the Central Himalayas of Nepal for Flood Prediction., Kyoto University, Japan: Department of Civil and Earth Resources Engineering, 2011.

[55] M. Noor, T. Ismail, E. Chung, S. Shahid and J. H. Sung, "Uncertainty in Rainfall Intensity Duration Frequency Curves of Peninsular Malaysia under Changing Climate Scenarios," *Water,* p. 1750, 2018.

[56] S. C. Acharya, R. Nathan, J. Q. Wang, C. Su and N. Eizenberg, "Ability of an Australian reanalysis dataset to characterise sub-daily precipitation," *Hydrology and Earth System Sciences,* pp. 432-452, 2019.

[57] T. Kiduse, Comparison and Evaluation of Satellite-Based Rainfall Products for Hydrological Modeling (Case of Wabe Watershed, Ethiopia). A Thesis in Hydraulics Engineering, Addis Ababa: Addis Ababa University, 2019.

[58] I. a. E. Ministry of Water, "Daily flow data at some selected gauge stations," 2021.

[59] P. Wondimu, Evaluating the Impact of Land Use Change on Urban Drainage System and Proposed Low Impact development measures in addis ababa, ethiopia, Addis Ababa: AAU, 2020.

[60] S. Dawit, "Flood risk analysis in Illu Floodplain, Upper Awash River Basin, Ethiopia: A Thesis submitted to the school of graduate studies of Addis Ababa Univeristy in Partial Fulfillment of the requirements for the degree of Master of Science in Hydraulic Engin'g," *AAU, PG Thesis*, pp. 1-50, 2015.

[61] S. Alaghmand, R. Bin Abdullah, I. Abustan and S. Eslamian, "Comparison between capabilities of HEC-RAS and MIKE11 hydraulic models in river flood risk modelling (a case study of Sungai Kayu Ara River Basin, Malaysia)," *Int. J. Hydrol. Sci. Technol.*, vol. 2, no. 3, pp. 270-291, 2012.

[62] W. Abeyou, "Hydrological balance of Lake Tana, Upper Blue Nile Basin, Ethioia," Ethiopia, 2008.

[63] A. Kilikevicius, J. Skeivalas, K. Kilikeviciene and J. Matijosius, "Analysis of Dynamic Parameters of a Railway Bridge," *Applied Sciences*, pp. 1-17, 2019.

[64] K. J. Beven and M. J. Kirkby, "A physically based, variable contributing area model of basin hydrology/Un Modele a base physique de zone d'appel variable de l'hydologie du bassin versant.," *Hydrol. Sci. J.*, pp. 43-69, 1979.

[65] J. Dehotin, P. Breil, I. Braud, A. de Lavenne, M. Lagouy and B. Sarrazin, "Detecting surface runoff location in a small catchment using distributed and simple observation method.," *J. Hydrol. 525,*, pp. 113-129, 2015.

[66] J. Smith, M. Baeck, K. Meierdiercks, A. Miller and W. Krajewski, "Radar rainfall estimation for flash flood forecasting in small urban watersheds.," *Adv. Water Resour. ,* pp. 2087-2097, 2007.

[67] J. Michaud and S. Sorooshian, "Effect of rainfall sampling errors on simulations of desert flash floods.," *Water Resour. Res.,* pp. 2765-2775, 1994.

[68] Y. Kun, D. B. Giuliano and P. Florian, Flood Hazard Mapping in Data-Scarce Areas. In Global Flood Hazard; Schumann, G.J., Bates, P.D., Apel, H., Aronica, G.T., Eds.;, Washington: American Geophysical Union, 2018.

[69] M. D. Caceres, N. Martin-StPaul, M. Turco, A. Cabon and V. Granda, "Estimating daily meteorological data and downscaling climate models over landscapes.," *Environ. Model. Softw. ,* pp. 186-196, 2018.

[70] W. Krajewski and J. Smith, "Radar hydrology: Rainfall estimation," *Adv. Water Resour.,* pp. 1387-1394, 2002.

[71] J. Diez-Sierra and M. del Jesus, "Subdaily Rainfall Estimation through Daily Rainfall Downscaling Using Ramdom Forests in Spain," *Water*, p. 125, 2019.

[72] B. Golding, N. Roberts, G. Leoncini, K. Mylne and R. Swinbank, "MOGRESPS-UK Convection-Permitting Ensemble Products for Surface Water Flood Forecasting: Rationale and First Results," *J. Hydrometeorol.,*, pp. 1383-1406, 2016.

[73] P. A. Kucera, E. E. Ebert, F. J. Turk, V. Levizzani, D. Kirschbaum, F. J. Tapiador, A. Loew and M. Borsche, "Precipitation from space: Advancing earth system science," *Bull. Am. Meteorol. Soc.,* pp. 365-375, 2013.

[74] A. Paschalis, S. Fatichi, P. Molnar, S. Rimkus and P. Burlando, "On the effects of small scale space-time variability of rainfall on basin flood response,," *J. Hydrol.,* pp. 313-327, 2014.

[75] C. C. Sampson, T. J. Fewtrell, F. O'Loughlin, F. Pappenberger, P. B. Bates, J. E. Freer and H. L. Cloke, "The impact of uncertain precipitation data on insurance loss estimates using a flood catastrophe model," *Hydrol. Earth Syst. Sci*, pp. 2305-2324, 2014.

[76] H. Seyyedi, E. N. Anagnostou, E. Beighley and J. McCollum, "Satellite-driven downscaling of global reanalysis precipitation products for hydrological applications," *Hydrol. Earth Syst. Sci.,* pp. 5077-5091, 2014.

[77] E. Hagan and X. X. Lu, "Let us create flood hazard maps for developing countries," *Nat Hazards*, pp. 841-843, 2011.

[78] S. Hettiarachchi, C. Wasko and A. Sharma, "Increase in flood risk resulting from climate change in a developed urban watershed-the role of storm temporal patterns," *Hydrol. Earth Syst. Sci.*, pp. 2041-2056, 2018.

[79] V. T. Nguyen, N. Desramaut and T. D. Nguyen, "Optimal rainfall temporal patterns for urban drainage design in the context of climate change," *Water Sci. Technol.*, pp. 1170-1176, 2010.

[80] M. Rogger, B. Kohl, H. Pirkl, A. Viglione, J. Komma, R. Kirnbauer, R. Merz and G. Bloschl, "Runoff models and flood frequency statistics for desgin flood estimatino in Austria - Do they tell a consistent story?," *Journal of Hydrology*, pp. 30-43, 2012.

[81] R. Bettess, Hydraulic Aspects of Bridges: Assessment of the Risk of Scour., UK: HR Wallingford, 1993.

[82] K. D. Kirby, A. Kitchen, M. Escaramela and O. L. Chesterton, Manual on scour at bridges and other hydraulic structures. 2nd ed., London: CIRIA, 2015.

[83] B. W. Melville and S. E. Coleman, "Bridge Scour," *Water Resources Publications*, 2000.

APPENDIX A

Double mass curves plotted to check the rainfall data consistencies recorded for the selected meteorological gauge stations within the case study area.

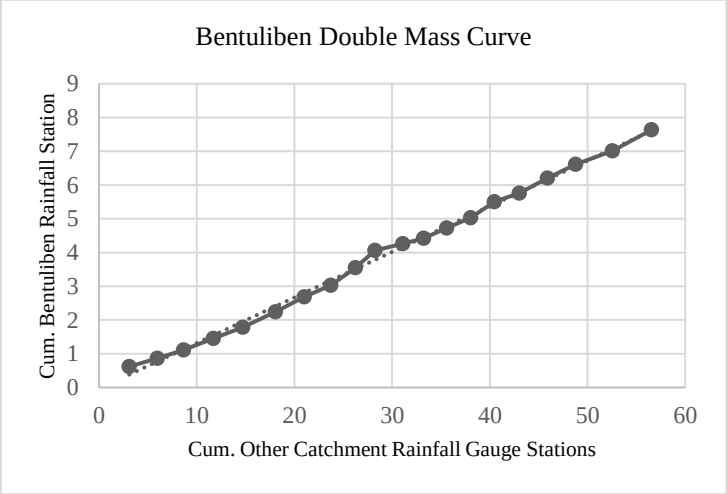

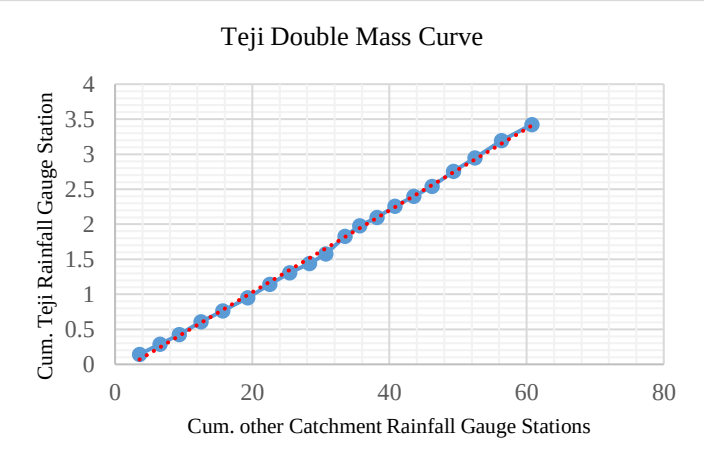

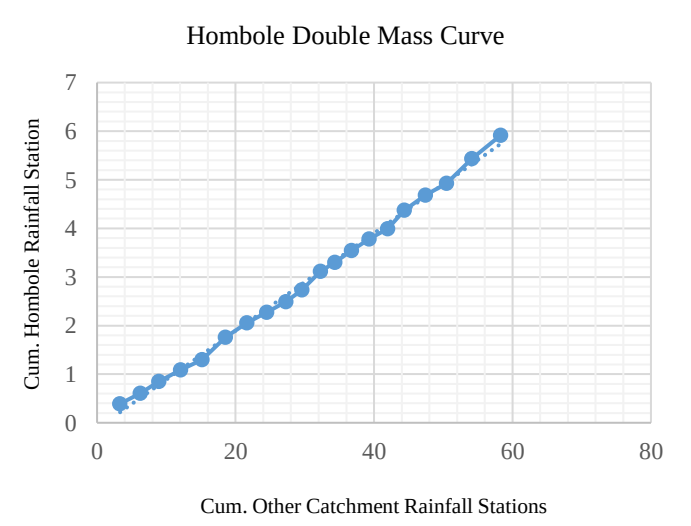

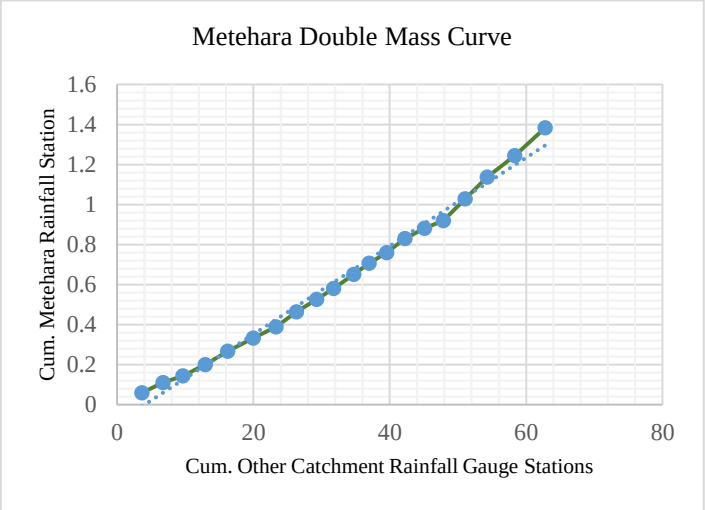
Metehara Double Mass Curve
Cum. Metehara Rainfall Station
1.6
1.4
1.2
1
0.8
0.6
0.4
0.2
0
0
20
40
60
80
Cum. Other Catchment Rainfall Gauge Stations

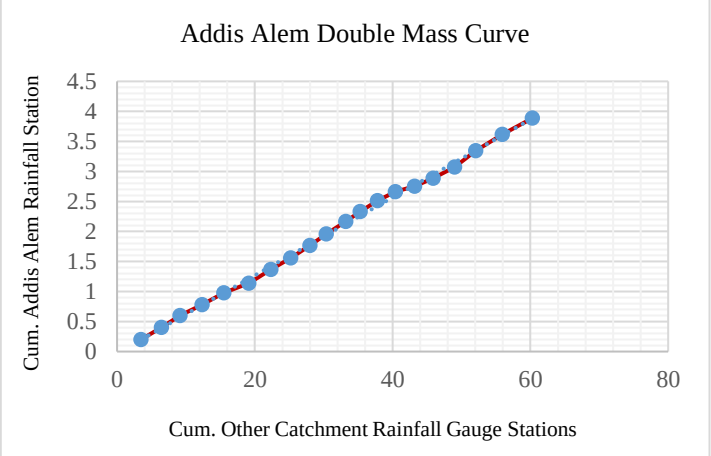
Addis Alem Double Mass Curve
Cum. Addis Alem Rainfall Station
4.5
4
3.5
3
2.5
2
1.5
1
0.5
0
0
20
40
60
80
Cum. Other Catchment Rainfall Gauge Stations

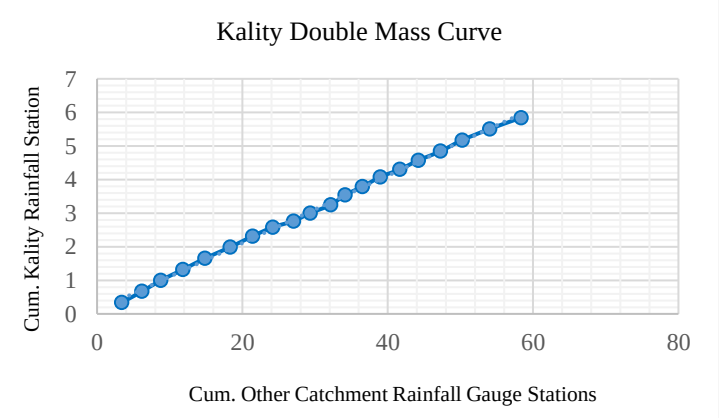
Kality Double Mass Curve
Cum. Kality Rainfall Station
7
6
5
4
3
2
1
0
0
20
40
60
80
Cum. Other Catchment Rainfall Gauge Stations

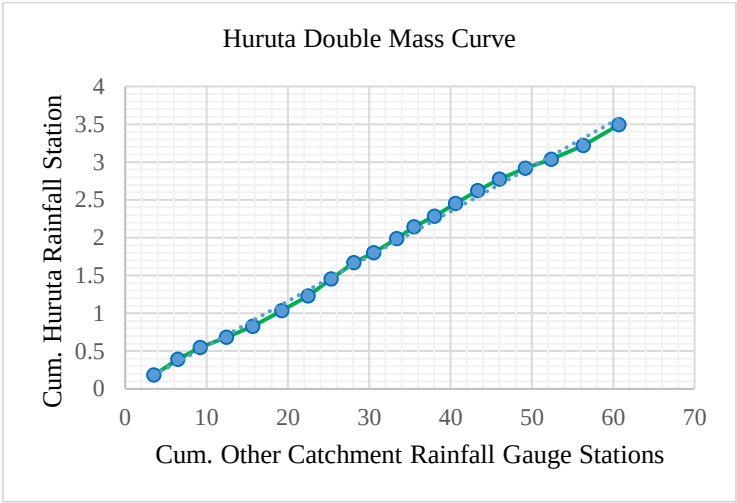
Huruta Double Mass Curve
Cum. Huruta Rainfall Station
0
0.5
1
1.5
2
2.5
3
3.5
4
0
10
20
30
40
50
60
70
Cum. Other Catchment Rainfall Gauge Stations

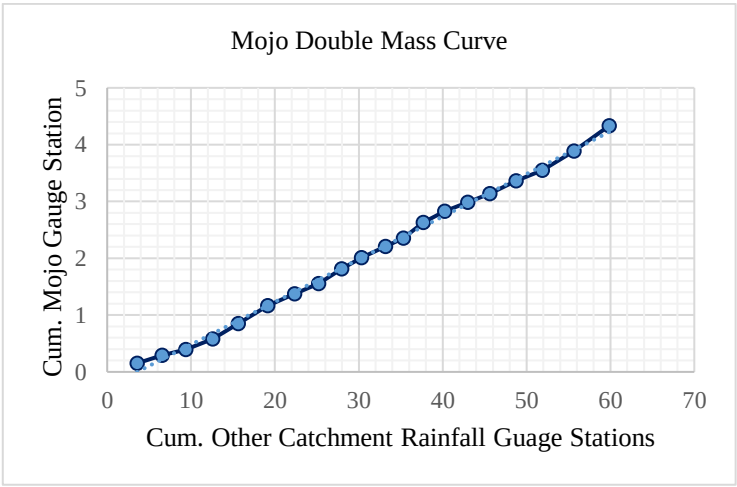
Mojo Double Mass Curve
Cum. Mojo Gauge Station
0
1
2
3
4
5
0
10
20
30
40
50
60
70
Cum. Other Catchment Rainfall Guage Stations

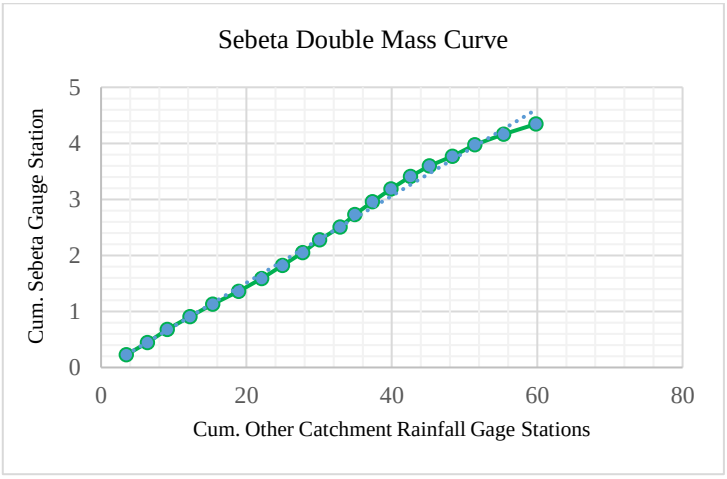
Sebeta Double Mass Curve
Cum. Sebeta Gauge Station
0
1
2
3
4
5
0
20
40
60
80
Cum. Other Catchment Rainfall Gage Stations

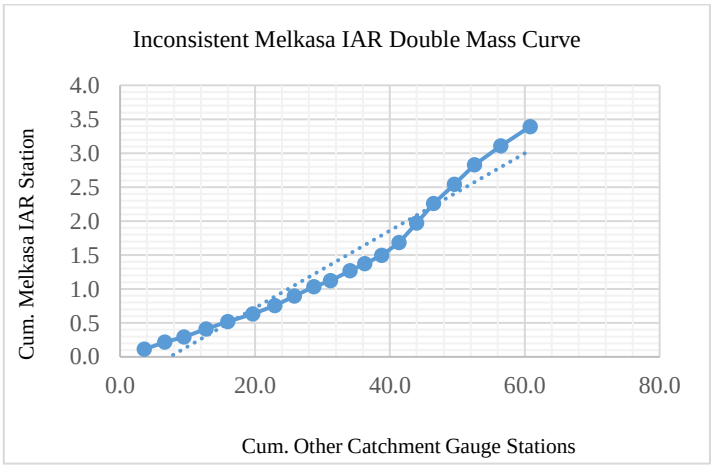
Inconsistent Melkasa IAR Double Mass Curve
Cum. Melkasa IAR Station
4.0
3.5
3.0
2.5
2.0
1.5
1.0
0.5
0.0
0.0
20.0
40.0
60.0
80.0
Cum. Other Catchment Gauge Stations

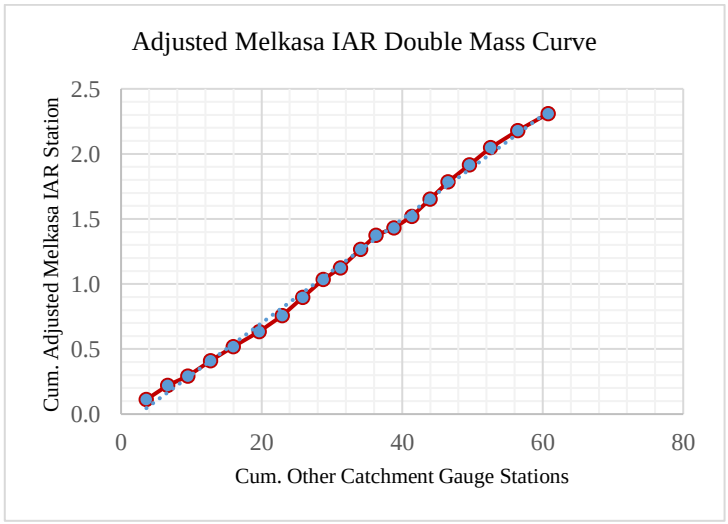
Adjusted Melkasa IAR Double Mass Curve
Cum. Adjusted Melkasa IAR Station
2.5
2.0
1.5
1.0
0.5
0.0
0
20
40
60
80
Cum. Other Catchment Gauge Stations

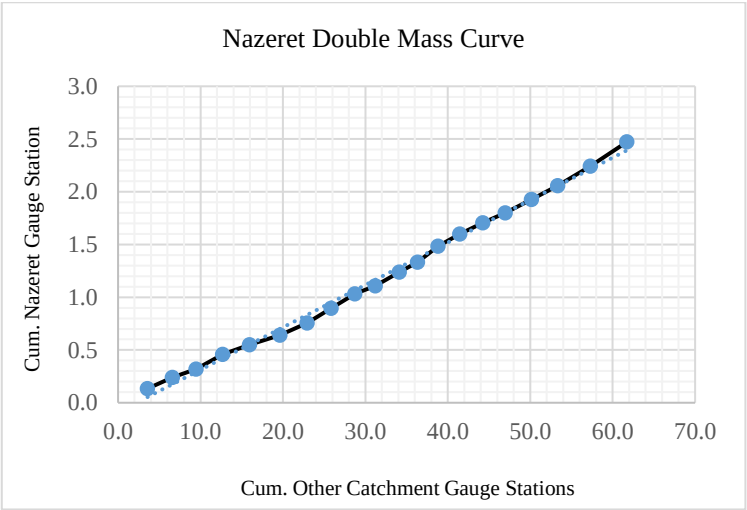
Nazeret Double Mass Curve
Cum. Nazeret Gauge Station
3.0
2.5
2.0
1.5
1.0
0.5
0.0
0.0
10.0
20.0
30.0
40.0
50.0
60.0
70.0
Cum. Other Catchment Gauge Stations

APPENDIX B

Model Parameters used for the calibration of the HEC-HMS Model in the case study area are presented in the following tables

Table 1: SCS Runoff Curve Number for the Sub-basins

Element	SCS CN	Element	SCS CN
WHombole	87.726	WJP14	87.953
WJP01	87.779	WJP15	86.223
WJP02	87.807	WJP16	87.619
WJP03	87.815	WJP17	87.911
WJP04	88.011	WJP18	87.816
WJP05	87.985	WJP19	87.656
WJP06	87.842	WJP20	87.498
WJP07	87.694	WJP21	87.327
WJP08	87.246	WJP22	87.806
WJP09	88.515	WJP23	87.877
WJP10	87.605	WJP24	87.608
WJP11	86.277	WJP25	87.626
WJP12	87.504	WJP26	87.9
WJP13	85.074	WJP27	86.945

Element	SCS CN	Element	SCS CN
WJP28	87.626	WJP40	87.775
WJP29	87.735	WJP41	87.108
WJP30	87.975	WJP42	87.914
WJP31	87.882	WJP43	88.071
WJP32	87.854	WJP44	87.692
WJP33	87.909	WJP45	87.165
WJP34	87.832	WJP46	87.705
WJP35	87.876	WJP47	84.303
WJP36	87.685	WMelkaKuntire	87.838
WJP37	87.456	WMojo	87.300
WJP38	87.586	WNuraHE	87.413
WJP39	87.75	WOutlet	87.950

Table 2: SCS Unit Hydrograph Lag Time for the Sub-basins

Subbasins	Parameter	Units	Value
WHombole	SCS UH - Lag Time	Min	298.08
WJP01	SCS UH - Lag Time	Min	19.22
WJP02	SCS UH - Lag Time	Min	21.19
WJP03	SCS UH - Lag Time	Min	24.15
WJP04	SCS UH - Lag Time	Min	22.08
WJP05	SCS UH - Lag Time	Min	29.34
WJP06	SCS UH - Lag Time	Min	31.06
WJP07	SCS UH - Lag Time	Min	27.71

WJP08	SCS UH - Lag Time	Min	29.81
WJP09	SCS UH - Lag Time	Min	9.07
WJP10	SCS UH - Lag Time	Min	21.56
WJP11	SCS UH - Lag Time	Min	24.81
WJP12	SCS UH - Lag Time	Min	15.35
WJP13	SCS UH - Lag Time	Min	12.66
WJP14	SCS UH - Lag Time	Min	23.08
WJP15	SCS UH - Lag Time	Min	28.33
WJP16	SCS UH - Lag Time	Min	32.47
WJP17	SCS UH - Lag Time	Min	156.51
WJP18	SCS UH - Lag Time	Min	36.84
WJP19	SCS UH - Lag Time	Min	275.77
WJP20	SCS UH - Lag Time	Min	48.22
WJP21	SCS UH - Lag Time	Min	53.45
WJP22	SCS UH - Lag Time	Min	18.76
WJP23	SCS UH - Lag Time	Min	30.13
WJP24	SCS UH - Lag Time	Min	27.13
WJP28	SCS UH - Lag Time	Min	91.43
WJP29	SCS UH - Lag Time	Min	252.04
WJP30	SCS UH - Lag Time	Min	27.13
WJP31	SCS UH - Lag Time	Min	130.28
WJP32	SCS UH - Lag Time	Min	57.11
WJP33	SCS UH - Lag Time	Min	119.48
WJP34	SCS UH - Lag Time	Min	340.93
WJP35	SCS UH - Lag Time	Min	36.39
WJP36	SCS UH - Lag Time	Min	64.96
WJP37	SCS UH - Lag Time	Min	138.42
WMelkaKuntire	SCS UH - Lag Time	Min	337.16
WMojo	SCS UH - Lag Time	Min	142.83

Table 3: Muskingum Constant K (hr) for the reaches within the study area.

Reach	Parameter	Units	Value
R01	Muskingum - K	Hr	26.41
R02	Muskingum - K	Hr	27.12
R03	Muskingum - K	Hr	26.89
R04	Muskingum - K	Hr	26.74
R05	Muskingum - K	Hr	27.07
R06	Muskingum - K	Hr	25.19
R07	Muskingum - K	Hr	26.11
R08	Muskingum - K	Hr	27.40
R09	Muskingum - K	Hr	27.01
R10	Muskingum - K	Hr	27.77

Reach	Parameter	Units	Value
R11	Muskingum - K	Hr	28.39
R12	Muskingum - K	Hr	28.09
R13	Muskingum - K	Hr	28.89

R14	Muskingum - K	Hr	28.62
R15	Muskingum - K	Hr	29.27
R16	Muskingum - K	Hr	29.09
R17	Muskingum - K	Hr	29.54
R18	Muskingum - K	Hr	29.42
R19	Muskingum - K	Hr	29.64
R20	Muskingum - K	Hr	36.67

Reach	Parameter	Units	Value
R21	Muskingum - K	Hr	56.55
R22	Muskingum - K	Hr	46.08
R23	Muskingum - K	Hr	39.12
R24	Muskingum - K	Hr	44.53
R25	Muskingum - K	Hr	42.20
R26	Muskingum - K	Hr	47.76
R27	Muskingum - K	Hr	46.36
R28	Muskingum - K	Hr	49.35
R29	Muskingum - K	Hr	48.74
R30	Muskingum - K	Hr	48.54
R31	Muskingum - K	Hr	42.43
R32	Muskingum - K	Hr	45.75
R33	Muskingum - K	Hr	54.02
R34	Muskingum - K	Hr	56.47

JPs	Shape Length (m)	Slope	ElevUP (m)	ElevDS (m)	Slope (10%)	Elev (10%)	Slope (85%)	Elev (85%)	LengthDown (m)	LongestFL (m)
1	7348.29	0.1249	3022	2104	0.1138	2126	0.1138	2753	331413.69	7348.29
2	8117.96	0.1460	3292	2107	0.1229	2124	0.1229	2872	306282.27	8117.96
3	9162.72	0.1202	3207	2106	0.1169	2128	0.1169	2931	307664.90	9162.72
4	7182.39	0.1314	3126	2182	0.0973	2208	0.0973	2732	310871.21	7182.39
5	8085.72	0.1065	3042	2181	0.0876	2212	0.0876	2743	311895.69	8085.72
6	12052.09	0.0963	3376	2215	0.0941	2241	0.0941	3092	316781.59	12052.09
7	1154.70	0.0641	2326	2252	0.0704	2254	0.0704	2315	309443.82	1154.70
8	6564.56	0.0457	2554	2254	0.0477	2257	0.0477	2492	315039.93	6564.56
9	17834.81	0.0363	2669	2021	0.0228	2070	0.0228	2375	292615.95	17834.81
10	13269.55	0.0663	2793	1913	0.0302	1928	0.0302	2229	264939.59	13269.55
11	5178.69	0.0620	2365	2044	0.0314	2046	0.0314	2168	286656.89	5178.69
12	3782.38	0.2004	2844	2086	0.1745	2097	0.1745	2592	285611.55	3782.38
13	6461.97	0.0197	2178	2051	0.0182	2056	0.0182	2144	293771.87	6461.97
14	7819.53	0.0327	2278	2022	0.0302	2040	0.0302	2217	282505.33	7819.53
15	6897.25	0.0845	2844	2261	0.0559	2272	0.0559	2561	315245.47	6897.25
16	4293.99	0.0871	2425	2051	0.0683	2057	0.0683	2277	284325.00	4293.99
17	51767.87	0.0257	3379	2046	0.0140	2071	0.0140	2616	335086.76	51767.87
18	6281.06	0.1065	2716	2047	0.0881	2049	0.0881	2464	287892.03	6281.06
19	83527.54	0.0138	3200	2047	0.0072	2065	0.0072	2517	370221.01	83527.54
20	13409.12	0.0269	2245	1884	0.0159	1890	0.0159	2050	259554.58	13409.12
21	3553.75	0.0324	2211	2096	0.0229	2100	0.0229	2161	294909.67	3553.75
22	3120.54	0.0205	1931	1867	0.0073	1868	0.0073	1885	242424.47	3120.54
23	31372.43	0.0322	2475	1465	0.0283	1488	0.0283	2155	144054.13	31372.43

24	27821.47	0.0056	2019	1862	0.0023	1864	0.0023	1911	259845.42	27821.47
25	4350.79	0.0457	2272	2073	0.0432	2084	0.0432	2225	280356.80	4350.79
26	4856.94	0.0445	2446	2230	0.0299	2231	0.0299	2340	310410.70	4856.94
27	4777.72	0.0266	2173	2046	0.0232	2051	0.0232	2134	288653.27	4777.72
28	4279.42	0.1552	2838	2174	0.1461	2220	0.1461	2689	293885.47	4279.42
29	10462.51	0.0176	2244	2060	0.0186	2069	0.0186	2215	298974.04	10462.51
30	49801.07	0.0131	2522	1869	0.0154	1881	0.0154	2457	290298.12	49801.07
31	25593.80	0.0277	2484	1776	0.0207	1788	0.0207	2185	200470.13	25593.80
32	7138.90	0.0483	2429	2084	0.0319	2098	0.0319	2269	283704.90	7138.90
33	18797.01	0.0126	1970	1734	0.0090	1758	0.0090	1885	224414.62	18797.01
34	7122.70	0.0261	1977	1791	0.0227	1804	0.0227	1925	217728.94	7122.70
35	80452.63	0.0095	2522	1761	0.0098	1819	0.0098	2409	290922.48	80452.63
36	13389.22	0.0129	1767	1594	0.0092	1602	0.0092	1694	163671.66	13389.22
37	14503.42	0.0291	2045	1623	0.0269	1674	0.0269	1967	168507.10	14503.42
38	5138.45	0.0051	1878	1852	0.0044	1855	0.0044	1872	229861.62	5138.45
39	9817.01	0.0275	1830	1560	0.0096	1602	0.0096	1673	132357.07	9817.01
40	9520.49	0.0321	1773	1467	0.0297	1483	0.0297	1695	123764.62	9520.49
41	98383.43	0.0170	3361	1688	0.0145	1729	0.0145	2796	308689.77	98383.43
42	9631.81	0.0244	1917	1682	0.0260	1702	0.0260	1890	172112.95	9631.81
43	133945.52	0.0091	2158	941	0.0051	945	0.0051	1456	133945.52	133945.52
44	8034.69	0.0433	1951	1603	0.0430	1621	0.0430	1880	162196.51	8034.69
45	123110.86	0.0126	3550	1994	0.0041	2023	0.0041	2403	393200.80	123110.86
46	4331.05	0.0531	1964	1734	0.0400	1744	0.0400	1874	173567.70	4331.05
47	16508.24	0.0295	2320	1833	0.0124	1840	0.0124	1994	236849.73	16508.24

APPENDIX C

Graphical Representations of the simulated daily flows from 2000 to 2019 for all the selected drainage structures

JP11 - Frame Bridge (K17 + 024.07)

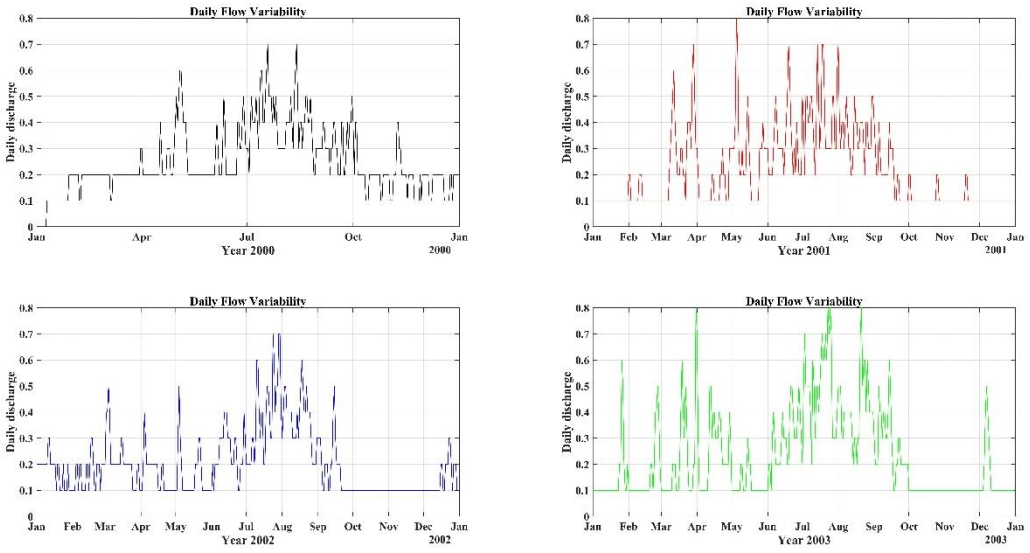

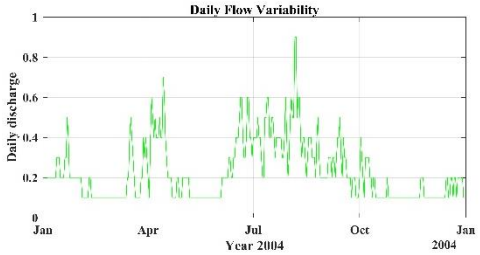
Daily Flow Variability
Daily discharge
Jan Apr Jul Oct Jan
Year 2004 2004

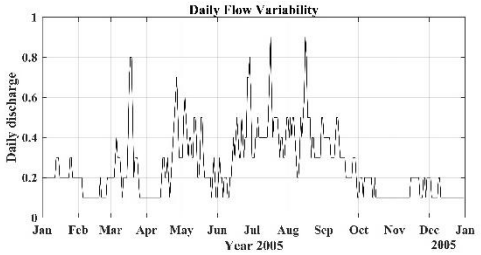
Daily Flow Variability
Daily discharge
Jan Feb Mar Apr May Jun Jul Aug Sep Oct Nov Dec Jan
Year 2005 2005

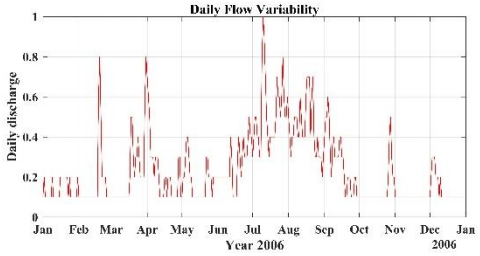
Daily Flow Variability
Daily discharge
Jan Feb Mar Apr May Jun Jul Aug Sep Oct Nov Dec Jan
Year 2006 2006

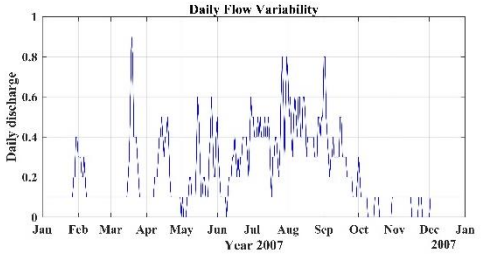
Daily Flow Variability
Daily discharge
Jan Feb Mar Apr May Jun Jul Aug Sep Oct Nov Dec Jan
Year 2007 2007

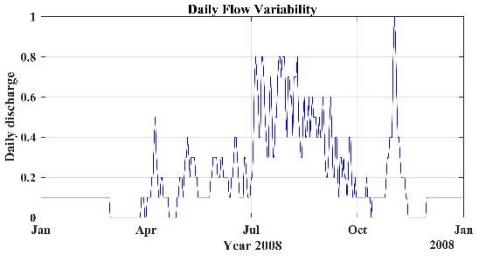
Daily Flow Variability
Daily discharge
Jan Apr Jul Oct Jan
Year 2008 2008

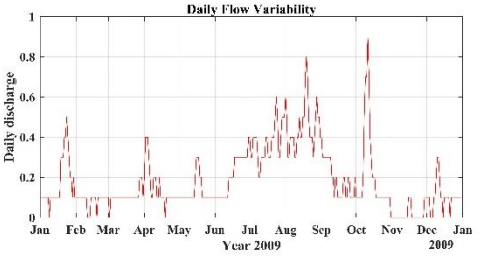
Daily Flow Variability
Daily discharge
Jan Feb Mar Apr May Jun Jul Aug Sep Oct Nov Dec Jan
Year 2009 2009

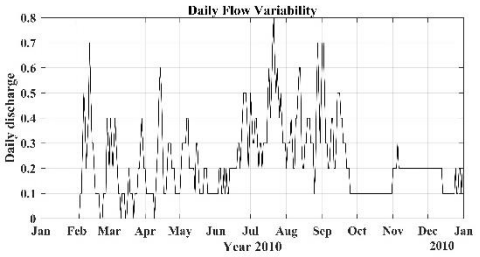
Daily Flow Variability
Daily discharge
Jan Feb Mar Apr May Jun Jul Aug Sep Oct Nov Dec Jan
Year 2010 2010

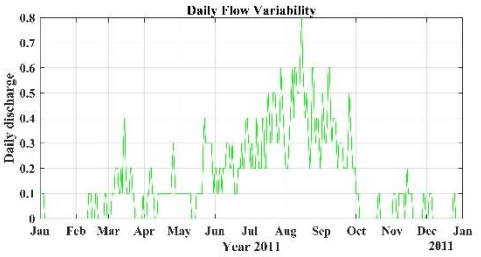
Daily Flow Variability
Daily discharge
Jan Feb Mar Apr May Jun Jul Aug Sep Oct Nov Dec Jan
Year 2011 2011

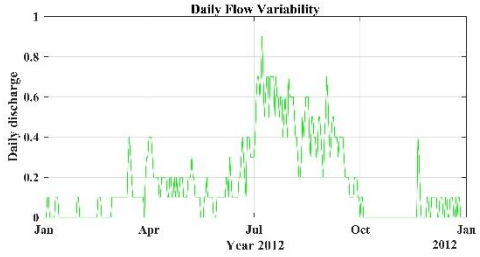
Daily Flow Variability
Daily discharge
Jan Apr Jul Oct Jan
Year 2012 2012

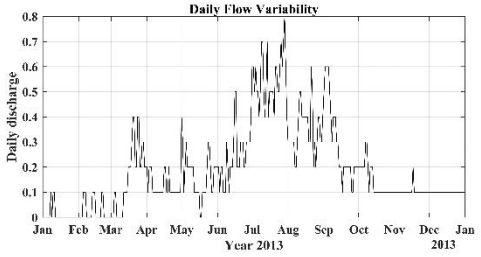
Daily Flow Variability
Daily discharge
Jan Feb Mar Apr May Jun Jul Aug Sep Oct Nov Dec Jan
Year 2013 2013

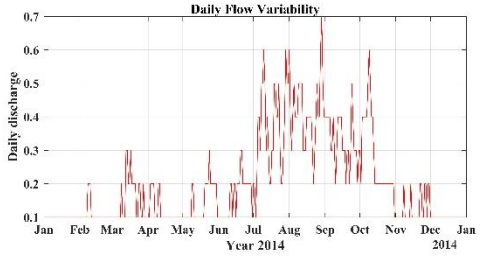
Daily Flow Variability
Daily discharge
Jan Feb Mar Apr May Jun Jul Aug Sep Oct Nov Dec Jan
Year 2014 2014

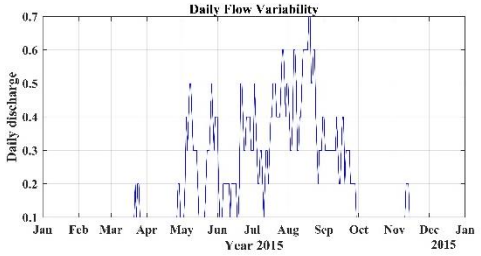
Daily Flow Variability
Daily discharge
Jan Feb Mar Apr May Jun Jul Aug Sep Oct Nov Dec Jan
Year 2015 2015

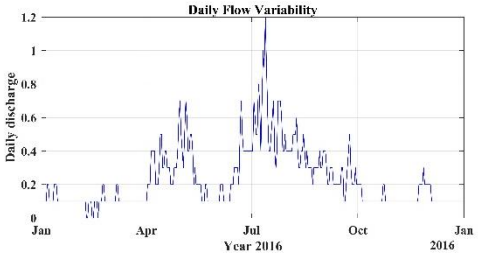

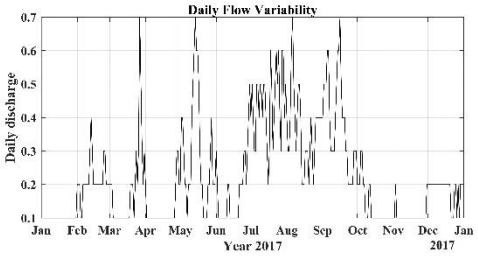

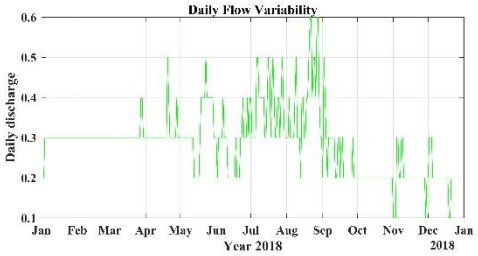

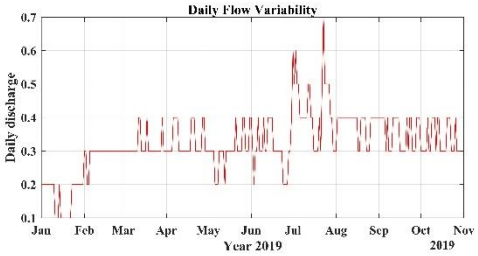

JP35 Simply Supported T – Beam Bridge

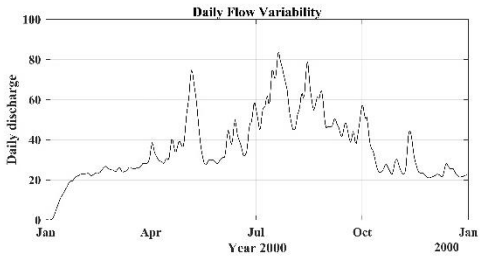

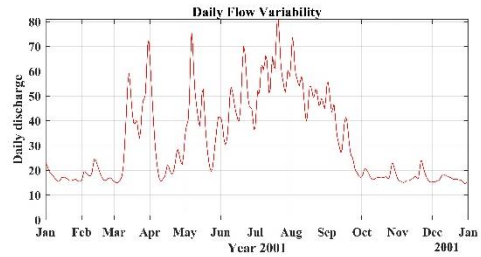

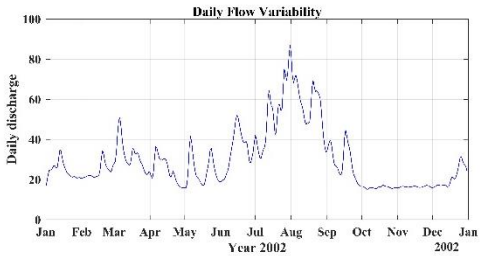

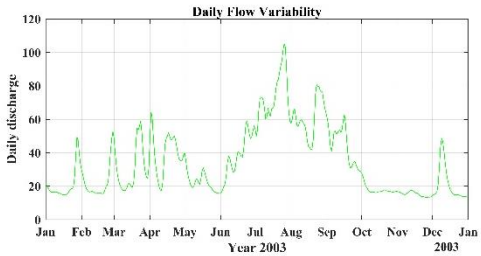

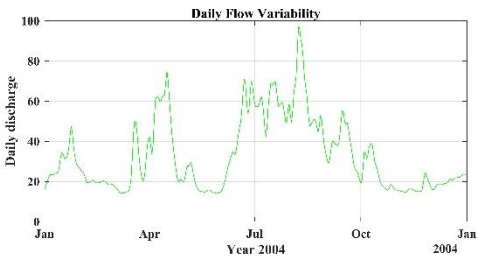

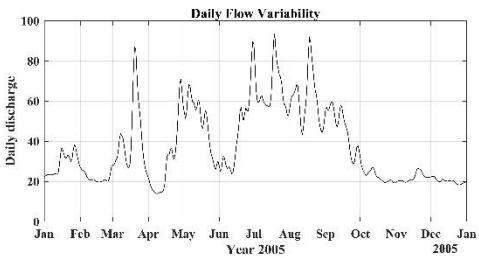

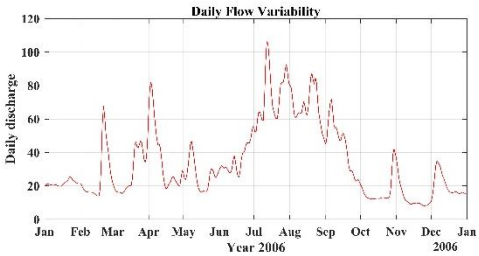

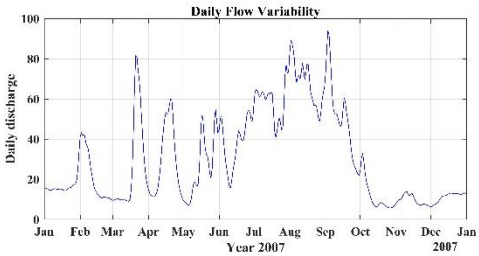

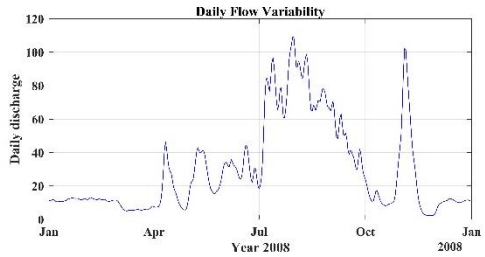
Daily Flow Variability
Daily discharge
Jan
Apr
Jul
Oct
Jan
Year 2008
2008

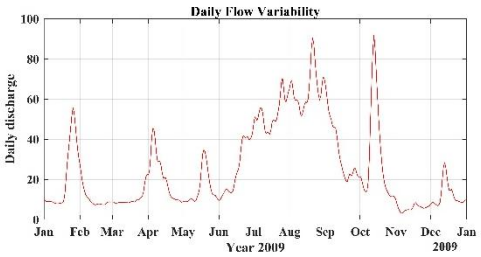
Daily Flow Variability
Daily discharge
Jan Feb Mar Apr May Jun Jul Aug Sep Oct Nov Dec Jan
Year 2009
2009

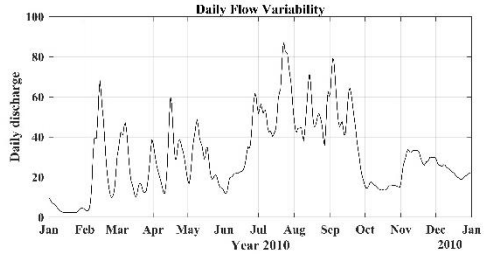
Daily Flow Variability
Daily discharge
Jan Feb Mar Apr May Jun Jul Aug Sep Oct Nov Dec Jan
Year 2010
2010

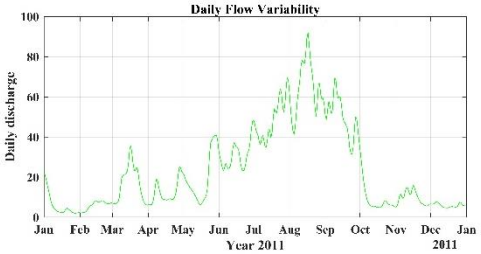
Daily Flow Variability
Daily discharge
Jan Feb Mar Apr May Jun Jul Aug Sep Oct Nov Dec Jan
Year 2011
2011

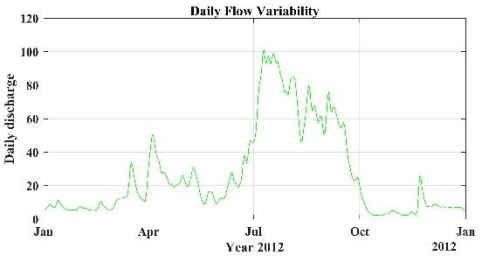
Daily Flow Variability
Daily discharge
Jan
Apr
Jul
Oct
Jan
Year 2012
2012

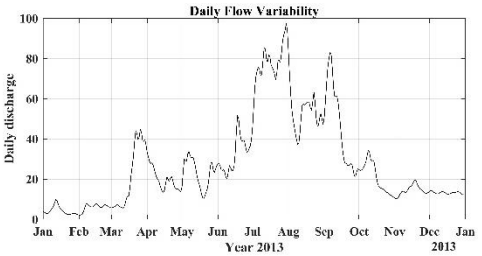
Daily Flow Variability
Daily discharge
Jan Feb Mar Apr May Jun Jul Aug Sep Oct Nov Dec Jan
Year 2013
2013

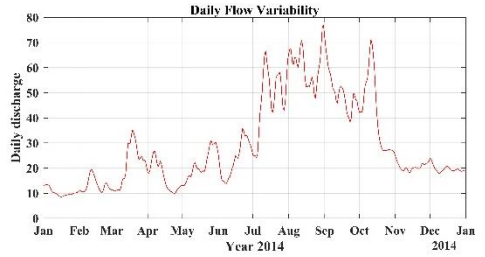
Daily Flow Variability
Daily discharge
Jan Feb Mar Apr May Jun Jul Aug Sep Oct Nov Dec Jan
Year 2014
2014

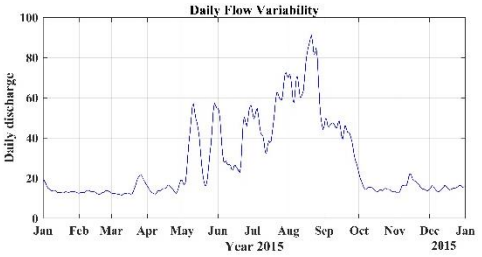
Daily Flow Variability
Daily discharge
Jan Feb Mar Apr May Jun Jul Aug Sep Oct Nov Dec Jan
Year 2015
2015

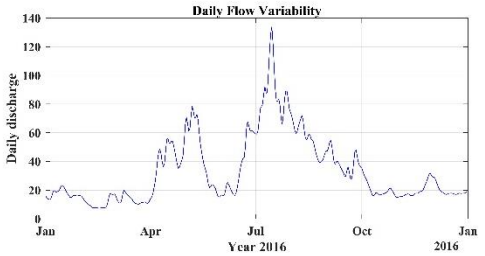
Daily Flow Variability
Daily discharge
Jan
Apr
Jul
Oct
Jan
Year 2016
2016

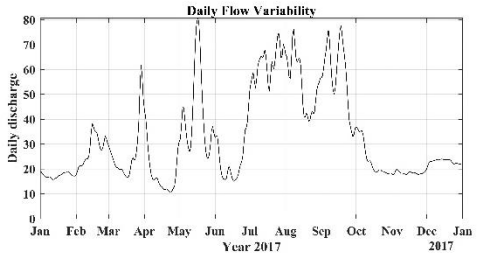
Daily Flow Variability
Daily discharge
Jan Feb Mar Apr May Jun Jul Aug Sep Oct Nov Dec Jan
Year 2017
2017

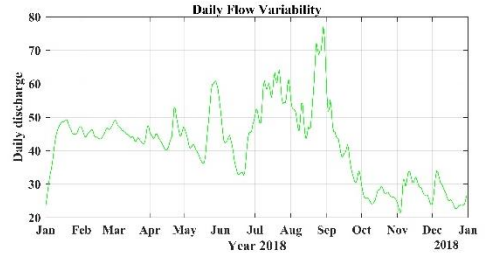
Daily Flow Variability
Daily discharge
Jan Feb Mar Apr May Jun Jul Aug Sep Oct Nov Dec Jan
Year 2018
2018

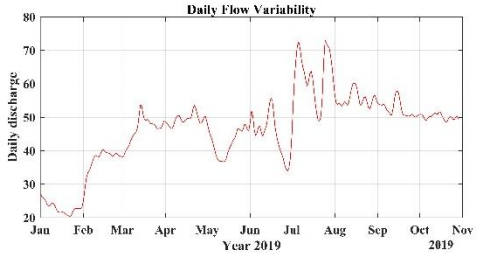
Daily Flow Variability
Daily discharge
Jan Feb Mar Apr May Jun Jul Aug Sep Oct Nov
Year 2019
2019

APPENDIX D

Particle size distribution curves (PSDCs) for the subgrade materials near JP03 to JP47

Mileage culvert 03	DK3+000	Mileage culvert 04	DK9+800
Report Date	1/9/2015	Report Date	8/2/2015
Digging Depth	1.8 m	Digging Depth	3.3 m
Sieve Sizes (mm)	Particle Size Passing (%)	Sieve Sizes (mm)	Particle Size Passing (%)
<200		<200	
<60		<60	100
<40		<40	93.8
<20	100	<20	73.9
<10	92.5	<10	49.5
<5	80.4	<5	28.3
<2	70.1	<2	20.7
<1	63.6	<1	18.6
<0.5	58.7	<0.5	15.3
<0.25	25.5	<0.25	11.2
<0.075	13.2	<0.075	8.4
Uniformity Coefficient Cu		Uniformity Coefficient Cu	78.49
Coefficient of Curvature Cc		Coefficient of Curvature Cc	12.88
Particle Density (g/cm^3)	2.562	Particle Density (g/cm^3)	2.55
Sample Description	Yellow and Brown, Powdery	Sample Description	Grayish yellow, granular
Name of the soil	Low Liquid Limit Soil	Name of the soil	Bad Graded Fine Breccia
Group of the Filling Material	C	Group of the Filling Material	B
Conclusion	Meets the design requirements	Conclusion	Meets the design requirements

Mileage 5	DK10+115	Mileage 6	DK10+500
Report Date	10/5/2013	Report Date	7/5/2014
Digging Depth	2.0 m	Digging Depth	1.5 m
Sieve Sizes (mm)	Particle Size Passing (%)	Sieve Sizes (mm)	Particle Size Passing (%)
<200	100	<200	100
<60	86	<60	87.1
<40	78.7	<40	80.4
<20	70.1	<20	72.5
<10	60.5	<10	63.7
<5	50.8	<5	54.7
<2	44.2	<2	48.6
<1	33.5	<1	38.7
<0.5	25.7	<0.5	31.6
<0.25	17	<0.25	23.5
<0.075	9.1	<0.075	16.3
Uniformity Coefficient Cu	102.62	Uniformity Coefficient Cu	172.66
Coefficient of Curvature Cc	0.65	Coefficient of Curvature Cc	0.56
Particle Density (g/cm^3)	2.49	Particle Density (g/cm^3)	2.49

Sample Description	Yellow, Angular crush stone, No impurities	Sample Description	Yellow, Angular crush stone, No impurities
Name of the soil	bad graded soil-containing fine breccia	Name of the soil	Soil fine breccia
Group of the Filling Material	B	Group of the Filling Material	B
Conclusion	Meets the design requirements	Conclusion	Meets the design requirements

Mileage 7	DK11+100	Mileage 8	DK11+500
Report Date	5/5/2014	Report Date	25/4/2014
Digging Depth	0.3 m	Digging Depth	1.5 m
Sieve Sizes (mm)	Particle Size Passing (%)	Sieve Sizes (mm)	Particle Size Passing (%)
<200	100	<200	100
<60	85.8	<60	87.1
<40	77.8	<40	80.5
<20	69.2	<20	72.5
<10	60.8	<10	63.7
<5	52.6	<5	54.8
<2	47.4	<2	48.6
<1	45.3	<1	38.7
<0.5	41.3	<0.5	31.6
<0.25	37.6	<0.25	23.6
<0.075	26.1	<0.075	16.4
Uniformity Coefficient Cu		Uniformity Coefficient Cu	173.21
Coefficient of Curvature Cc		Coefficient of Curvature Cc	0.56
Particle Density (g/cm^3)	2.48	Particle Density (g/cm^3)	2.47
Sample Description	Yellow, Round granular, No impurities	Sample Description	Yellow, Angular crush stone, No impurities
Name of the soil	soil fine round gravel	Name of the soil	Soil fine breccia
Group of the Filling Material	B	Group of the Filling Material	B
Conclusion	Meets the design requirements	Conclusion	Meets the design requirements

Mileage 10	DK14+980	Mileage FB11	DK16+600
Report Date	27/3/2014	Report Date	3/4/2014
Digging Depth	0.8 m	Digging Depth	3.0 m
Sieve Sizes (mm)	Particle Size Passing (%)	Sieve Sizes (mm)	Particle Size Passing (%)
<200	100	<200	
<60	98.5	<60	100
<40	95.5	<40	95.7
<20	79.4	<20	81.5
<10	59.7	<10	57.7
<5	46.3	<5	45.1
<2	35	<2	31.2
<1	33.3	<1	24.9
<0.5	28.4	<0.5	19.1
<0.25	25.2	<0.25	13.5
<0.075	19.5	<0.075	8.8
Uniformity Coefficient Cu	263.96	Uniformity Coefficient Cu	137.5
Coefficient of Curvature Cc	1.13	Coefficient of Curvature Cc	3.48
Particle Density (g/cm^3)	2.4	Particle Density (g/cm^3)	2.53
Sample Description	Yellow, Arris, No impurities	Sample Description	Grayish yellow, silty sand

Name of the soil	Soil fine breccia	Name of the soil	Bad Graded Soil-Containing Breccia
Group of the Filling Material	B	Group of the Filling Material	B
Conclusion	Meets the design requirements	Conclusion	Meets the design requirements

Mileage 9	DK14+200	Mileage culvert 12	DK25+00
Report Date	11/4/2014	Report Date	15/9/2012
Digging Depth	0.5 m	Digging Depth	2.5 m
Sieve Sizes (mm)	Particle Size Passing (%)	Sieve Sizes (mm)	Particle Size Passing (%)
<200	100	<200	
<60	88.1	<60	
<40	77	<40	100
<20	70.4	<20	99.3
<10	62.5	<10	95.2
<5	54.7	<5	78.4
<2	42.6	<2	57.8
<1	38.8	<1	39.2
<0.5	30.1	<0.5	23
<0.25	25.1	<0.25	14
<0.075	5	<0.075	9.2
Uniformity Coefficient Cu	70.85	Uniformity Coefficient Cu	22.22
Coefficient of Curvature Cc	0.25	Coefficient of Curvature Cc	2.31
Particle Density (g/cm^3)	2.5	Particle Density (g/cm^3)	2.52
Sample Description	Yellow, Arris, No impurities	Sample Description	Yellow and brown, powdery
Name of the soil	bad graded soil-containing fine breccia	Name of the soil	low liquid limit silty clay
Group of the Filling Material	B	Group of the Filling Material	C
Conclusion	Meets the design requirements	Conclusion	Meets the design requirements

Mileage 35	DK93+600	Mileage 36	DK94+440
Report Date	18/10/2012	Report Date	12/2/2014
Digging Depth	1.0 m	Digging Depth	2.0 m
Sieve Sizes (mm)	Particle Size Passing (%)	Sieve Sizes (mm)	Particle Size Passing (%)
<200		<200	100
<60		<60	91
<40	100	<40	79.6
<20	98.6	<20	69.1
<10	98.2	<10	59.3
<5	97.7	<5	49.3
<2	95.3	<2	42.5
<1	93.2	<1	31.5
<0.5	77	<0.5	23.6
<0.25	53.8	<0.25	14.6
<0.075	47.3	<0.075	6.6
Uniformity Coefficient Cu		Uniformity Coefficient Cu	71.73
Coefficient of Curvature Cc		Coefficient of Curvature Cc	0.51
Particle Density (g/cm^3)		Particle Density (g/cm^3)	2.51
Sample Description	yellow, powdery	Sample Description	Angular crush stone with soil

Name of the soil	low liquid limit silt clay	Name of the soil	bad graded soil-containing fine breccia
Group of the Filling Material	C	Group of the Filling Material	B
Conclusion	Meets the design requirements	Conclusion	Meets the design requirements

Mileage 43	DK106+869.94 - DK108.084.34	Mileage 44	DK111+521
Report Date	20/12/2014	Report Date	18/4/2014
Digging Depth	0.5 m	Digging Depth	0.5 m
Sieve Sizes (mm)	Particle Size Passing (%)	Sieve Sizes (mm)	Particle Size Passing (%)
<200	100	<200	100
<60	93.3	<60	90.1
<40	84.2	<40	85.1
<20	66.4	<20	76
<10	50.7	<10	64.8
<5	40.3	<5	52.4
<2	31.3	<2	40.2
<1	27.8	<1	35.5
<0.5	20.9	<0.5	25.1
<0.25	12.3	<0.25	19.7
<0.075	5	<0.075	6.4
Uniformity Coefficient Cu	81.72	Uniformity Coefficient Cu	65.9
Coefficient of Curvature Cc	0.85	Coefficient of Curvature Cc	0.55
Particle Density (g/cm^3)	2.5	Particle Density (g/cm^3)	
Sample Description	Yellow, Arris, No impurities	Sample Description	Yellow, Arris, No impurities
Name of the soil	bad graded soil-containing fine breccia	Name of the soil	Bad Graded soil-containing fine Breccia
Group of the Filling Material	B	Group of the Filling Material	B
Conclusion	Meets the design requirements	Conclusion	Meets the design requirements

Mileage 45	DK111+100	Mileage 46	DK113+150
Report Date	18/4/2014	Report Date	18/8/2014
Digging Depth	0.5 m	Digging Depth	2.0 m
Sieve Sizes (mm)	Particle Size Passing (%)	Sieve Sizes (mm)	Particle Size Passing (%)
<200	100	<200	
<60	90.1	<60	
<40	85.1	<40	
<20	76	<20	100
<10	64.8	<10	100
<5	52.4	<5	98.5
<2	40.2	<2	96.3
<1	35.5	<1	93.3
<0.5	25.1	<0.5	87.3
<0.25	19.7	<0.25	55.4
<0.075	6.4	<0.075	44.4
Uniformity Coefficient Cu	65.9	Uniformity Coefficient Cu	
Coefficient of Curvature Cc	0.55	Coefficient of Curvature Cc	
Particle Density (g/cm^3)		Particle Density (g/cm^3)	
Sample Description	Yellow, Arris, No impurities	Sample Description	Yellow, powdery, No impurities
Name of the soil	Bad Graded soil-containing fine Breccia	Name of the soil	low liquid limit silt
Group of the Filling Material	B	Group of the Filling Material	C
Conclusion	Meets the design requirements	Conclusion	Meets the design requirements

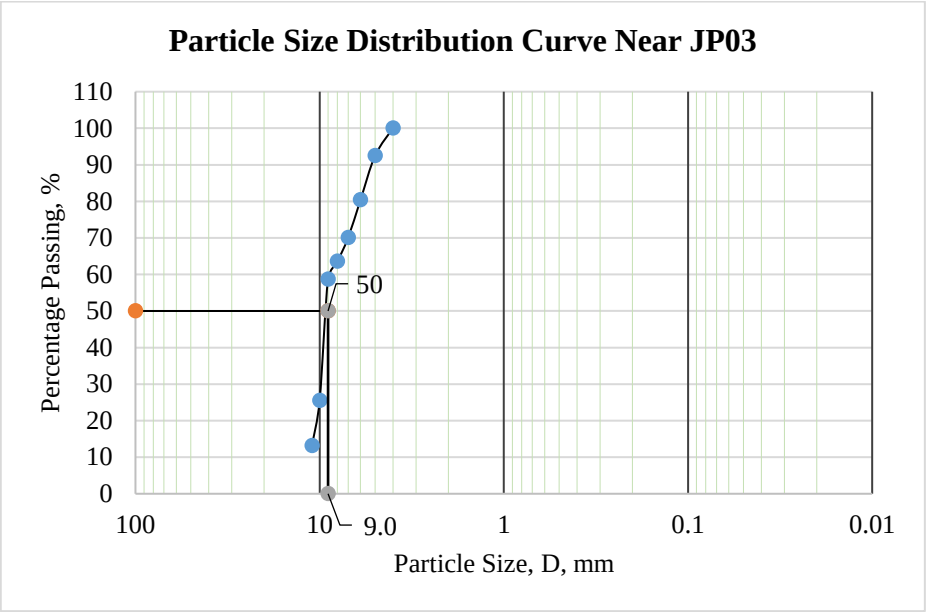
Particle Size Distribution Curve Near JP03
Percentage Passing, %
110
100
90
80
70
60
50
40
30
20
10
0
50
100
10
9.0
1
0.1
0.01
Particle Size, D, mm

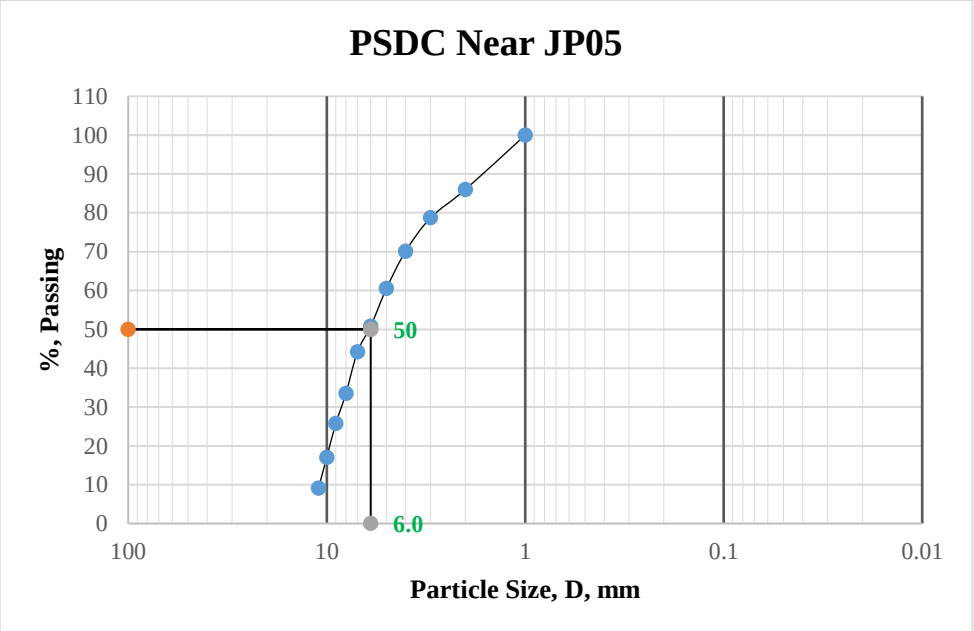
PSDC Near JP05
%, Passing
110
100
90
80
70
60
50
40
30
20
10
0
50
6.0
100
10
1
0.1
0.01
Particle Size, D, mm

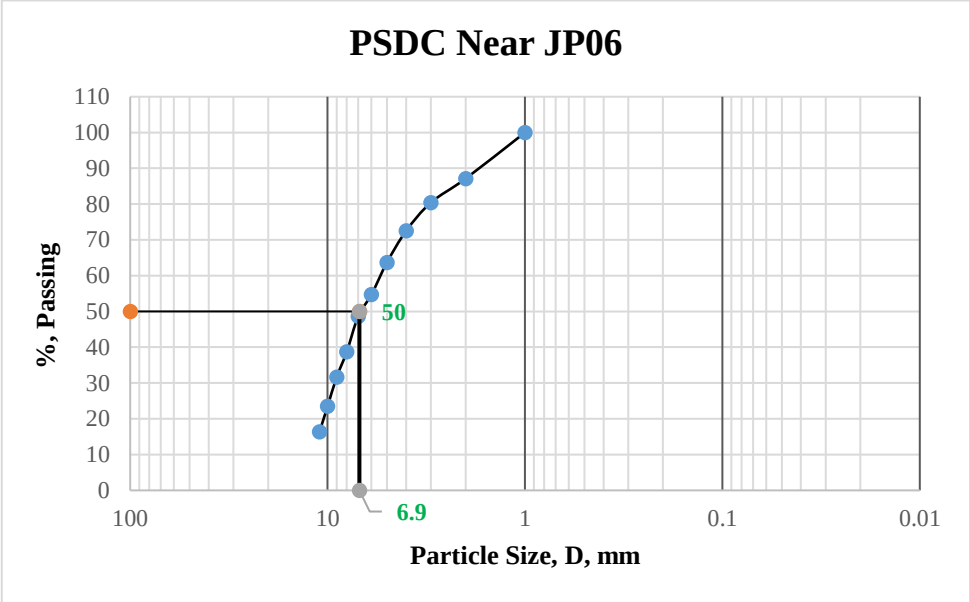
PSDC Near JP06
110
100
90
80
70
60
50
40
30
20
10
0
%, Passing
50
6.9
100
10
1
0.1
0.01
Particle Size, D, mm

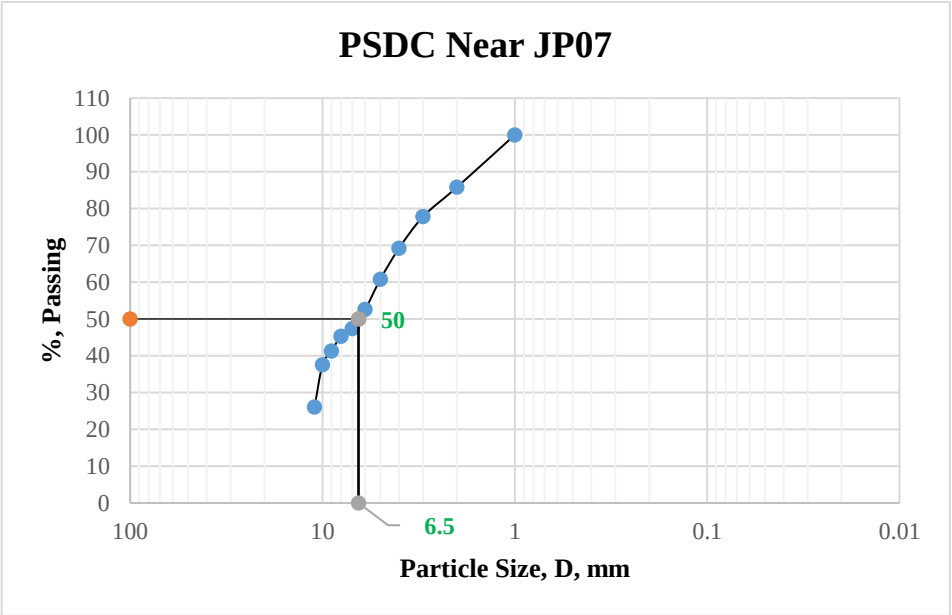
PSDC Near JP07
110
100
90
80
70
60
50
40
30
20
10
0
%, Passing
50
6.5
100
10
1
0.1
0.01
Particle Size, D, mm

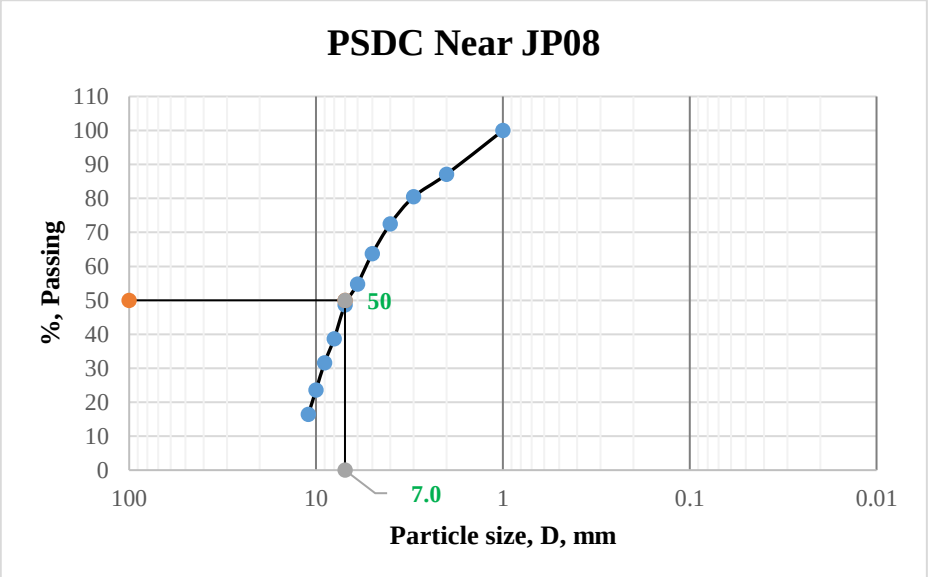
PSDC Near JP08
110
100
90
80
70
60
50
40
30
20
10
0
%, Passing
50
7.0
100
10
1
0.1
0.01
Particle size, D, mm

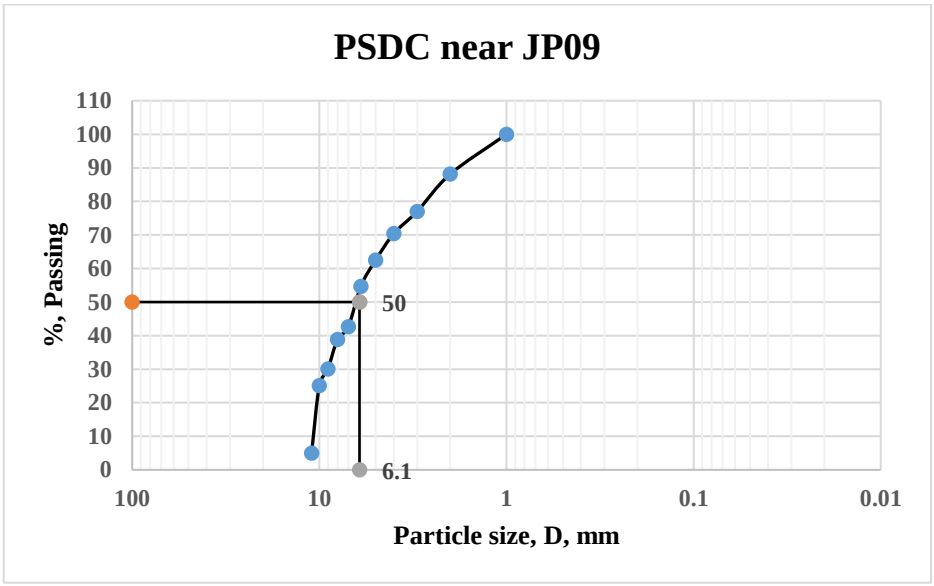
PSDC near JP09
110
100
90
80
70
60
50
40
30
20
10
0
%, Passing
50
6.1
100
10
1
0.1
0.01
Particle size, D, mm

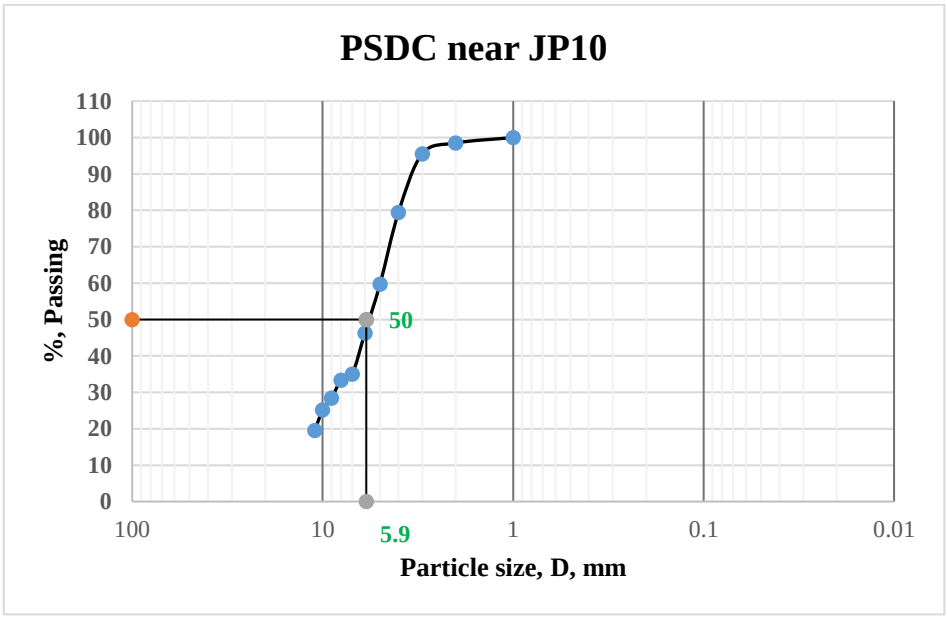
PSDC near JP10
110
100
90
80
70
60
50
40
30
20
10
0
%, Passing
50
5.9
100
10
1
0.1
0.01
Particle size, D, mm

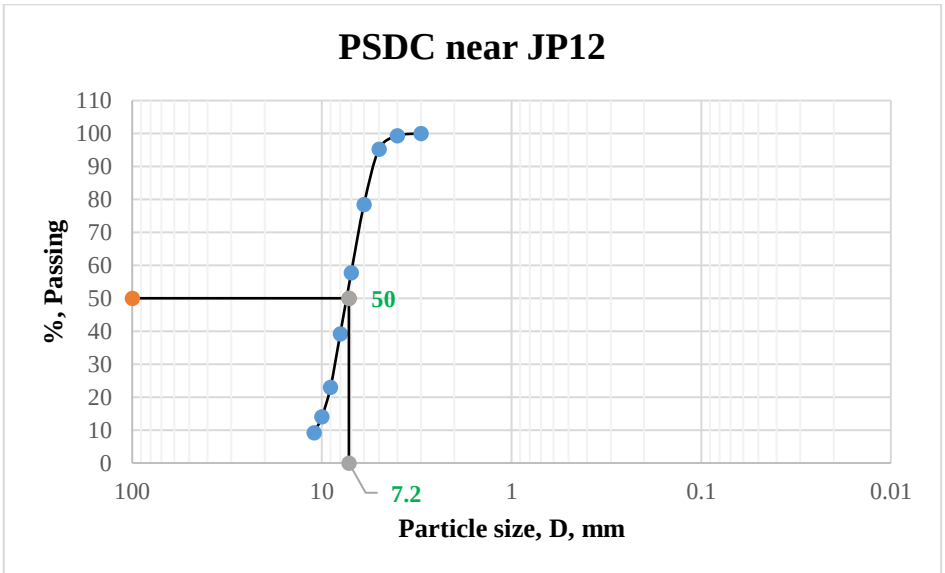
PSDC near JP12
110
100
90
80
70
60
50
40
30
20
10
0
%, Passing
50
7.2
100
10
1
0.1
0.01
Particle size, D, mm

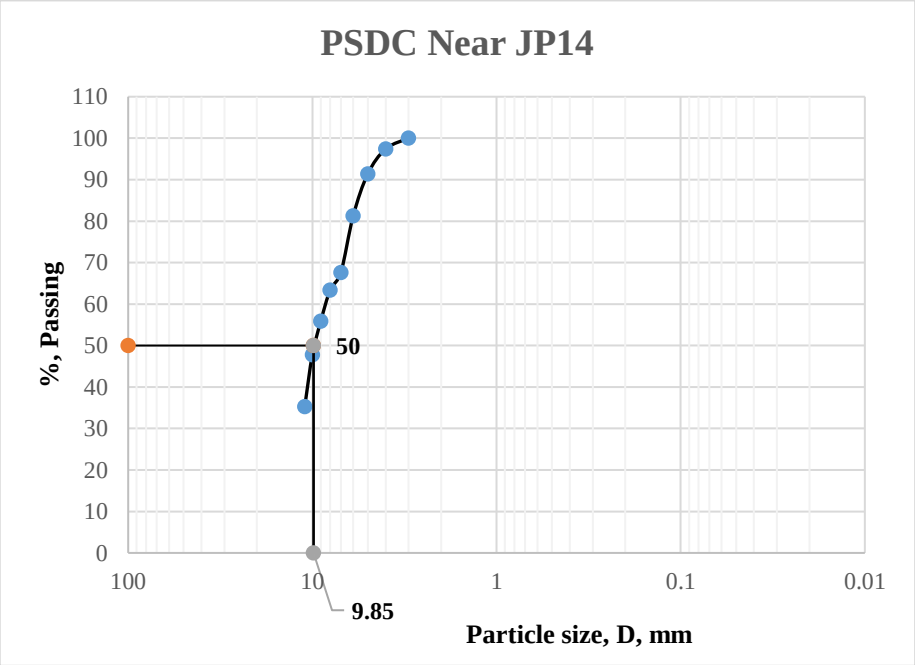
PSDC Near JP14
110
100
90
80
70
60
50
40
30
20
10
0
%, Passing
50
100
10
1
0.1
0.01
9.85
Particle size, D, mm

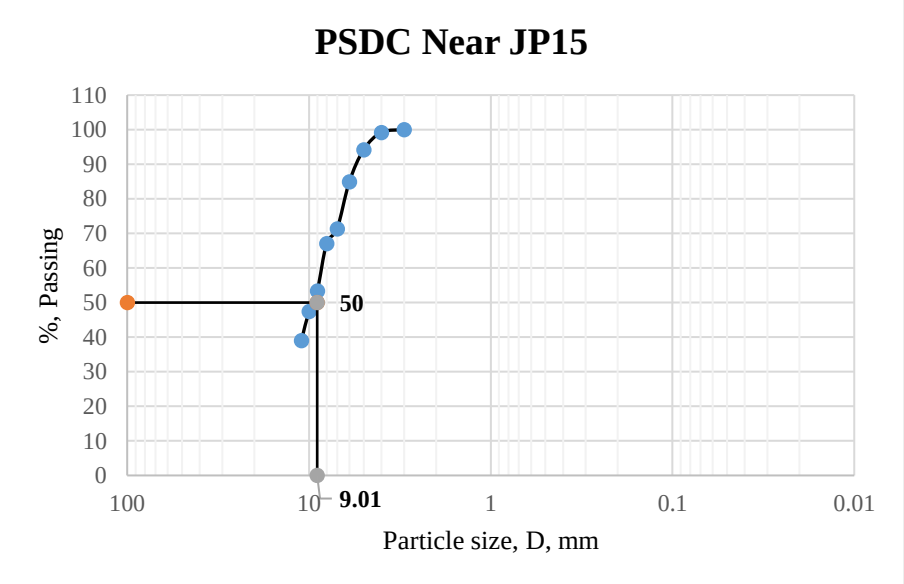
PSDC Near JP15
110
100
90
80
70
60
50
40
30
20
10
0
%, Passing
50
100
10
1
0.1
0.01
9.01
Particle size, D, mm

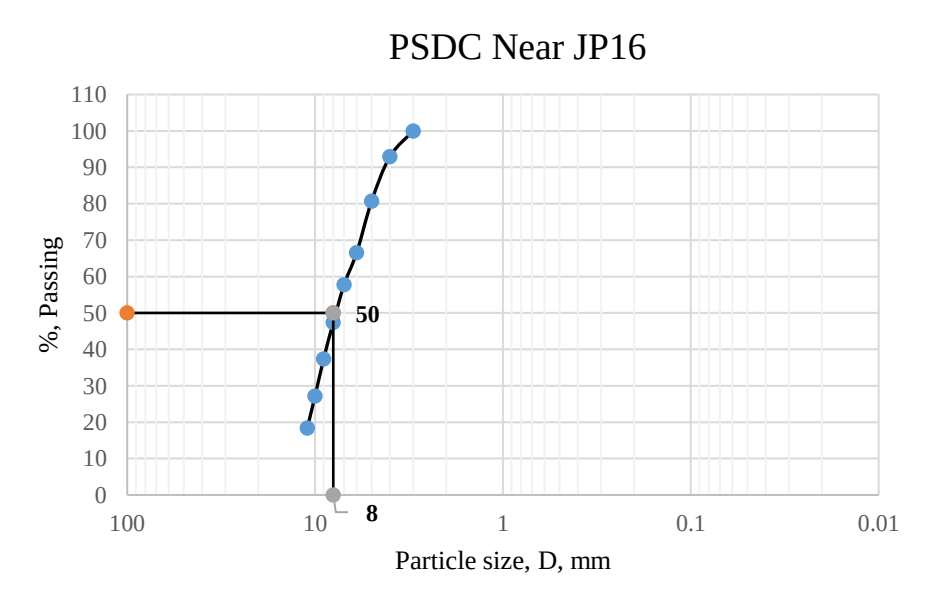
PSDC Near JP16
110
100
90
80
70
60
50
40
30
20
10
0
%, Passing
50
100
10
1
0.1
0.01
8
Particle size, D, mm

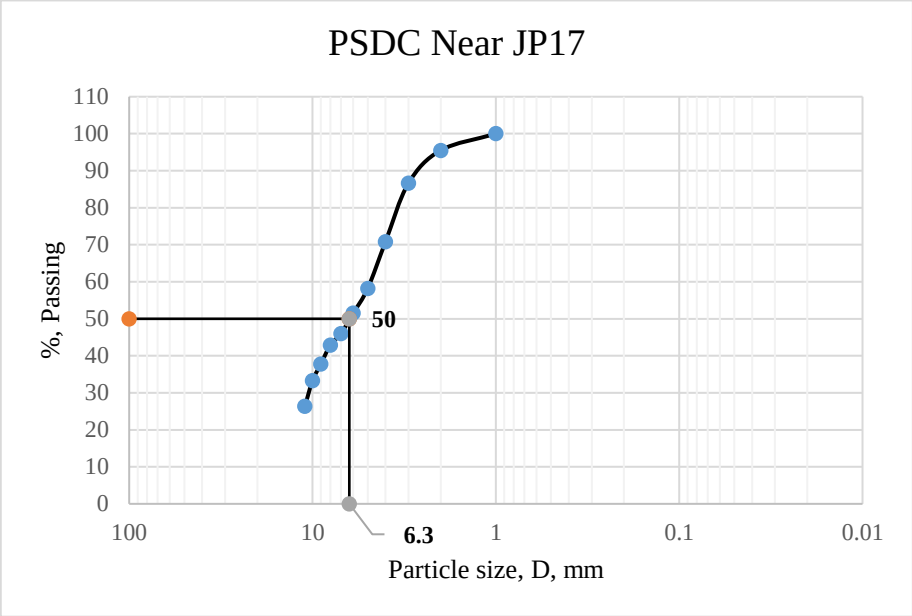
PSDC Near JP17
110
100
90
80
70
60
50
40
30
20
10
0
%, Passing
50
100
10
6.3
1
0.1
0.01
Particle size, D, mm

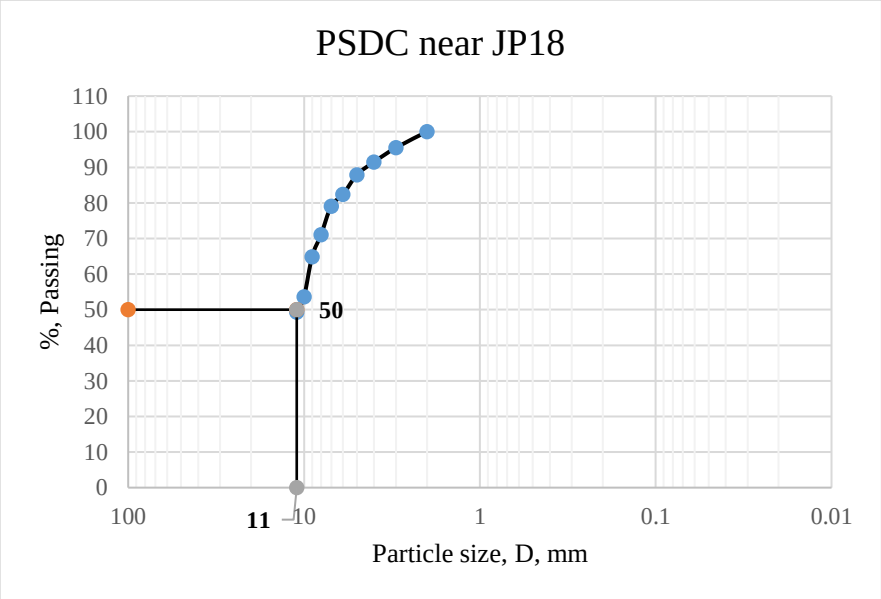
PSDC near JP18
110
100
90
80
70
60
50
40
30
20
10
0
%, Passing
50
100
11
10
1
0.1
0.01
Particle size, D, mm

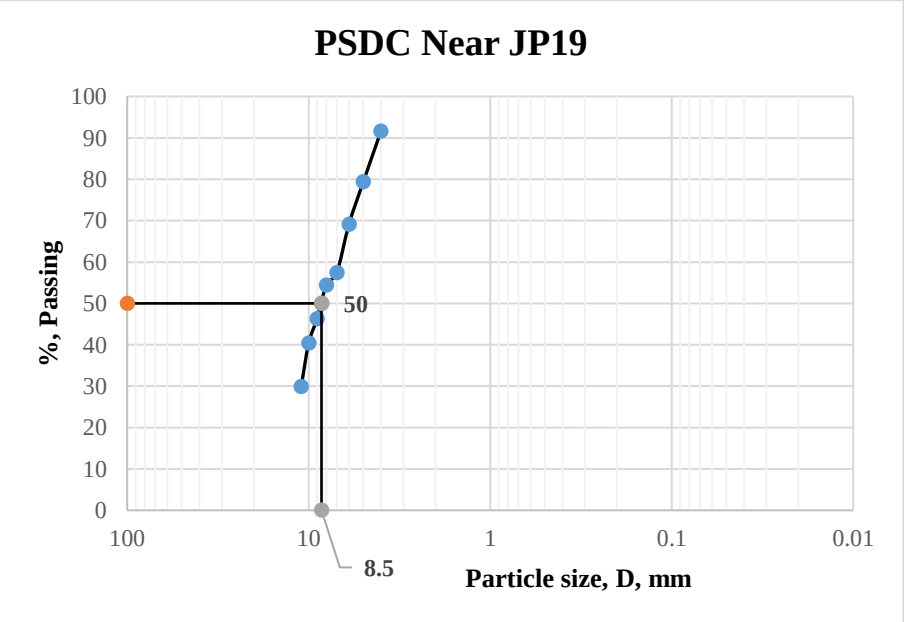
PSDC Near JP19
100
90
80
70
60
50
40
30
20
10
0
%, Passing
50
100
10
8.5
1
0.1
0.01
Particle size, D, mm

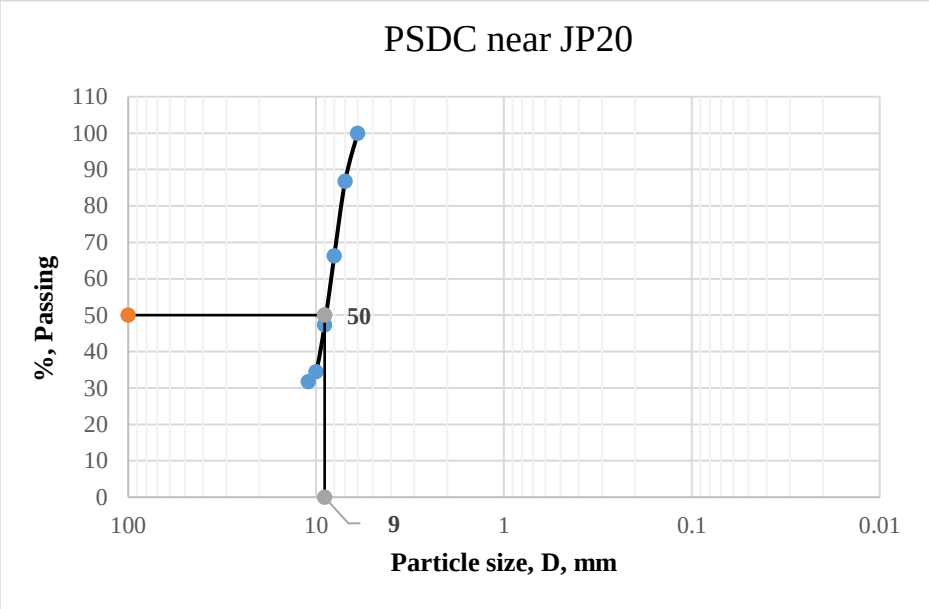
PSDC near JP20
110
100
90
80
70
60
50
40
30
20
10
0
%, Passing
50
100
10
9
1
0.1
0.01
Particle size, D, mm

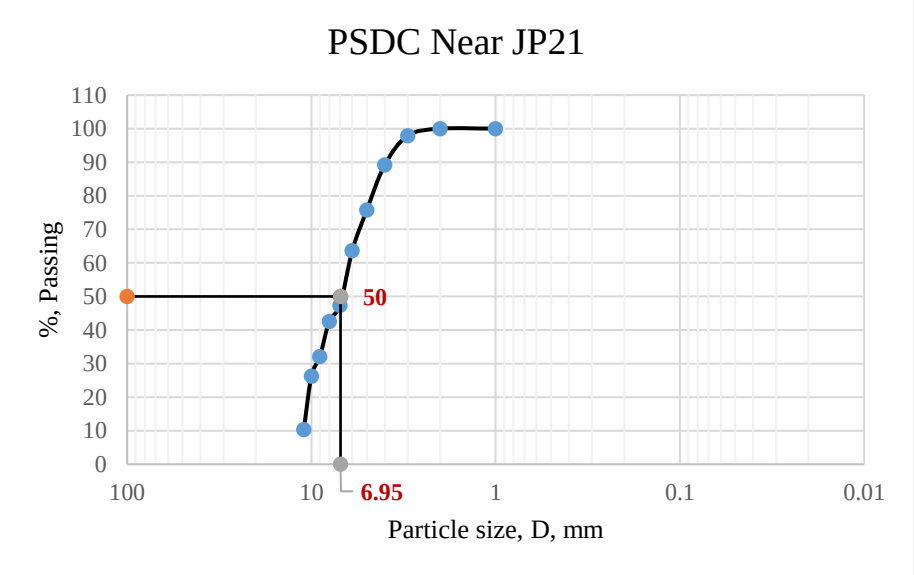
PSDC Near JP21
110
100
90
80
70
60
50
40
30
20
10
0
%, Passing
50
100
10
6.95
1
0.1
0.01
Particle size, D, mm

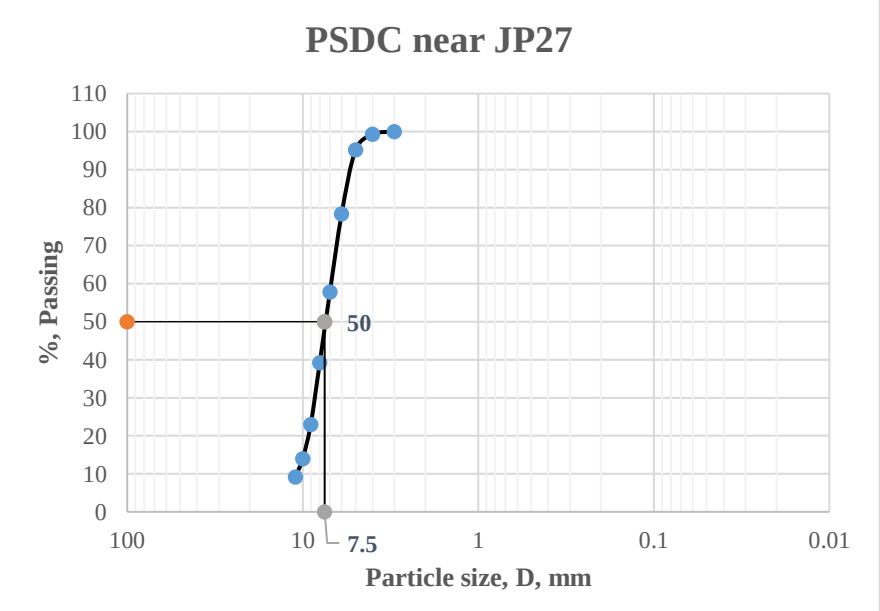
PSDC near JP27
110
100
90
80
70
60
50
40
30
20
10
0
%, Passing
50
100
10
7.5
1
0.1
0.01
Particle size, D, mm

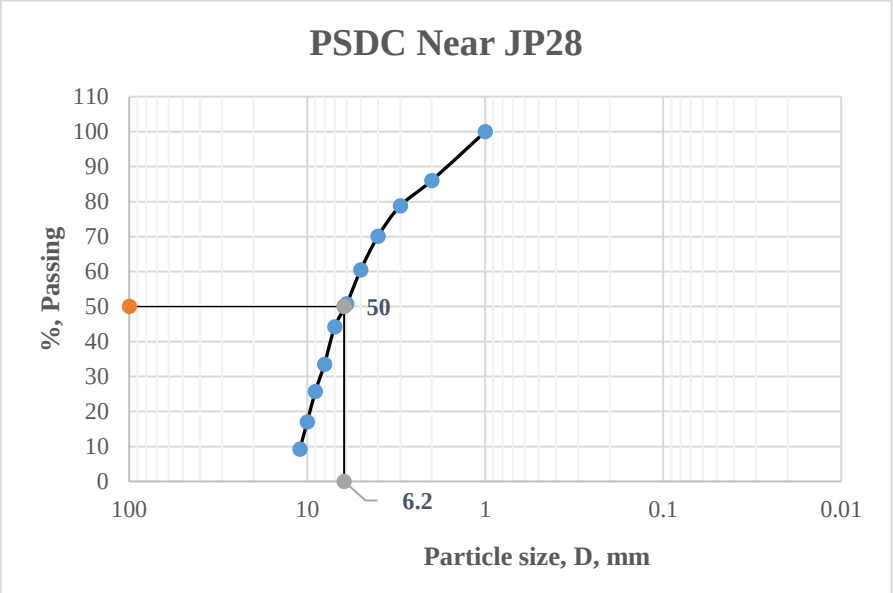
PSDC Near JP28
110
100
90
80
70
60
50
40
30
20
10
0
%, Passing
50
6.2
100
10
1
0.1
0.01
Particle size, D, mm

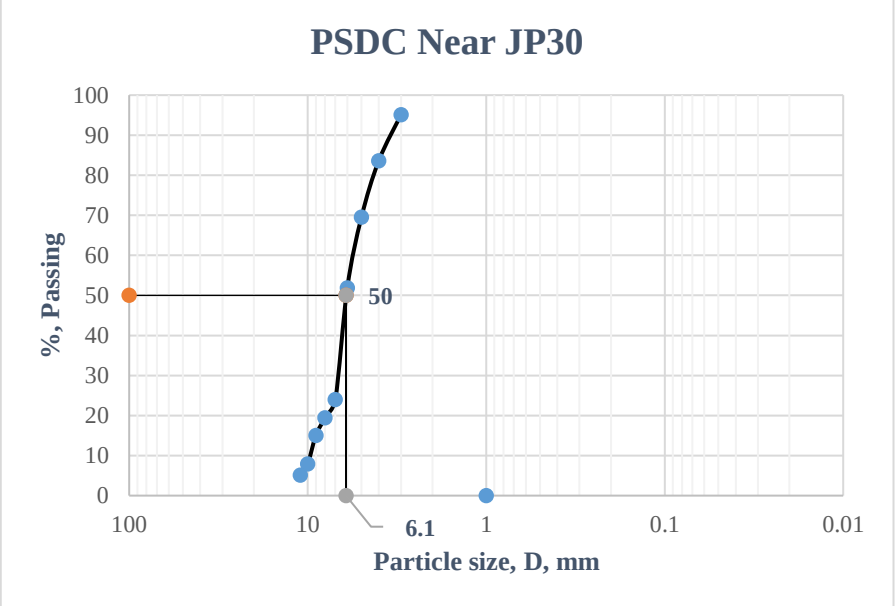
PSDC Near JP30
100
90
80
70
60
50
40
30
20
10
0
%, Passing
50
6.1
100
10
1
0.1
0.01
Particle size, D, mm

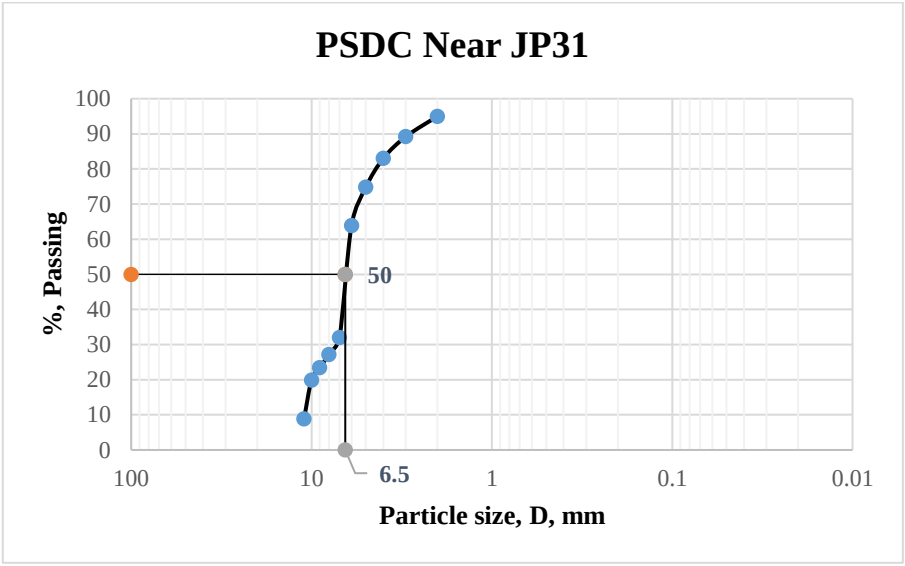
PSDC Near JP31
%, Passing
100
90
80
70
60
50
40
30
20
10
0
50
6.5
100
10
1
0.1
0.01
Particle size, D, mm

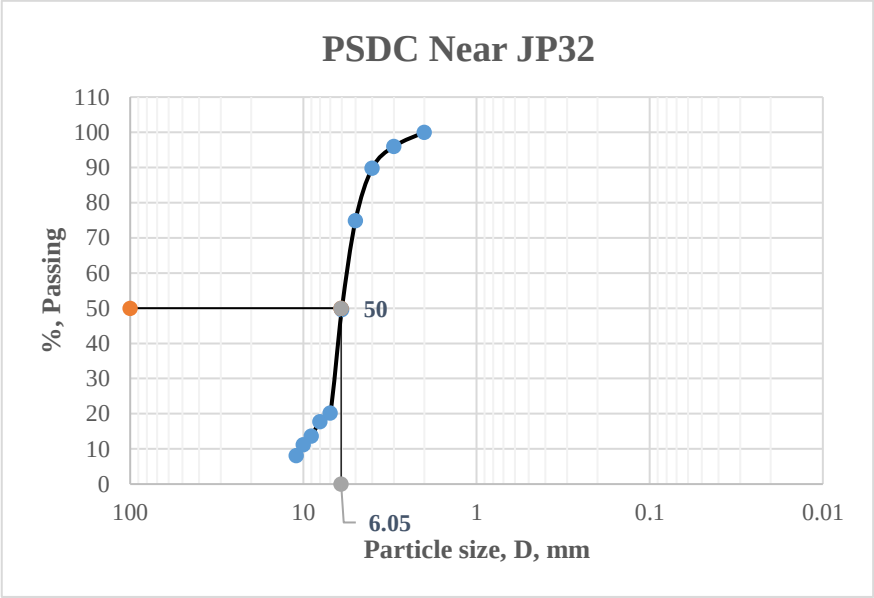
PSDC Near JP32
%, Passing
110
100
90
80
70
60
50
40
30
20
10
0
50
6.05
100
10
1
0.1
0.01
Particle size, D, mm

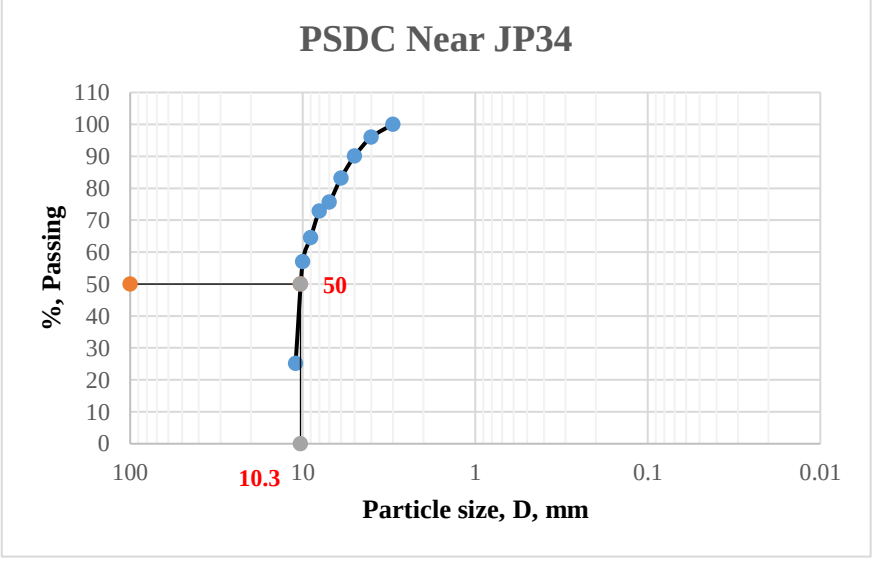
PSDC Near JP34
%, Passing
110
100
90
80
70
60
50
40
30
20
10
0
50
10.3
100
10
1
0.1
0.01
Particle size, D, mm

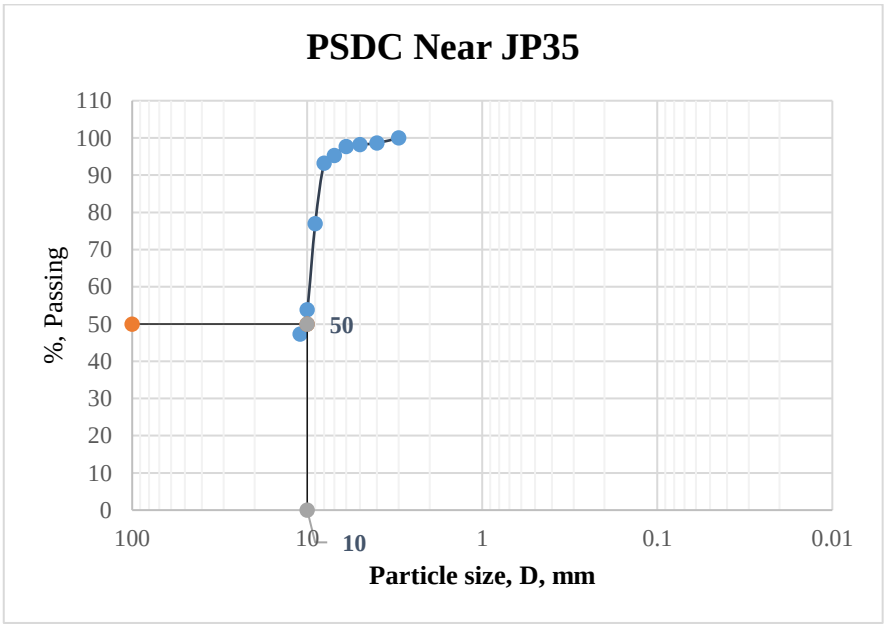
PSDC Near JP35
110
100
90
80
70
60
50
40
30
20
10
0
%, Passing
50
100
10
10
1
0.1
0.01
Particle size, D, mm

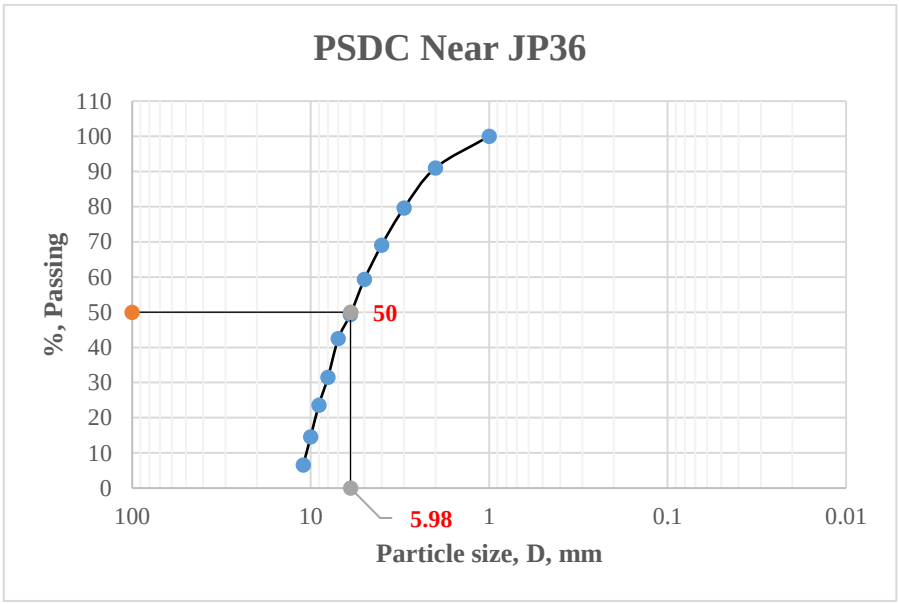
PSDC Near JP36
110
100
90
80
70
60
50
40
30
20
10
0
%, Passing
50
100
10
5.98
1
0.1
0.01
Particle size, D, mm

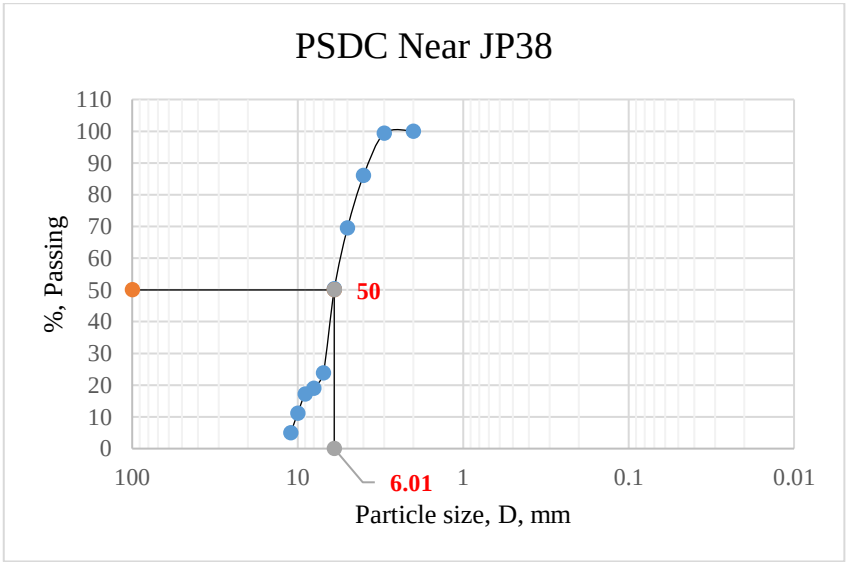
PSDC Near JP38
110
100
90
80
70
60
50
40
30
20
10
0
%, Passing
50
100
10
6.01
1
0.1
0.01
Particle size, D, mm

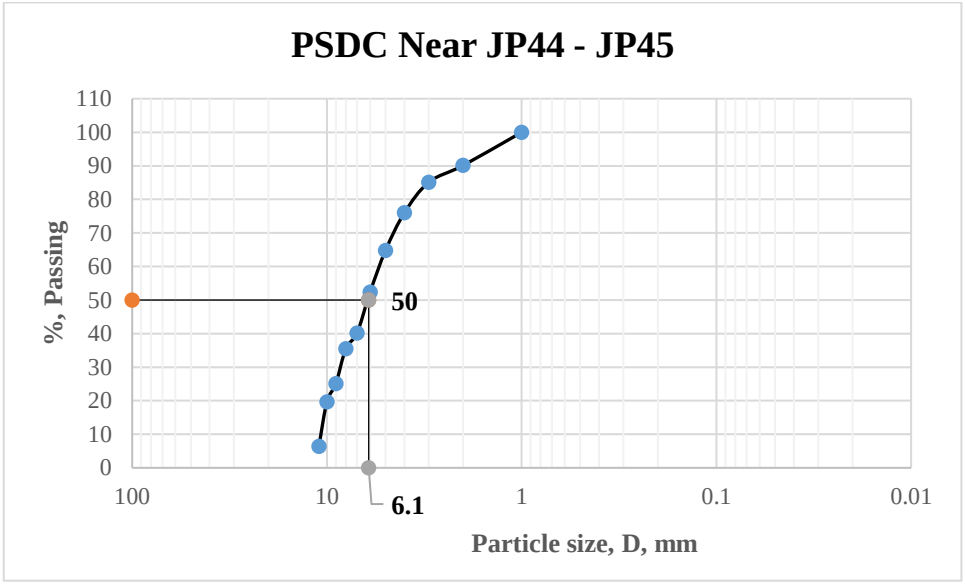
PSDC Near JP44 - JP45
%, Passing
110
100
90
80
70
60
50
40
30
20
10
0
50
100
10
6.1
1
0.1
0.01
Particle size, D, mm

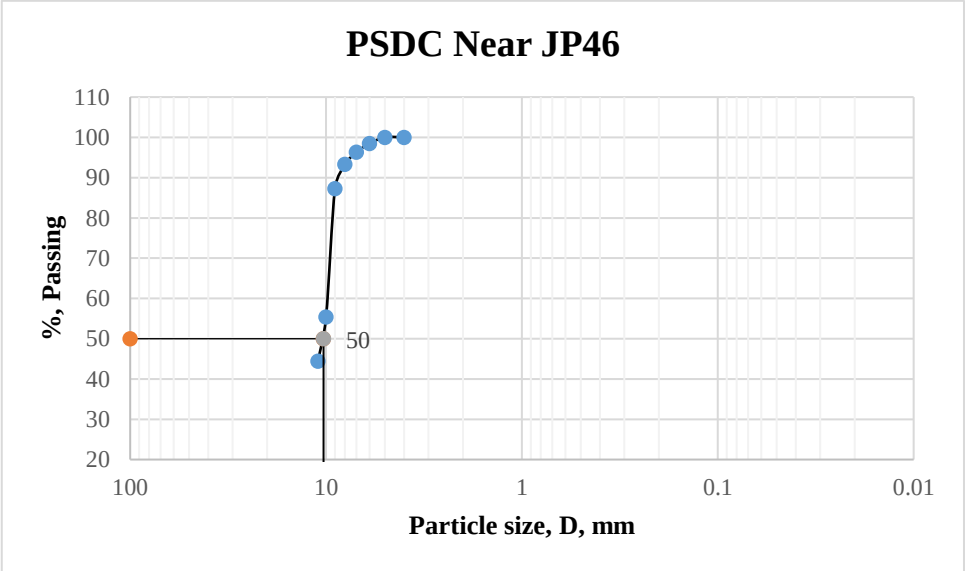
PSDC Near JP46
%, Passing
110
100
90
80
70
60
50
40
30
20
50
100
10
1
0.1
0.01
Particle size, D, mm

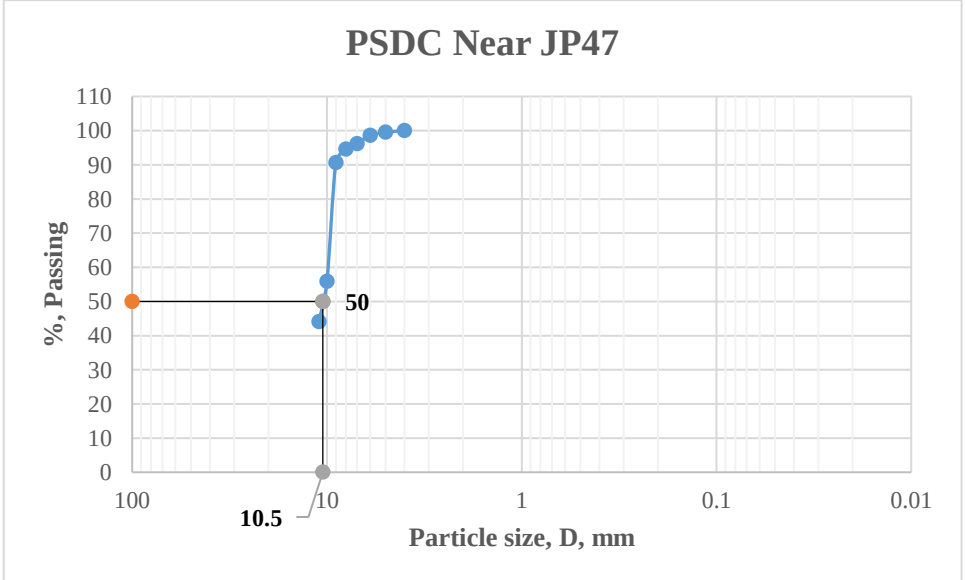
PSDC Near JP47
%, Passing
110
100
90
80
70
60
50
40
30
20
10
0
50
100
10.5
10
1
0.1
0.01
Particle size, D, mm

APPENDIX F

The table shows the information about the flow characteristics of each junction point and their respective estimated scour depth (m)

SLAB BOX CULVERTS

JP01

T (yrs)	Peak Q(cms)	Yo(m)	Vn(m/s)	A(sqm)	Yc (m)	Vc (m/s)	Vc/Vn	Fr	Ymax (m)	Ys (m)
2	13.8	0.5	6.905	1.999	0.404	1.992	0.288	3.118	1.380	0.880
5	19.1	0.619	7.72	2.474	0.775	2.757	0.357	3.133	1.645	1.026
10	22.6	0.692	8.166	2.768	1.085	3.262	0.399	3.134	1.802	1.110
25	27.2	0.784	8.677	3.135	1.571	3.926	0.452	3.129	1.991	1.207
50	30.7	0.851	9.022	3.403	2.002	4.431	0.491	3.123	2.126	1.275
100	34.2	0.916	9.335	3.664	2.484	4.936	0.529	3.114	2.253	1.337
200	37.7	0.979	9.622	3.918	3.018	5.442	0.566	3.105	2.375	1.396
500	42.3	1.061	9.968	4.244	3.800	6.105	0.613	3.090	2.527	1.466

JP02

T (yrs)	Peak Q(cms)	Yo(m)	Vn(m/s)	A(sqm)	Yc (m)	Vc (m/s)	Vc/Vn	Fr	Ymax (m)	Ys (m)
2	14.3	0.315	7.558	1.892	0.193	1.376	0.182	4.299	1.438	1.123
5	19.8	0.387	8.535	2.320	0.370	1.905	0.223	4.380	1.714	1.327
10	23.5	0.431	9.093	2.584	0.521	2.261	0.249	4.422	1.880	1.449
25	28.3	0.485	9.735	2.907	0.756	2.723	0.280	4.463	2.079	1.594
50	32	0.524	10.179	3.144	0.967	3.079	0.303	4.490	2.222	1.698
100	35.6	0.561	10.579	3.365	1.196	3.426	0.324	4.510	2.353	1.792
200	39.2	0.597	10.95	3.580	1.450	3.772	0.344	4.525	2.479	1.882
500	44.1	0.644	11.419	3.862	1.836	4.244	0.372	4.543	2.642	1.998

JP03

T(yrs)	Peak Q(cms)	Yo(m)	Vn(m/s)	A(sqm)	Yc (m)	Vc (m/s)	Vc/Vn	Fr	Ymax (m)	Ys (m)
2	28.9	0.714	6.745	4.285	0.788	2.781	0.412	2.549	1.766	1.052
5	39.7	0.879	7.527	5.274	1.488	3.820	0.508	2.563	2.096	1.217
10	47.2	0.986	7.979	5.916	2.103	4.542	0.569	2.566	2.302	1.316
25	56.8	1.116	8.482	6.697	3.045	5.466	0.644	2.563	2.544	1.428
50	64	1.21	8.817	7.259	3.866	6.158	0.698	2.559	2.713	1.503
100	71.3	1.302	9.127	7.812	4.798	6.861	0.752	2.554	2.876	1.574
200	78.6	1.392	9.412	8.351	5.831	7.563	0.804	2.547	3.031	1.639
500	88.2	1.507	9.755	9.042	7.343	8.487	0.870	2.537	3.226	1.719

JP04

T(yrs)	Peak Q(cms)	Yo(m)	Vn(m/s)	A(sqm)	Yc (m)	Vc (m/s)	Vc/Vn	Fr	Ymax (m)	Ys (m)
2	26.6	0.581	9.164	2.903	0.962	3.072	0.335	3.839	1.947	1.366
5	36.7	0.716	10.245	3.582	1.831	4.238	0.414	3.866	2.316	1.600
10	43.5	0.802	10.852	4.008	2.572	5.023	0.463	3.869	2.539	1.737
25	52.3	0.907	11.536	4.534	3.718	6.039	0.523	3.867	2.804	1.897
50	59	0.983	11.999	4.917	4.731	6.813	0.568	3.864	2.993	2.010
100	65.6	1.057	12.415	5.284	5.849	7.575	0.610	3.855	3.169	2.112
200	72.3	1.129	12.803	5.647	7.105	8.348	0.652	3.847	3.340	2.211
500	81.1	1.222	13.27	6.112	8.939	9.365	0.706	3.833	3.554	2.332

JP10

T(yrs)	Peak Q(cms)	Yo(m)	Vn(m/s)	A(sqm)	Yc (m)	Vc (m/s)	Vc/Vn	Fr	Ymax (m)	Ys (m)
2	6.9	0.542	4.245	1.625	0.180	1.328	0.313	1.841	1.089	0.547
5	9.5	0.673	4.706	2.019	0.341	1.828	0.388	1.832	1.294	0.621
10	11.3	0.758	4.967	2.275	0.482	2.175	0.438	1.821	1.421	0.663
25	13.7	0.868	5.264	2.603	0.709	2.637	0.501	1.804	1.577	0.709
50	15.4	0.942	5.448	2.827	0.895	2.964	0.544	1.792	1.680	0.738
100	17.2	1.019	5.624	3.058	1.117	3.310	0.589	1.779	1.783	0.764
200	19	1.095	5.783	3.285	1.363	3.657	0.632	1.764	1.882	0.787
500	21.3	1.19	5.968	3.569	1.713	4.099	0.687	1.747	2.002	0.812

JP24

T(yrs)	Peak Q(cms)	Yo(m)	Vn(m/s)	A(sqm)	Yc (m)	Vc (m/s)	Vc/Vn	Fr	Ymax (m)	Ys (m)
2	21.9	1.017	7.178	3.051	1.811	4.215	0.587	2.273	1.958	0.941
5	30.3	1.287	7.847	3.861	3.466	5.831	0.743	2.208	2.333	1.046
10	36.1	1.466	8.21	4.397	4.920	6.947	0.846	2.165	2.565	1.099
25	43.6	1.69	8.599	5.070	7.177	8.391	0.976	2.112	2.840	1.150
50	49.2	1.854	8.846	5.562	9.139	9.469	1.070	2.074	3.032	1.178
100	54.8	2.015	9.064	6.046	11.338	10.546	1.164	2.039	3.213	1.198
200	60.4	2.175	9.258	6.524	13.773	11.624	1.256	2.004	3.387	1.212
500	67.9	2.386	9.487	7.157	17.406	13.067	1.377	1.961	3.608	1.222

JP27

T(yrs)	Peak Q(cms)	Yo(m)	Vn(m/s)	A(sqm)	Yc (m)	Vc (m/s)	Vc/Vn	Fr	Ymax (m)	Ys (m)
2	3.91	0.489	3.999	0.978	0.130	1.129	0.282	1.826	0.837	0.348
5	5.47	0.618	4.424	1.236	0.254	1.579	0.357	1.797	1.003	0.385
10	6.54	0.702	4.656	1.405	0.363	1.888	0.405	1.774	1.104	0.402
25	7.93	0.808	4.91	1.615	0.534	2.289	0.466	1.744	1.226	0.418
50	8.97	0.884	5.074	1.768	0.683	2.589	0.510	1.723	1.310	0.426
100	10.03	0.96	5.222	1.921	0.855	2.895	0.554	1.702	1.391	0.431
200	11.08	1.035	5.353	2.070	1.043	3.199	0.598	1.680	1.468	0.433
500	12.48	1.132	5.51	2.265	1.323	3.603	0.654	1.653	1.566	0.434

JP45

T(yrs)	Peak Q(cms)	Yo(m)	Vn(m/s)	A(sqm)	Yc (m)	Vc (m/s)	Vc/Vn	Fr	Ymax (m)	Ys (m)
2	7.24	0.309	5.852	1.237	0.071	0.836	0.143	3.361	0.970	0.661
5	10.1	0.382	6.602	1.530	0.139	1.166	0.177	3.410	1.161	0.779
10	12.08	0.429	7.037	1.717	0.198	1.395	0.198	3.430	1.279	0.850
25	14.62	0.486	7.526	1.943	0.291	1.688	0.224	3.447	1.418	0.932
50	16.54	0.526	7.855	2.106	0.372	1.910	0.243	3.458	1.516	0.990
100	18.46	0.566	8.157	2.263	0.463	2.132	0.261	3.462	1.608	1.042
200	20.4	0.604	8.44	2.417	0.566	2.356	0.279	3.467	1.697	1.093
500	22.96	0.654	8.782	2.614	0.716	2.651	0.302	3.467	1.809	1.155

JP46

T(yrs)	Peak Q(cms)	Yo(m)	Vn(m/s)	A(sqm)	Yc (m)	Vc (m/s)	Vc/Vn	Fr	Ymax (m)	Ys (m)
2	7.10	0.36	3.946	1.799	0.069	0.820	0.208	2.100	0.838	0.478

5	9.90	0.444	4.455	2.222	0.133	1.143	0.257	2.135	1.002	0.558
10	11.80	0.497	4.745	2.487	0.189	1.363	0.287	2.149	1.102	0.605
25	14.20	0.56	5.067	2.802	0.274	1.640	0.324	2.162	1.218	0.658
50	16.00	0.606	5.284	3.028	0.348	1.848	0.350	2.167	1.299	0.693
100	17.90	0.652	5.495	3.258	0.435	2.067	0.376	2.173	1.380	0.728
200	19.70	0.694	5.679	3.469	0.527	2.275	0.401	2.176	1.454	0.760
500	22.10	0.748	5.906	3.742	0.664	2.552	0.432	2.180	1.547	0.799

FRAME BRIDGES

JP19

T(yrs)	Peak Q(cms)	Yo(m)	Vn(m/s)	A(sqm)	Yc (m)	Vc (m/s)	Vc/Vn	Fr	Ymax (m)	Ys (m)
2	52.02	1.959	3.916	13.284	2.554	5.006	1.278	0.893	2.462	0.503
5	71.98	2.404	4.302	16.732	4.890	6.926	1.610	0.886	2.934	0.530
10	85.75	2.683	4.518	18.980	6.940	8.251	1.826	0.881	3.225	0.542
25	103.63	3.022	4.758	21.780	10.136	9.972	2.096	0.874	3.572	0.550
50	117.14	3.262	4.916	23.828	12.951	11.272	2.293	0.869	3.816	0.554
100	130.72	3.492	5.061	25.829	16.128	12.579	2.485	0.865	4.049	0.557
200	144.38	3.714	5.193	27.803	19.675	13.893	2.675	0.860	4.272	0.558
500	162.59	3.997	5.354	30.368	24.951	15.645	2.922	0.855	4.555	0.558

JP25

T(yrs)	Peak Q(cms)	Yo(m)	Vn(m/s)	A(sqm)	Yc (m)	Vc (m/s)	Vc/Vn	Fr	Ymax (m)	Ys (m)
2	44.27	0.402	4.216	10.500	0.100	0.990	0.235	2.123	1.612	1.210
5	61.37	0.489	4.789	12.815	0.192	1.372	0.286	2.187	1.923	1.434
10	73.15	0.544	5.127	14.268	0.273	1.635	0.319	2.219	2.114	1.570
25	88.16	0.609	5.511	15.997	0.396	1.971	0.358	2.255	2.338	1.729
50	99.56	0.655	5.777	17.234	0.505	2.225	0.385	2.279	2.497	1.842
100	110.96	0.699	6.023	18.423	0.627	2.480	0.412	2.300	2.648	1.949
200	122.36	0.742	6.254	19.565	0.763	2.735	0.437	2.318	2.791	2.049
500	137.56	0.796	6.54	21.034	0.964	3.075	0.470	2.340	2.973	2.177

JP26

T(yrs)	Peak Q(cms)	Yo(m)	Vn(m/s)	A(sqm)	Yc (m)	Vc (m/s)	Vc/Vn	Fr	Ymax (m)	Ys (m)
2	43.6	0.329	5.079	8.584	0.097	0.975	0.192	2.827	1.655	1.326
5	60.2	0.4	5.764	10.444	0.185	1.346	0.233	2.910	1.970	1.570
10	71.6	0.444	6.167	11.610	0.261	1.600	0.260	2.955	2.164	1.720
25	86.3	0.497	6.633	13.011	0.379	1.929	0.291	3.004	2.393	1.896
50	97.4	0.534	6.952	14.010	0.483	2.177	0.313	3.037	2.555	2.021
100	108.5	0.57	7.249	14.968	0.600	2.425	0.335	3.066	2.708	2.138
200	119.7	0.605	7.53	15.896	0.730	2.676	0.355	3.091	2.856	2.251
500	134.5	0.649	7.876	17.077	0.921	3.006	0.382	3.121	3.041	2.392

JP28

T(yrs)	Peak Q(cms)	Yo(m)	Vn(m/s)	A(sqm)	Yc (m)	Vc (m/s)	Vc/Vn	Fr	Ymax (m)	Ys (m)
2	37.40	0.505	6.068	6.163	0.330	1.799	0.297	2.726	1.867	1.362
5	51.80	0.616	6.863	7.548	0.633	2.492	0.363	2.792	2.227	1.611
10	61.60	0.685	7.323	8.412	0.895	2.964	0.405	2.825	2.445	1.760
25	74.30	0.769	7.851	9.464	1.303	3.575	0.455	2.858	2.705	1.936
50	83.90	0.829	8.212	10.217	1.661	4.037	0.492	2.880	2.889	2.060

100	93.50	0.886	8.545	10.942	2.063	4.499	0.526	2.898	3.063	2.177
200	103.20	0.941	8.858	11.650	2.513	4.965	0.561	2.915	3.231	2.290
500	116.10	1.012	9.245	12.558	3.181	5.586	0.604	2.934	3.443	2.431

JP30

T(yrs)	Peak Q(cms)	Yo(m)	Vn(m/s)	A(sqm)	Yc (m)	Vc (m/s)	Vc/Vn	Fr	Ymax (m)	Ys (m)
2	48.5	0.619	3.254	14.905	0.143	1.185	0.364	1.320	1.809	1.190
5	67.0	0.752	3.684	18.187	0.273	1.637	0.444	1.356	2.154	1.402
10	79.0	0.830	3.923	20.138	0.380	1.930	0.492	1.375	2.355	1.525
25	95.5	0.931	4.215	22.657	0.555	2.333	0.554	1.395	2.609	1.678
50	107.5	1.000	4.408	24.387	0.703	2.627	0.596	1.407	2.781	1.781
100	119.5	1.066	4.587	26.052	0.869	2.920	0.637	1.418	2.944	1.878
200	131.5	1.130	4.754	27.661	1.052	3.213	0.676	1.428	3.101	1.971
500	147.5	1.211	4.963	29.720	1.324	3.604	0.726	1.440	3.299	2.088

JP34

T(yrs)	Peak Q(cms)	Yo(m)	Vn(m/s)	A(sqm)	Yc (m)	Vc (m/s)	Vc/Vn	Fr	Ymax (m)	Ys (m)
2	17.6	0.751	2.823	6.235	0.164	1.270	0.450	1.040	1.412	0.661
5	24.8	0.929	3.188	7.779	0.327	1.790	0.561	1.056	1.699	0.770
10	29.9	1.044	3.402	8.789	0.475	2.158	0.634	1.063	1.879	0.835
25	36.4	1.181	3.639	10.003	0.703	2.627	0.722	1.069	2.090	0.909
50	41.3	1.278	3.797	10.877	0.906	2.981	0.785	1.072	2.238	0.960
100	46.3	1.373	3.945	11.736	1.138	3.341	0.847	1.075	2.380	1.007
200	51.3	1.464	4.081	12.570	1.397	3.702	0.907	1.077	2.516	1.052
500	57.9	1.58	4.246	13.636	1.780	4.179	0.984	1.078	2.685	1.105

SIMPLY SUPPORT T-BEAM BRIDGES

JP38

T(yrs)	Peak Q(cms)	Yo(m)	Vn(m/s)	A(sqm)	Yc (m)	Vc (m/s)	Vc/Vn	Fr	Ys/Yo	Ys (m)	Risk FPR = Ys/fd	Risk (%)
2	10.1	0.357	5.292	1.909	0.121	1.090	0.206	2.828	12.766	4.558	0.142	14.2
5	14.1	0.441	5.982	2.357	0.236	1.522	0.254	2.876	11.209	4.943	0.154	15.4
10	16.7	0.491	6.36	2.626	0.331	1.802	0.283	2.898	10.487	5.149	0.161	16.1
25	20.2	0.555	6.808	2.967	0.484	2.180	0.320	2.918	9.713	5.391	0.168	16.8
50	22.8	0.6	7.107	3.208	0.617	2.460	0.346	2.929	9.249	5.549	0.173	17.3
100	25.4	0.643	7.381	3.441	0.766	2.741	0.371	2.939	8.854	5.693	0.178	17.8
200	28.0	0.685	7.636	3.667	0.931	3.022	0.396	2.946	8.506	5.827	0.182	18.2
500	31.5	0.74	7.953	3.961	1.178	3.399	0.427	2.952	8.097	5.992	0.187	18.7

JP39

T(yrs)	Peak Q(cms)	Yo(m)	Vn(m/s)	A(sqm)	Yc (m)	Vc (m/s)	Vc/Vn	Fr	Ys/Yo	Ys (m)	Risk FPR = Ys/fd	Risk (%)
2	24.9	1.30	3.589	6.938	0.689	2.600	0.724	1.006	1.751	2.271	0.055	5.5
5	34.4	1.63	3.957	8.693	1.315	3.591	0.908	0.991	1.503	2.442	0.059	5.9
10	41.0	1.84	4.162	9.851	1.868	4.281	1.028	0.979	1.378	2.538	0.061	6.1
25	49.4	2.11	4.383	11.271	2.712	5.158	1.177	0.964	1.254	2.642	0.064	6.4
50	55.7	2.30	4.526	12.307	3.447	5.815	1.285	0.953	1.179	2.711	0.065	6.5
100	62.1	2.49	4.656	13.338	4.285	6.483	1.392	0.941	1.113	2.774	0.067	6.7

200	68.5	2.68	4.773	14.352	5.214	7.152	1.498	0.931	1.056	2.832	0.068	6.8
500	76.9	2.93	4.911	15.659	6.571	8.029	1.635	0.916	0.991	2.901	0.070	7.0

JP40

T(yrs)	Peak Q(cms)	Yo(m)	Vn(m/s)	A(sqm)	Yc (m)	Vc (m/s)	Vc/Vn	Fr	Ys/Yo	Ys (m)	Risk FPR = Ys/fd	Risk (%)
2	4.44	0.547	4.061	1.093	0.167	1.282	0.316	1.753	4.104	2.245	0.077	7.7
5	6.12	0.686	4.461	1.372	0.318	1.767	0.396	1.720	3.513	2.410	0.083	8.3
10	7.29	0.778	4.683	1.557	0.451	2.104	0.449	1.695	3.217	2.503	0.086	8.6
25	8.76	0.89	4.919	1.781	0.652	2.529	0.514	1.665	2.925	2.603	0.090	9.0
50	9.90	0.975	5.075	1.951	0.833	2.858	0.563	1.641	2.740	2.671	0.092	9.2
100	11.01	1.056	5.211	2.113	1.030	3.178	0.610	1.619	2.586	2.731	0.094	9.4
200	12.12	1.136	5.333	2.273	1.248	3.499	0.656	1.598	2.452	2.786	0.096	9.6
500	13.62	1.243	5.481	2.485	1.576	3.932	0.717	1.570	2.295	2.853	0.098	9.8

JP41

T(yrs)	Peak Q(cms)	Yo(m)	Vn(m/s)	A(sqm)	Yc (m)	Vc (m/s)	Vc/Vn	Fr	Ys/Yo	Ys (m)	Risk FPR = Ys/fd	Risk (%)
2	12.90	0.299	5.023	2.568	0.076	0.866	0.172	2.933	3.676	1.099	0.027	2.7
5	18.03	0.367	5.709	3.157	0.149	1.210	0.212	3.009	3.253	1.194	0.029	2.9
10	21.55	0.41	6.109	3.528	0.213	1.447	0.237	3.046	3.043	1.248	0.030	3.0
25	26.10	0.462	6.567	3.974	0.313	1.752	0.267	3.085	2.831	1.308	0.032	3.2
50	29.53	0.499	6.877	4.293	0.400	1.982	0.288	3.108	2.702	1.348	0.033	3.3
100	32.98	0.535	7.167	4.601	0.500	2.214	0.309	3.128	2.590	1.385	0.034	3.4
200	36.45	0.57	7.439	4.900	0.610	2.447	0.329	3.146	2.491	1.420	0.035	3.5
500	41.05	0.614	7.772	5.282	0.774	2.756	0.355	3.167	2.380	1.461	0.036	3.6

JP44

T(yrs)	Peak Q(cms)	Yo(m)	Vn(m/s)	A(sqm)	Yc (m)	Vc (m/s)	Vc/Vn	Fr	Ys/Yo	Ys (m)	Risk FPR = Ys/fd	Risk (%)
2	46.3	0.877	10.557	4.386	10.775	10.281	0.974	3.599	10.888	9.549	0.318	31.8
5	64.0	1.092	11.725	5.458	20.588	14.212	1.212	3.582	9.423	10.289	0.343	34.3
10	76.2	1.231	12.383	6.154	29.186	16.921	1.366	3.563	8.697	10.706	0.357	35.7
25	91.9	1.402	13.109	7.010	42.452	20.407	1.557	3.535	7.964	11.166	0.372	37.2
50	103.8	1.528	13.59	7.638	54.157	23.050	1.696	3.510	7.508	11.472	0.382	38.2
100	115.6	1.649	14.02	8.245	67.171	25.670	1.831	3.486	7.124	11.747	0.392	39.2
200	127.5	1.769	14.415	8.845	81.712	28.312	1.964	3.460	6.785	12.002	0.400	40.0
500	143.3	1.925	14.89	9.624	103.218	31.821	2.137	3.426	6.395	12.310	0.410	41.0

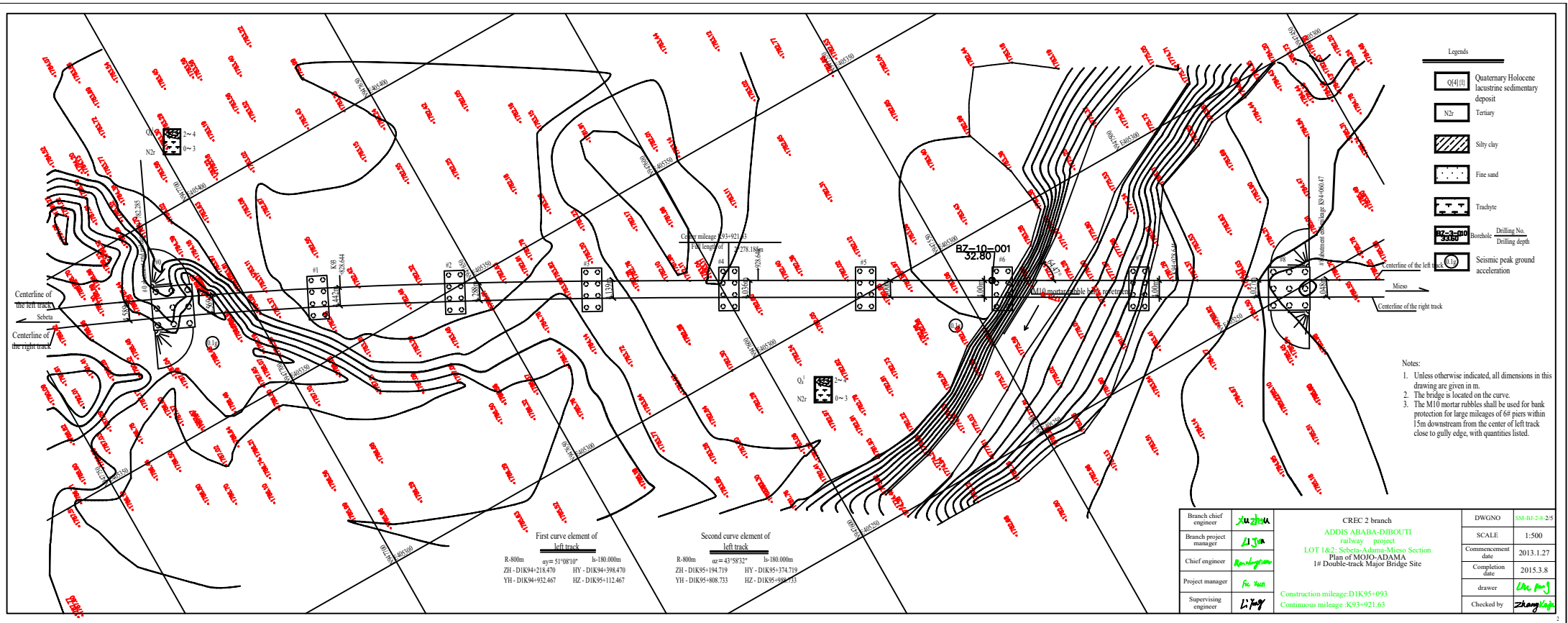
Legends
Q[4] [l] Quaternary Holocene lacustrine sedimentary deposit
N2r Tertiary
Silty clay
Fine sand
Trachyte
BZ-3-010 33.50 Borehole Drilling No. / Drilling depth
0.12 Seismic peak ground acceleration
Centerline of the left track
Sebeta
Centerline of the right track
Mieso
Centerline of the left track
Centerline of the right track
BZ-10-001 32.80
M10 mortar rubble bank protection
Abutment Mileage K94+066.47
Center mileage K93+921.63
Total length of bridge 278.18m
First curve element of left track
R-800m αy= 51°08'10" ls-180.000m
ZH - D1K94+218.470 HY - D1K94+398.470
YH - D1K94+932.467 HZ - D1K95+112.467
Second curve element of left track
R-800m αz= 43°58'32" ls-180.000m
ZH - D1K95+194.719 HY - D1K95+374.719
YH - D1K95+808.733 HZ - D1K95+988.733
Notes:
1. Unless otherwise indicated, all dimensions in this drawing are given in m.
2. The bridge is located on the curve.
3. The M10 mortar rubbles shall be used for bank protection for large mileages of 6# piers within 15m downstream from the center of left track close to gully edge, with quantities listed.
Branch chief engineer
Branch project manager
Chief engineer
Project manager
Supervising engineer
CREC 2 branch
ADDIS ABABA-DJBOUTI railway project
LOT 1&2: Sebeta-Adama-Mieso Section
Plan of MOJO-ADAMA 1# Double-track Major Bridge Site
Construction mileage:D1K95+093
Continuous mileage :K93+921.63
DWGNO SM-BJ-2-8-2/5
SCALE 1:500
Commencement date 2013.1.27
Completion date 2015.3.8
drawer
Checked by

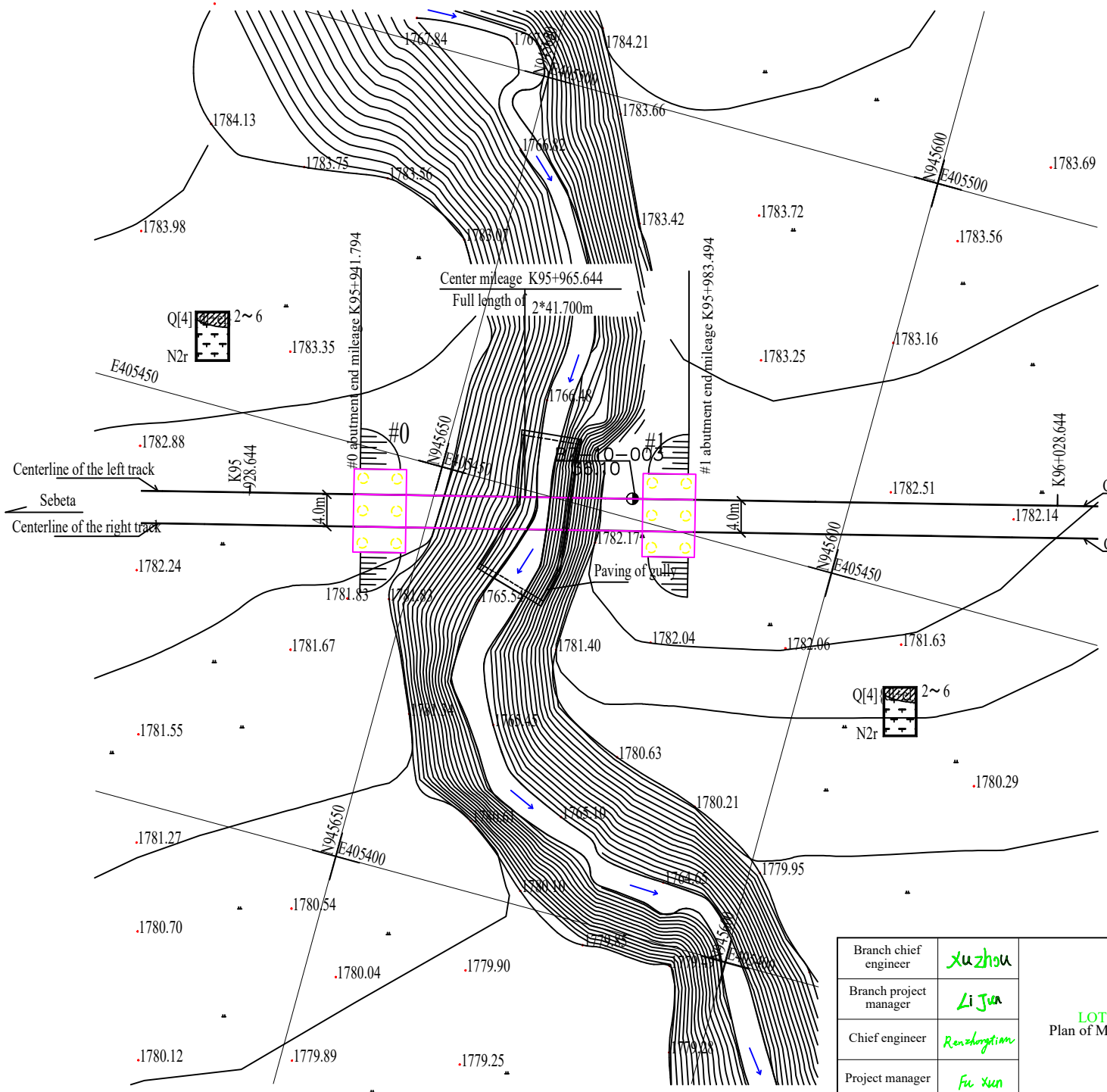

Legends

Q[4]{dl+el}	Quaternary Holocene drift-eluvium
N2r	Tertiary
	Silty clay
	Trachyte
BZ-10-003 36.10	Borehole — Drilling No. / Drilling depth

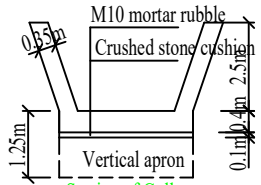

Section of Gully Paving

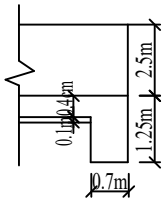

Schematic Diagram of Vertical Aprons at Both Ends

Notes:

1. All dimensions in this drawing are given in meters.
2. The bridge is located on the straight line.
3. The M10 mortar rubbles have been paved within the range of 20m upstream and downstream of the gulley between two abutments for protection. The 1.25m deep vertical apron have been provided at both ends of the paved place, with relevant quantities listed.

Branch chief engineer	Xu Zhou
Branch project manager	Li Jun
Chief engineer	Ren Zhongtian
Project manager	Fu Xun
Supervising engineer	Li Yong

CREC 2 branch

ADDIS ABABA-DJBOUTI railway project

LOT 1&2: Sebeta-Adama-Mieso Section

Plan of MOJO-ADAMA # 2 Double-track Medium Bridge

Construction mileage:D1K97+134

Continuous mileage :K95+965.644

DWGNO	SM-BJ-2-9-2/3
SCALE	
Commencement date	2013.2.25
Completion date	2015.3.12
drawer	Liu Peng
Checked by	Zhang Keju

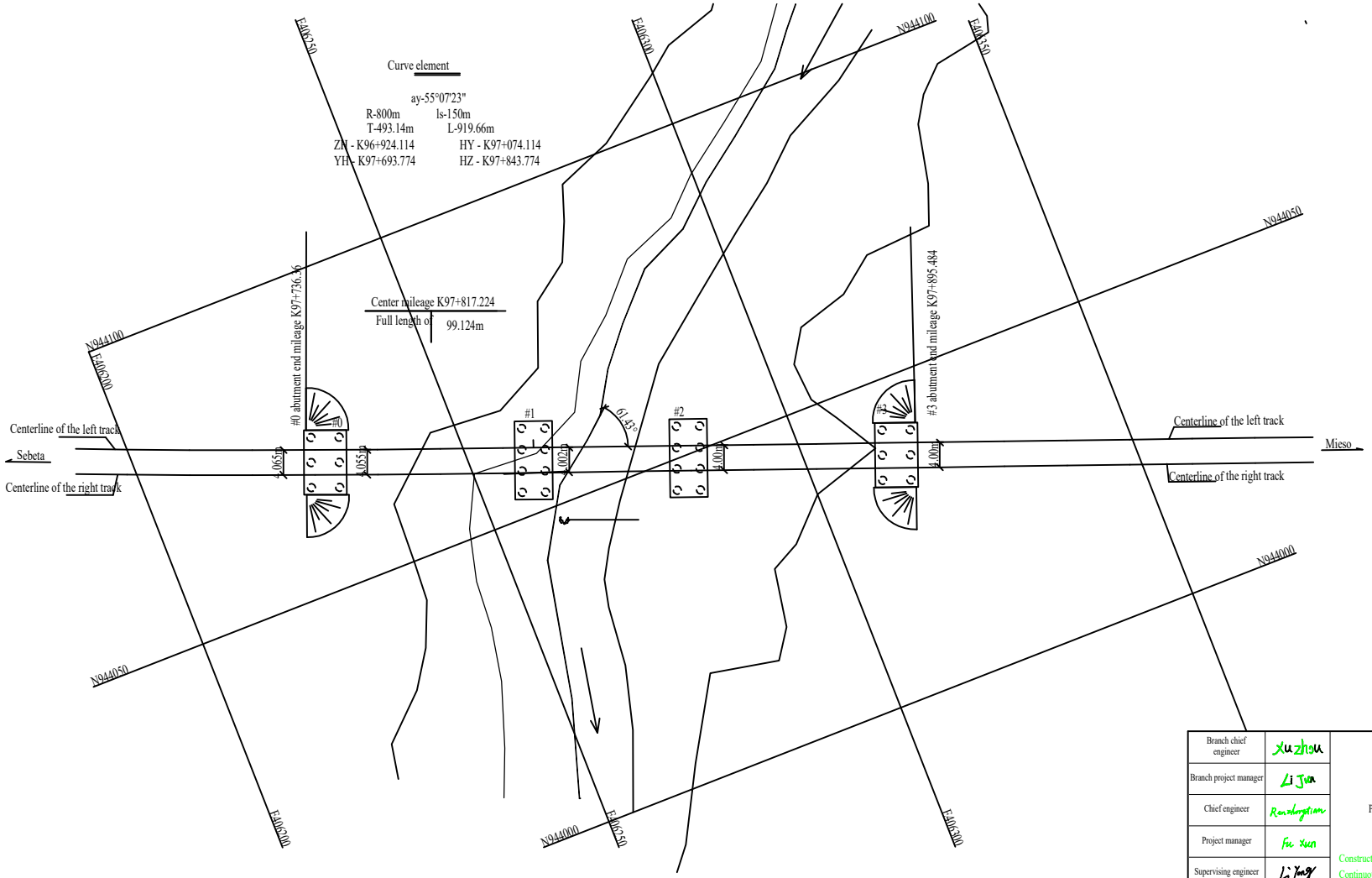

Legends

- Q[4]{dl+el} Quaternary Holocene drift-eluvium
- N2r Tertiary
- Silty clay
- Trachyte

Notes:

1. Unless otherwise indicated, all dimensions in this drawing are given in m.
2. This bridge is located on gentle curve and straight line.

Branch chief engineer	Xu zhou	CREC 2 branch ADDIS ABABA-DJBOUTI railway project LOT 1&2: Sebeta-Adama-Mieso Section Plan of MOJO-ADAMA #3 Double-track Medium Bridge Construction mileage:DK98+903 Continuous mileage :K97+817.22	DWGNO SM-BJ-2-10-2/7
Branch project manager	Li Jun		SCALE 1:500
Chief engineer	Ruanlongtian		Commencement date 2013.12.31
Project manager	Fu xun		Completion date 2015.3.16
Supervising engineer	Li Yong		drawer Liu peng
			Checked by Zhang Kejia

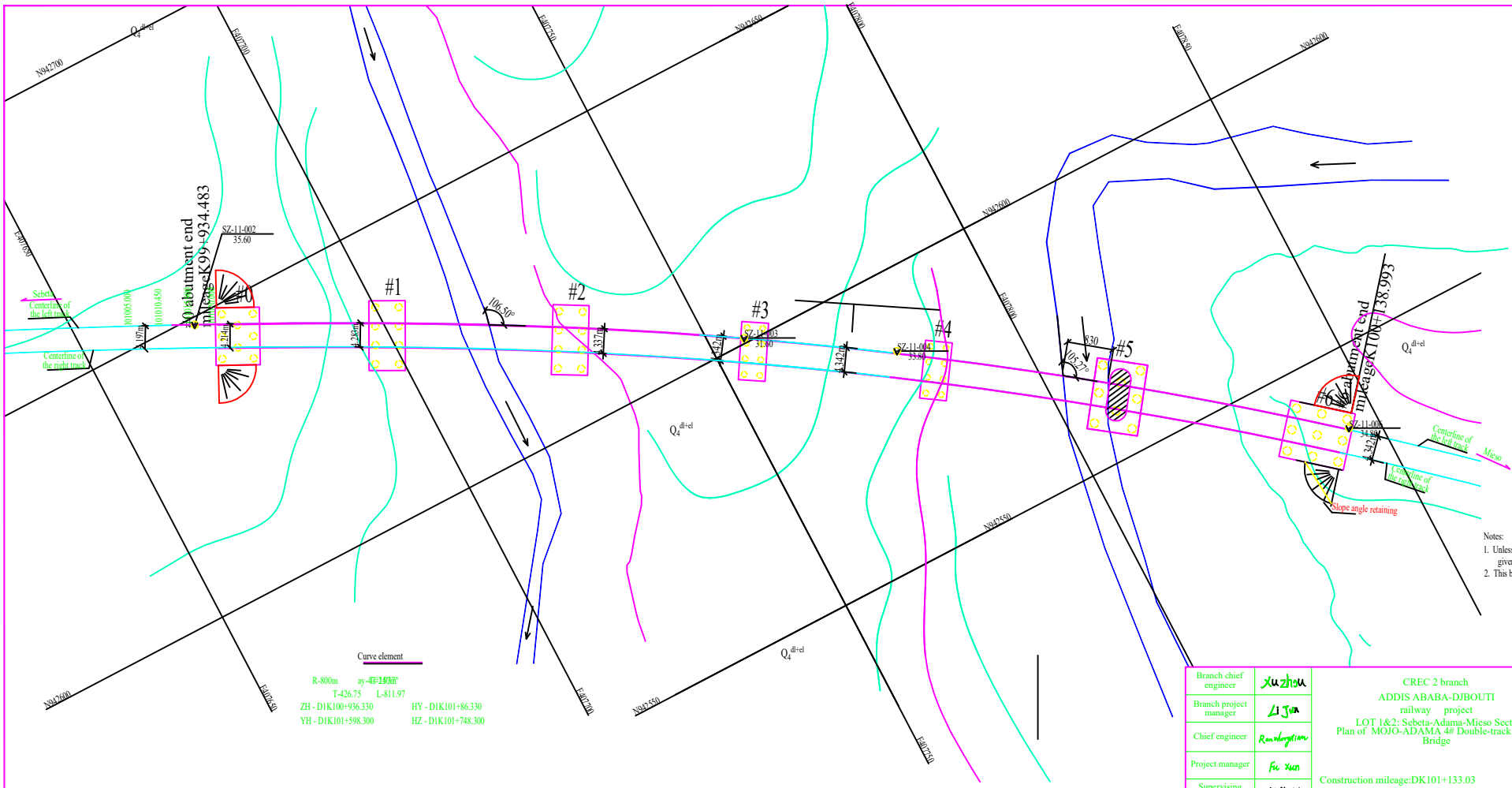

Branch chief engineer	Xuzhou	CREC 2 branch ADDIS ABABA-DJBOUTI railway project LOT 1&2: Sebeta-Adama-Mieso Section Plan of MOJO-ADAMA 4# Double-track Major Bridge Construction mileage:DK101+133.03 Continuous mileage :K100+19.144	DWGNO: SM-BJ-2-11-2/9
Branch project manager	Li Jun		SCALE: 1:500
Chief engineer	Ranzhengtian		Commencement date: 2013.11.12
Project manager	Fu Xun		Completion date: 2015.3.24
Supervising engineer	Li Jing		drawer: Liu peng
			Checked by: Zhang Kegu

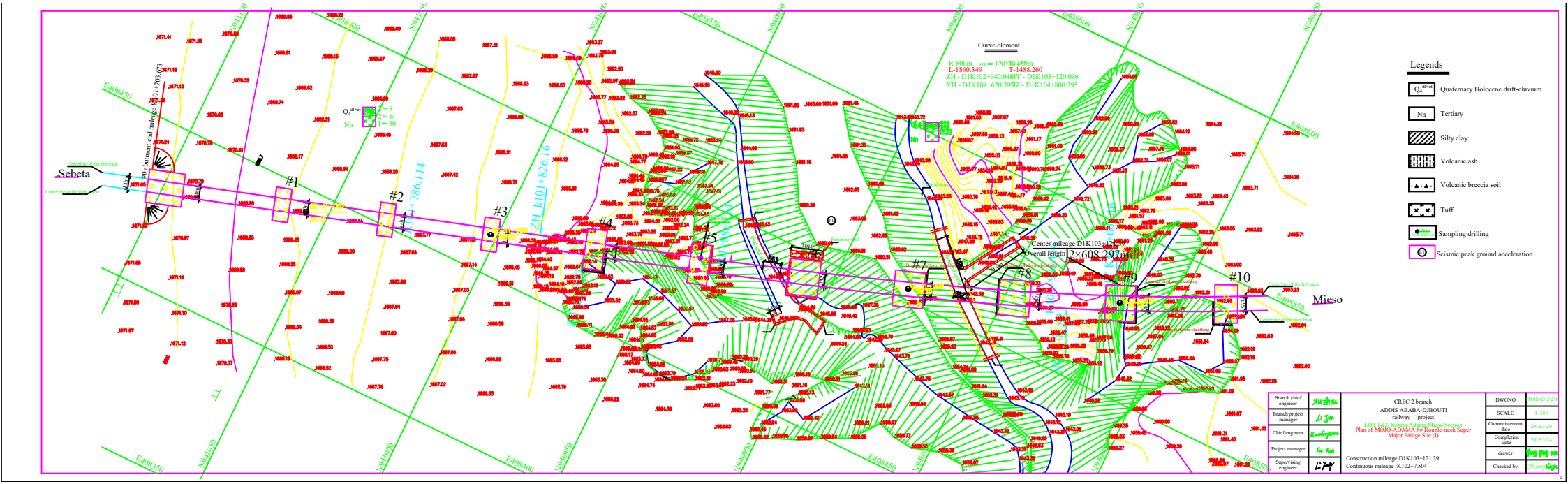
Sebeta
Mieso
#1
#2
#3
#4
#5
#6
#7
#8
#9
#10
ZH - K101+826.16
HY - K101+786.114
Curve element
R-800m αz= 120°16'48"
L-1860.349 T-1488.260
ZH - D1K102+940.046 HY - D1K103+120.046
YH - D1K104+620.395 HZ - D1K104+800.395
Center mileage D1K103+121.39
Overall length 2×608.297m
Legends
Quaternary Holocene drift-eluvium
Tertiary
Silty clay
Volcanic ash
Volcanic breccia soil
Tuff
Sampling drilling
Seismic peak ground acceleration
CREC 2 branch
ADDIS ABABA-DJIBOUTI
railway project
LOT 1&2: Sebeta-Adama-Mieso Section
Plan of MOJO-ADAMA 8# Double-track Super Major Bridge Site (I)
Construction mileage:D1K103+121.39
Continuous mileage :K102+7.504
DWGNO
SCALE 1:500
Commencement date 2013.3.29
Completion date 2015.3.24
drawer
Checked by

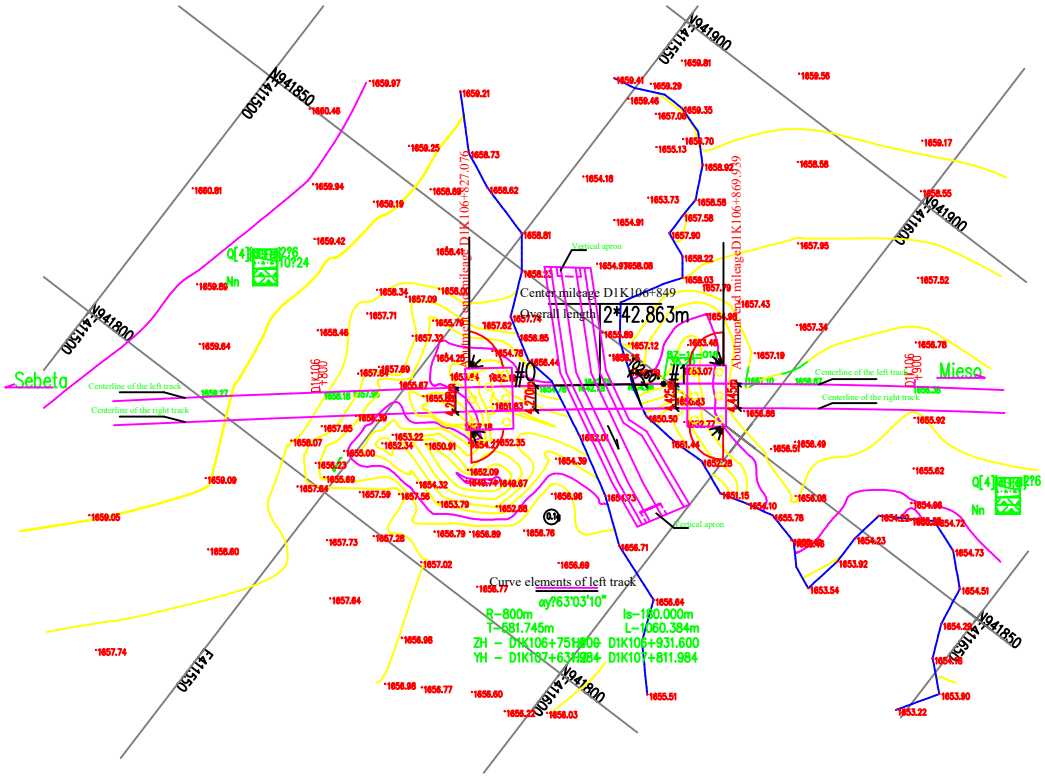

Notes:

1. This bridge was started to be built on 2013.11.23 and completed on 2014.7.24 .
2. All dimensions in this drawing are given in m.
3. The bridge is a medium double-track bridge located on gentle curve, and simple supported beams are subject to half-split midsagittal arrangement.
4. The bridge discharges flood on a seasonal basis, with a design flow: $Q_{[1/100]}$=8.53m3/s。
5. Geological data:

<4-4>	Volcanic ash	Slightly dense	α=0.15MPa
<4-6>	Volcanic breccia soil	Slightly dense	α=0.20MPa
<7-1>	Volcanic Breccia	W3	α=0.35MPa

6. Applicable general drawings:
(1) *Prefabricated post-tensioned simple supported T beam of mixed passenger and freight railway*, L=32m SM-BG-01
(2) *Bored (Dug) Pile* SM-BG-06
(3) *Double-track T-shaped Hollow Abutment* SM-BG-08
(4) *Waterproof Layer for Concrete Bridge and Culvert of Railway* SM-BG-09
(5) *Communication and Signal Cable Trough on Bridge* SM-BG-12
(6) *Atlas of Architectural Drawings for Railway Bridges* SM-BG-13
(7) *Inspection Equipment of Railway Bridge Pier and Abutment* SM-BG-15
(8) *Installation Drawing of Bearing for Railway Bridge* SM-BG-16
(9) *Earthquake-caused Beam Falling Prevention Measures* SM-BG-17
7. TJGZ-Q bearings are employed for the bridge. For 32m T beam, a 25mm thick layer of M50 stiff non-shrink cement mortar shall be paved between the bottom face of bearing and the top face of bearing pad stone.
8. The elevation of abutment top marked in the Elevation is that of bearing pad stone top.
9. The beam and two abutments shall be provided with 1.05m wide sidewalks with angle steel railings at both sides.
10. Guard rails shall be provided inside the stock rails on the bridge.
11. C35 reinforced concrete L-shaped ballast retaining blocks shall be provided on the outermost ballast retaining wall of the curve on the bridge.
12. Communication and signal cable troughs shall be provided outside the sidewalk railing at the left side of the deck.
13. 0# and 1# abutments of the bridge are provided with 1.25m diameter bored pile foundations. For 0# abutment, the stirrups shall be densified within a range of 6.5m from the pile top below the bottom surface of the bearing platform. For 1# abutment, the stirrups shall be densified within a range of 4.0m from the pile top below the bottom surface of the bearing platform, with the stirrup spacing being 10cm in the densified section.
14. All pile foundations of this bridge are per friction piles.
15. The cone shall be built with 35cm-thick M10 mortar rubbles and provided below with 10cm-thick crushed stone cushion. The cone drainage pipes shall be PVC pipes with an outside diameter of 125mm and a wall thickness of 8mm and arranged in a quincunx form at an interval of 1.5m.
16. M10 mortar rubble embankment inspection steps shall be provided on both sides of the embankment at the ends of the two abutments.
17. The subgrade side ditch behind the abutment have been connected to the proper positions or natural ditches below the bridge to avoid scouring on the abutment body and the foundation or the slope surface below the bridge. If the subgrade side ditch behind the abutment is connected to a position below the bridge, it shall be step-like downward along the landform, with the quantities listed.
18. Corrosion control of bridge decking and metallic components of inspection facilities were in accordance with the requirements in the applicable general drawings.
19. M10 mortar rubble paving along the gully have been adopted within a range of 30m upstream and downstream of the ditch.

Legends

- Quaternary Holocene alluvial deluvium
- Tertiary
- Volcanic ash
- Volcanic breccia soil
- Volcanic Breccia
- Faults with unidentified properties
- Borehole (No., basic depth (m))
- Seismic peak ground acceleration

Schematic Diagram of Section of Riverbed Protection (upstream of ditch)

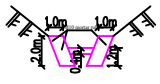

Schematic Diagram of Section of Riverbed Protection (downstream of ditch)

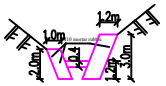

Branch chief engineer	
Branch project manager	
Chief engineer	
Project manager	
Supervising engineer	

CREC 3rd Branch
ADDIS ABABA-DJBOUTI railway project
Sebeta-Meiso lot D1K103+425.856-D1K150+000 section
Bridge-built Drawing of MOJO-ADAMA #6 Double-track Medium Bridge
Construction mileage: D1K106+849
Continuous mileage : K105+735

DWGNO	SM-BJ-22-1/2
SCALE	As shown in the drawing
Commencement date	2013.11.23
Completion date	2014.07.24
Drawer	
Checked by	

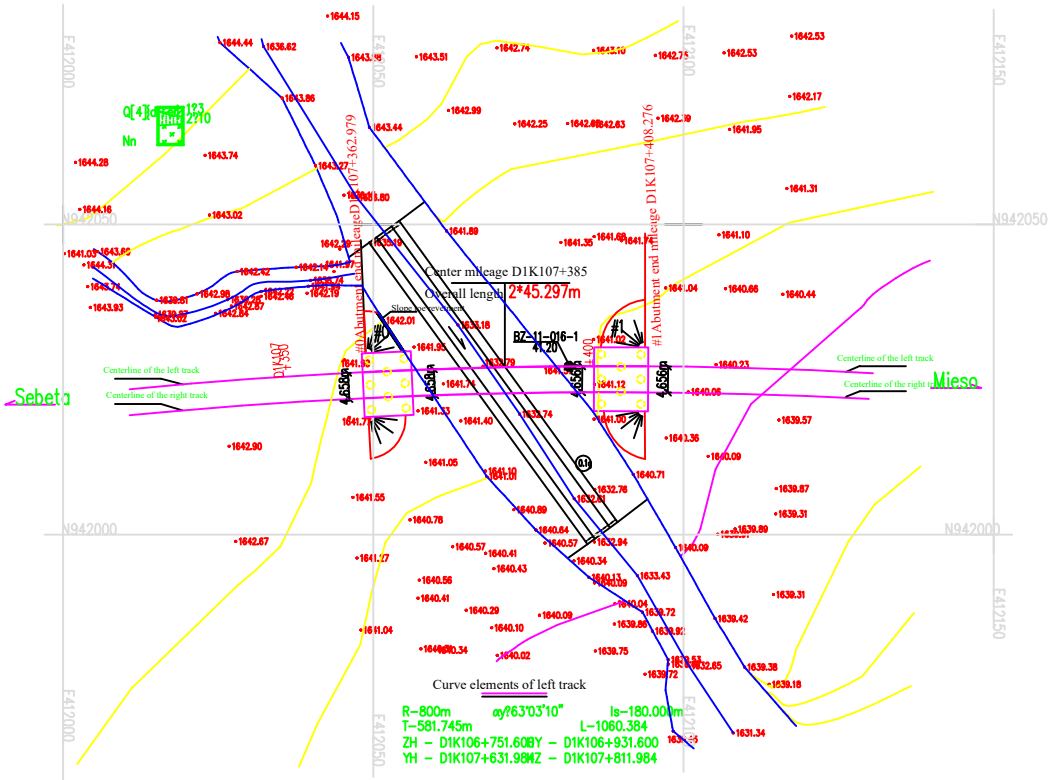

Notes:

1. This bridge was started to be built on 2014.4.1 and completed on 2014.7.21 .
2. All dimensions in this drawing are given in m.
3. The bridge is a medium double-track bridge located on gentle curve, and simple supported beams are subject to half-split midsagittal arrangement.
4. The bridge discharges flood on a seasonal basis, with a design flow: Q[1/100]=21.3m3/s。
5. Geological data:

<4-3	Silty clay	Slightly dense	α=0.16MPa
<4-4	Volcanic ash	Loose	α=0.15MPa
<7-1	Volcanic Breccia	W4 W3	α=0.20MPa α=0.35MPa

6. Applicable general drawings:
(1) Prefabricated post-tensioned simple supported T beam of mixed passenger and freight railway, L=32m SM-BG-01
(2) Bored (Dug) Pile SM-BG-06
(3) Double-track T-shaped Hollow Abutment SM-BG-08
(4) Waterproof Layer for Concrete Bridge and Culvert of Railway SM-BG-09
(5) Communication and Signal Cable Trough on Bridge SM-BG-12
(6) Atlas of Architectural Drawings for Railway Bridges SM-BG-13
(7) Inspection Equipment of Railway Bridge Pier and Abutment SM-BG-15
(8) Installation Drawing of Bearing for Railway Bridge SM-BG-16
(9) Earthquake-caused Beam Falling Prevention Measures SM-BG-17
7. TJGZ-Q bearings are employed for the bridge. For 32m T beam, a 25mm thick layer of M50 stiff non-shrink cement mortar shall be paved between the bottom face of bearing and the top face of bearing pad stone.
8. The elevation of abutment top marked in the Elevation is that of bearing pad stone top.
9. The beam and two abutments shall be provided with 1.05m wide sidewalks with angle steel railings at both sides.
10. Guard rails shall be provided inside the stock rails on the bridge.
11. C35 reinforced concrete L-shaped ballast retaining blocks shall be provided on the outermost ballast retaining wall of the curve on the bridge.
12. Communication and signal cable troughs shall be provided outside the sidewalk railing at the left side of the deck.
13. 0# and 1# abutments of the bridge are provided with 1.25m diameter bored pile foundations. For 0# abutment, the stirrups shall be densified within a range of 6.5m from the pile top below the bottom surface of the bearing platform. For 1# abutment, the stirrups shall be densified within a range of 4.0m from the pile top below the bottom surface of the bearing platform, with the stirrup spacing being 10cm in the densified section.
14. All pile foundations of this bridge are per friction piles.
15. The cone shall be built with 35cm-thick M10 mortar rubbles and provided below with 10cm-thick crushed stone cushion. The cone drainage pipes shall be PVC pipes with an outside diameter of 125mm and a wall thickness of 8mm and arranged in a quincunx form at an interval of 1.5m.
16. Both sides of the ditch shall be paved with 35cm thick M10 mortar rubbles within a range of 20m upstream and downstream along the bank with 10cm thick crushed stone bed course at the bottom .
17. M10 mortar rubble embankment inspection steps are provided on both sides of the embankment at the ends of the two abutments.
18. The subgrade side ditch behind the abutment are connected to the proper positions or natural ditches below the bridge to avoid scouring on the abutment body and the foundation or the slope surface below the bridge.
19. The spoil toe are protected with M10 mortar rubble.
20. Corrosion control of bridge decking and metallic components of inspection facilities are in accordance with the requirements in the applicable general drawings.
21. M10 mortar rubbles have been adopted for protection within a range of 30m upstream and downstream of river channel. The quantities of such works have been included.
22. Conical slope toe on the left side of 0# abutment have been provided with slope toe revetment .

Legends

- Quaternary Holocene drift-eluvium
- Nn Tertiary
- Silty clay
- Volcanic ash
- Volcanic Breccia
- No. / Hole depth (m) Borehole
- Seismic peak ground acceleration

Schematic Diagram of Section of Riverbed Protection

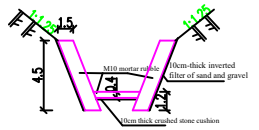

Branch chief engineer		CREC 3rd Branch ADDIS ABABA-DJBOUTI railway project Sebeta~Meiso lot D1K103+425.856-D1K150+000 section Bridge-built Drawing of MOJO-ADAMA #7 Double-track Medium Bridge Construction mileage: D1K107+385 Continuous mileage : K106+271	DWGNO	SM-BJ-23-1/3
Branch project manager			SCALE	As shown in the drawing
Chief engineer			Commencement date	2014.04.01
Project manager			Completion date	2014.07.21
Supervising engineer			Drawer	
			Checked by	

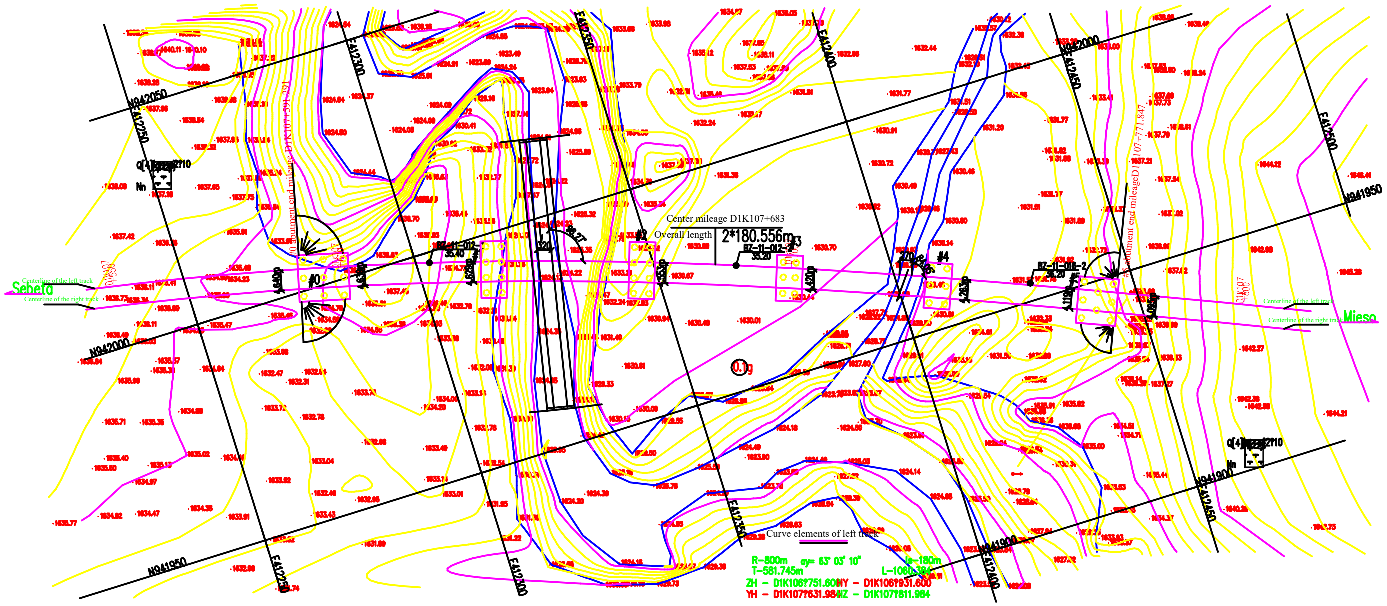

Notes:

1. This bridge was started to be built on 2014.1.5 and completed on 2014.5.8.
2. All dimensions in this drawing are given in m.
3. The bridge is a double-track medium bridge located on circular curve and gentle curve, and simple supported beams are subject to half-split midsagittal arrangement.
4. The bridge discharges flood on a seasonal basis, with a design flow: Q[1/100]=178.9m3/s。
5. Geological data:

<4-3>Q[4]{dl+el}	Silty clay	Stiff-plastic		σ=0.16MPa
<7-1>Nn	Volcanic Breccia	W4		σ=0.20MPa
		W3		σ=0.30MPa

6. Applicable general drawings:
(1) Prefabricated post-tensioned simple supported T beam of mixed passenger and freight railway, L=32m SM-BG-01
(2) Double-track round-ended solid pier in 7-degree seismic areas SM-BG-04
(3) Bored (Dug) Pile SM-BG-06
(4) Double-track T-shaped Hollow Abutment SM-BG-08
(5) Waterproof Layer for Concrete Bridge and Culvert of Railway SM-BG-09
(6) Communication and Signal Cable Trough on Bridge SM-BG-12
(7) Atlas of Architectural Drawings for Railway Bridges SM-BG-13
(8) Inspection Equipment of Railway Bridge Pier and Abutment SM-BG-15
(9) Installation Drawing of Bearing for Railway Bridge SM-BG-16
(10) Earthquake-caused Beam Falling Prevention Measures SM-BG-17
7. TJGZ-Q bearings are employed for the bridge. For 32m T beam, a 25mm thick layer of M50 stiff non-shrink cement mortar have been paved between the bottom face of bearing and the top face of bearing pad stone.
8. The elevation of abutment top marked in the Elevation is that of bearing pad stone top.
9. The beam and two abutments shall be provided with 1.05m wide sidewalks with angle steel railings at both sides.
10. Guard rails have been provided inside the stock rails on the bridge.
11. C35 reinforced concrete L-shaped ballast retaining blocks have been provided on the outermost ballast retaining wall of the curve on the bridge.
12. Communication and signal cable troughs have been provided outside the sidewalk railing at the left side of the deck.
13. Bored pile foundations with a diameter of 1.25m shall be adopted for 0~5# piers & abutments of this bridge. Stirrups shall be densified for 0~3# piers & abutments, and for 4~5# piers & abutments within the range of 5m and 4m respectively, from the pile top below the bottom surface of the bearing platform, with the stirrup spacing being 10cm in the densified section.
14. All pile foundations of this bridge are per friction piles.
15. The cone have been built with 35cm-thick M10 mortar rubbles and provided below with 10cm-thick crushed stone cushion. The cone drainage pipes shall be PVC pipes with an outside diameter of 125mm and a wall thickness of 8mm and arranged in a quincunx form at an interval of 1.5m.
16. M10 mortar rubble embankment inspection steps have been provided on both sides of the embankment at the ends of the two abutments
17. The subgrade side ditch behind the abutment shall be connected to the proper positions or natural ditches below the bridge to avoid scouring on the abutment body and the foundation or the slope surface below the bridge.
18. C20 concrete have been adopted for protection within a range of 50m upstream and 30m downstream of river channel. The quantities of such works have been included.
19. Corrosion control of bridge decking and metallic components of inspection facilities have been in accordance with the requirements in the applicable general drawings.

Legends

Q[4]{dl+el}	Quaternary Holocene drift-eluvium	f	Faults with unidentified properties
Nn	Tertiary	No. / Hole depth (m)	Borehole
	Silty clay	0.1g	Seismic peak ground acceleration
	Volcanic Breccia		

Branch chief engineer	Yang [signature]	CREC 3rd Branch ADDIS ABABA-DJBOUTI railway project Sebeta~Meiso lot D1K103+425.856-D1K150+000 section	DWGNO	SM-BJ-24-1/3
Branch project manager	[signature]		SCALE	As shown in the drawing
Chief engineer	[signature]	Bridge-built Drawing of MOJO-ADAMA #8 Double-track Major Bridge	Commencement date	2014.01.05
Project manager	Fu Xun		Completion date	2014.05.08
Supervising engineer	[signature]	Construction mileage: D1K107+683 Continuous mileage : K106+569	Drawer	[signature]
			Checked by	[signature]

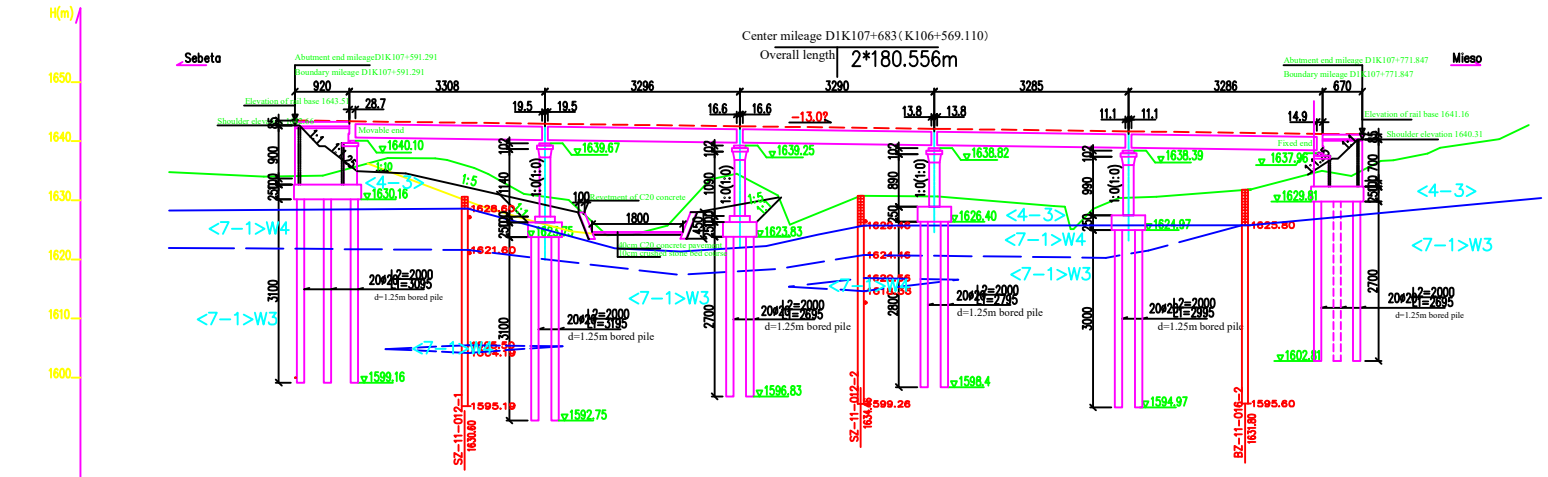

Elevation

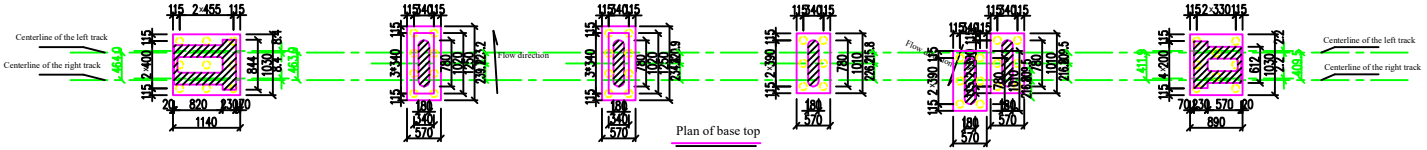

Plan of base top

Schematic Diagram of Curve

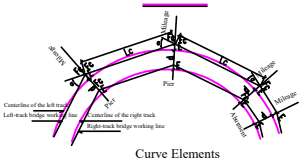

Curve Elements

ay= 63° 03' 10"

R=800m ls=180m

ZH – D1K106+751.608Y – D1K106+931.600

YH – D1K107+631.984Z – D1K107+811.984

Layout of Curves

Left track						Right track	
Abutment and pier No.	Abutment and beam joint mileage	Deflection distance (Fdeam)	Beam joint (Fe.beam)	Deflection angle (α)	Distance between centers of tracks	Mileage	Beam joint (Fe.beam)
0# abutment front	D1K107+591.291		0°19'46"	9.200		4.640	
0# abutment back	D1K107+600.491	28.7	1°30'29"	33.084	4.639	16.5	
1	D1K107+633.573	19.5	2°17'43"	32.061	4.629	10.1	
2	D1K107+666.534	16.6	1°53'47"	32.961	4.553	9.1	
3	D1K107+699.495	13.8	1°27'58"	32.914	4.420	8.1	
4	D1K107+732.267	11.1	1°22'39"	32.849	4.263	7.2	
5# abutment front	D1K107+765.116	14.9	0°24'43"	32.850	4.119	11.8	
5# abutment back	D1K107+771.847		0°3'24"	6.700	4.095		

Notes:

1. Except mileages and elevations which are expressed in m and where otherwise indicated, all dimensions in this drawing are given in cm.
2. The bridge is designed according to the topographical conditions.
3. Hydrological data: Q[1/100]=178.9m3/s; H[1/100]=1629.57m; V[1/100]=2.95m/s.
4. Route profile

Elevation of rail top 1643.80 1635.39

13.0?

569.998

Mileage D1K107+580 D1K108+150

5. Geological data:

<4-3>Q[4]al+pl Silty clay Stiff-plastic σ_0=0.16MPa

<7-1>Nn Volcanic Breccia W4 σ_0=0.20MPa

W3 σ_0=0.30MPa

Branch chief engineer		CREC 3rd Branch ADDIS ABABA-DJBOUTI railway project Sebeta~Meiso lot D1K103+425.856-D1K150+000 section Bridge-built Drawing of MOJO-ADAMA #8 Double-track Major Bridge Construction mileage: D1K107+683 Continuous mileage : K106+569	DWGNO SM-BJ-24-2/3
Branch project manager			SCALE As shown in the drawing
Chief engineer			Commencement date 2014.01.05
Project manager			Completion date 2014.05.08
Supervising engineer			Drawer Checked by

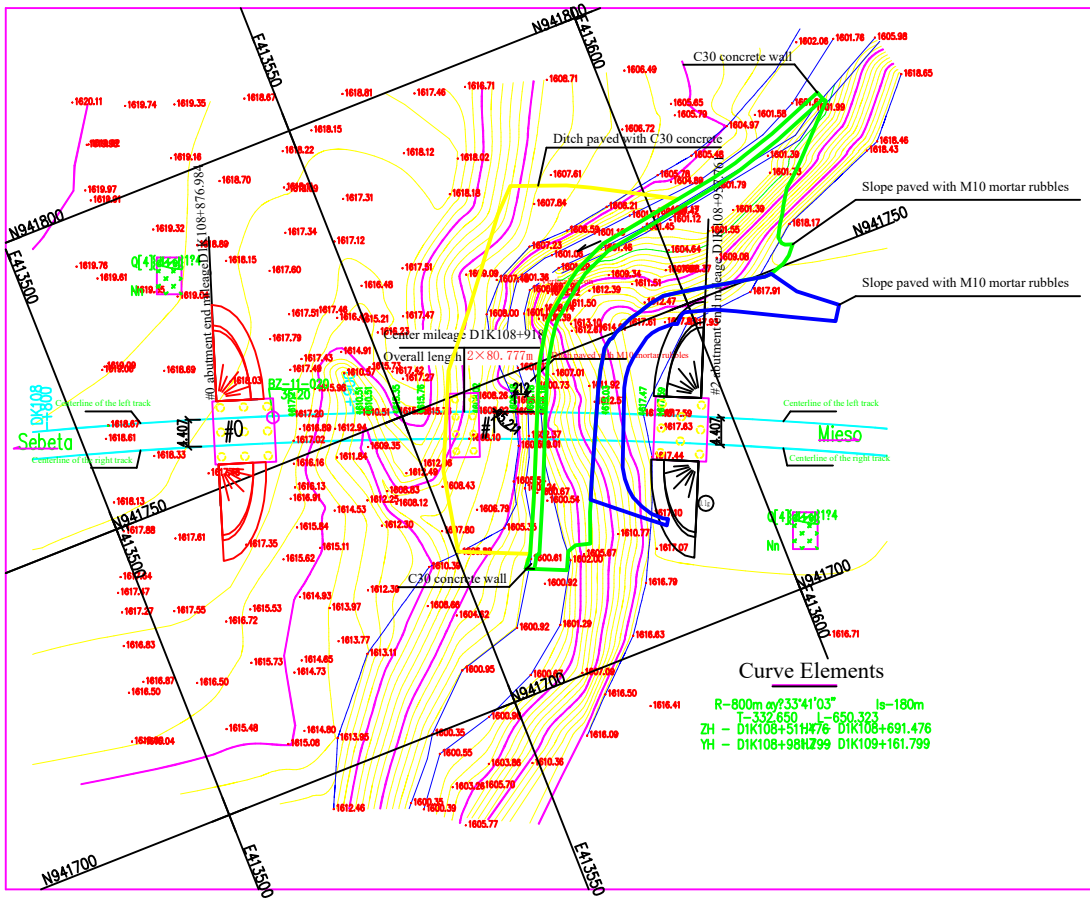

Notes:

1. This bridge was started to be built on 2014.2.19 and completed on 2014.10.7.
2. All dimensions in this drawing are given in m.
3. The bridge is a double-track medium bridge located on circular curve, and simple supported beams are subject to half-split midsagittal arrangement.
4. The bridge discharges flood on a seasonal basis, with a design flow: Q[1/100]=46.0m3/s。
5. Geological data:

<4-3>Q[4]dl+el Silty clay α_c=0.16MPa
<7-2>Nn Tuff W4 α_c=0.20MPa
W4 W3 Weathering boundary line of rock stratum W3 α_c=0.35MPa

6. Applicable general drawings:
(1) Prefabricated post-tensioned simple supported T beam of mixed passenger and freight railway, L=32m SM-BG-01
(2) Double-track round-ended solid pier in 7-degree seismic areas SM-BG-04
(3) Bored (Dug) Pile SM-BG-06
(4) Double-track T-shaped Hollow Abutment SM-BG-08
(5) Waterproof Layer for Concrete Bridge and Culvert of Railway SM-BG-09
(6) Communication and Signal Cable Trough on Bridge SM-BG-12
(7) Atlas of Architectural Drawings for Railway Bridges SM-BG-13
(8) Simple supported T beam refuge platform of railway SM-BG-14
(9) Inspection Equipment of Railway Bridge Pier and Abutment SM-BG-15
(10) Installation Drawing of Bearing for Railway Bridge SM-BG-16
(11) Earthquake-caused Beam Falling Prevention Measures SM-BG-17
7. TJGZ-Q bearings are employed for the bridge. For 32m T beam, a 25mm thick layer of M50 stiff non-shrink cement mortar shall be paved between the bottom face of bearing and the top face of bearing pad stone.
8. The abutment top elevations marked in the elevation are bearing pad stone top elevations and the top cap elevations marked in the drawing include the bearing pad stone heights.
9. The beam and two abutments have been provided with 1.05m wide sidewalks with angle steel railings at both sides.
10. This is a double-track bridge and refuge platforms have been provided on both sides of the piers.
11. Guard rails have been provided inside the stock rails on the bridge.

Apron Section

Schematic

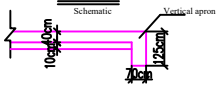

12. C35 reinforced concrete L-shaped ballast retaining blocks have been provided on the outermost ballast retaining wall of the curve on the bridge.
13. Communication and signal cable troughs shall be provided outside the sidewalk railing at the left side of the deck.
14. Electro support anchor bolt holes have been reserved on the pier top cap of this bridge.
15. 1.25m bored pile foundations have been adopted for 0#~2# piers & abutments of this bridge. Stirrups shall be densified for 0# and 2# abutments, and for 1# pier within the range of 5m and 8.5m respectively, from the pile top below the bottom surface of the bearing platform, with the stirrup spacing being 10cm in the densified section.
16. All pile foundations of this bridge are per friction piles.
17. The cone have been built with 35cm-thick M10 mortar rubbles and provided below with 10cm-thick crushed stone cushion. The cone drainage pipes shall be PVC pipes with an outside diameter of 125mm and a wall thickness of 8mm and arranged in a quincunx form at an interval of 1.5m.
18. M10 mortar rubble embankment inspection steps have been provided on both sides of the embankment at the ends of the two abutments.
19. The subgrade side ditch behind the abutment have been connected to the proper positions or natural ditches below the bridge to avoid scouring on the abutment body and the foundation or the slope surface below the bridge.
20. Spoil shall not be disposed under the bridge without permission.The spoil toe have been protected with M10 mortar rubble.
21. Corrosion control of bridge decking and metallic components of inspection facilities are in accordance with the requirements in the applicable general drawings.
22. Ditch paving have been provided between 1# pier and 2# abutment of the bridge within a range of 50m upstream and 30m downstream. Both ends of the ditch paving have been provided with 1.25m deep aprons. See section of ditch paving for details.
23. After excavation, 1# pier have been backfilled and compacted with 1:4 M10 mortar rubbles and wrapped by bearing platform .

Legends

Q[4]dl+el Quaternary Holocene diluvial-eluvium
Nn Tertiary
Silty clay
Tuff
BZ-11-020 35.20 Borehole No. / Hole depth (m)
0.16g Seismic peak ground acceleration

Branch chief engineer		DWGNO	SM-BJ-26-1/3
Branch project manager		SCALE	As shown in the drawing
Chief engineer		Commencement date	2014.02.19
Project manager		Completion date	2014.10.07
Supervising engineer		Drawer	
		Checked by	

CREC 3rd Branch
ADDIS ABABA-DJBOUTI railway project
Sebeta~Meiso lot D1K103+425.856-D1K150+000 section

Bridge-built Drawing of MOJO-ADAMA #10 Double-track Medium Bridge

Construction mileage: D1K108+918
Continuous mileage : K107+804